

[www.ghiocel-tech.com](http://www.ghiocel-tech.com)

4 South Main St., Phoenix Building, 3rd Floor, Pittsford, New York 14534

"We see the future today..."



# ENGINEERING ADVANCES FOR DETERMINISTIC AND PROBABILISTIC, LINEAR AND NONLINEAR SEISMIC SSI ANALYSES

TECHNICAL NEWSLETTER | No. 1 / 2015

## ACS SASSI NEWS

The **ACS SASSI** software is a software in a continuous fast development. In addition to the computational speed improvements through a full parallelization of the code that makes it hundreds of times faster than the university SASSI code, ACS SASSI includes a totally new set SSI analysis capabilities that extends the linearized SASSI methodology to nonlinear soil and structure and probabilistic SSI problems, including eventually incoherent seismic wave fields and inclined soil layering geometries.

The new added SSI capabilities makes ACS SASSI the most complete seismic SSI analysis engineering tool for nuclear structure projects. The recent versions

already included section-cut capabilities and powerful ACS SASSI-ANSYS integration capabilities.

**Option AA** or Advanced ANSYS, makes possible to run directly ANSYS FE structural models in ACS SASSI with no modelling limitation, including all ANSYS refined shell, beam and solid element types, rigid links, coupled nodes, or constraint equations, and even fluid elements. The structural animation at <http://www.ghiocel-tech.com/enggTools/pool-combined-thd.avi> shows the ACS SASSI-ANSYS fluid-structure interaction capability.

**Option A** or ANSYS includes fast automatic export of the seismic SSI boundary

conditions for performing a detailed nonlinear/linear stress SSI analysis using refined ANSYS FE models via the ACS SASSI-ANSYS integration capability.

By this July, we released the ACS SASSI Probabilistic SSI analysis capability option per the new ASCE 04-2015 recommended methods, **Option PRO**, and by this August, we will release the nonlinear structure capability, **Option NON**, applicable to the low-rise concrete shearwall buildings and foundation isolation problems. The nonlinear structure analysis capability is based on a highly efficient hybrid frequency-time domain SSI approach. The new **Option NON** will include nonlinear Shell, Springs and Beam elements. This makes Option NON highly applicable to

nonlinear structure applications, including foundation isolation and sliding effects.

The random vibration theory (RVT) capability for SSI analysis, **Option RVT**, will be released by late August or September.

**Option 2DSOIL** that will be available in the next upgrade, uses a soil deposit model in the 2D space with inclined soil layers. The classical 3D SASSI model with 1D free-field soil impedances and motions is replaced by a 3D SASSI model with 2D free-field soil impedances and motions. Also, in the next upgrade, a new nonlinear soil module, **SOILNON**, will be included. **SOILNON** implements identical theory and provides identical results with **DEEPSOIL** code. Comparisons between results obtained using SHAKE equivalent-linear methodology and **DEEPSOIL** nonlinear methodology can be done very efficiently by a single click selection. The **SOILNON** module uses automatically the soil constitutive curve input data to define the parameters of the soil hyperbolic nonlinear model.

**Option PRO** is consistent with probabilistic site response and SSI procedures in ASCE 04-2015 standard (see Chapters 2 and 5) and USNRC guidance for computing the FIRS for new applications. The **Option PRO** probabilistic modelling includes: i) Response spectra shape model for the seismic motion input, ii) Soil shear wave velocity  $V_s$  and hysteretic damping  $D$  profiles, defined for each soil layer for low shear strain values, iii) Soil shear modulus  $G$  and hysteretic damping  $D$ , as random functions of the soil shear strain values for each soil layer, and iv) Equivalent linear values for the effective structural material stiffness and damping for each group of elements depending on the stress levels in different parts of the structure.

**Option NON** is useful for including the concrete cracking in the SSI model in accordance to the new ASCE 04-2015 standard requirements (Section 3) and the USNRC SRP requirements for site-specific applications.

The nonlinear structural SSI analysis for low-rise shearwall structures using **Option NON** is a breakthrough capability. The nonlinear SSI analysis is performed using an innovative, accurate and efficient iterative hybrid approach. The runtime of the nonlinear SSI analysis is only about 2-3 times the runtime of the linear SSI analysis (thousands of times faster than a nonlinear time-domain SSI analysis using LS-DYNA with PML absorbent boundaries). The ductilities and inelastic absorption factors for each shearwall panel are computed based on the nonlinear time domain results after the last iteration. Comparative results between the new hybrid approach and the nonlinear time-integration approach showed very good matching. Please see the structural displacement animation that compares seismic responses for a fixed-base analysis for a 0.60g seismic input that is twice than the 0.30g seismic design input using the ACS SASSI fast hybrid nonlinear approach vs. PERFORM3D direct time-integration nonlinear approach (PERFORM3D is trademark of CSI) [http://www.ghiocel-tech.com/enggTools/ACS\\_SASSI\\_vs\\_Perform3D\\_Nonlinear\\_Response\\_for\\_Rigid\\_Foundation\\_0.6g\\_Acc.avi](http://www.ghiocel-tech.com/enggTools/ACS_SASSI_vs_Perform3D_Nonlinear_Response_for_Rigid_Foundation_0.6g_Acc.avi)

The computed SSI structural displacement responses with respect to the free-field input motion using ACS SASSI nonlinear approach for a linear, uncracked concrete structure and a cracked, nonlinear concrete structure founded on the same soft soil deposit for the large 0.60g seismic input (twice than design input) are compared at [http://www.ghiocel-tech.com/enggTools/ACS\\_SASSI\\_Linear\\_Elastic\\_vs\\_Equivalent\\_Linear\\_Response\\_For\\_Soil\\_Foundation\\_0.6g\\_Acc.avi](http://www.ghiocel-tech.com/enggTools/ACS_SASSI_Linear_Elastic_vs_Equivalent_Linear_Response_For_Soil_Foundation_0.6g_Acc.avi). The structural animation indicates clearly that the assumption that "the foundation motion is not influenced by the structural nonlinear behaviour", as some influential researchers wrote in their recent papers, is completely wrong.

**Option NON** can handle also nonlinear

spring and beam hysteretic models, applicable to seismic isolation problems, nonlinear pile SSI problems, and even sliding assessment problems.

**Option RVT** provides an approximate SSI analysis solution using a simplified random vibration theory for estimating the in-structure response spectra.

It should be noted that the combination of **Options PRO and NON** provides a state-of-the-art tool for performing practical, highly efficient and accurate probabilistic nonlinear SSI analyses for critical facilities under tight schedules.

## FEATURE ARTICLES

A number of unique state-of-the-art seismic SSI analysis capabilities will be very soon available to the nuclear engineering community through the new ACS SASSI SSI analysis options coming one after the other in the next couple of months: i) probabilistic and RVT SSI analysis, **Options PRO and RVT**, ii) nonlinear structural analysis for low-rise concrete shearwall buildings (nonlinear shells), **Option NON**, iii) foundation isolation modelling and pile SSI analysis including nonlinear effects (nonlinear springs), **Option NON**, iv) nonlinear soil behaviour for 1D and 2D soil layering models, the **SOILNON** module, and v) 3D SSI analysis using more realistic 2D modelling of soil layering impedances, soil motions and excavated soil, rather than the 1D modelling of soil impedances and motions, **Option 2DSOIL**.

While developing, testing, validating and practicing these new SSI capabilities, we learned many useful practical things related to seismic SSI analysis, in particular to the effects of motion incoherency coupled with SSSI, some pitfalls in the current deterministic SSI approach, limitations of the RVT approaches for SSI, that we would like to share with you in this 1st issue of our 2015 technical newsletter. ■

# SASSI FLEXIBLE VOLUME SUBSTRUCTURING METHODS FOR DEEPLY EMBEDDED STRUCTURES; HOW TO SELECT EXCAVATED SOIL INTERACTION NODES AND ELEMENT MESH SIZE

## ABSTRACT

The paper presents key aspects of the application of the SASSI Flexible Volume (FV) substructuring to deeply embedded structures, such as small modular reactors (SMR). Different substructuring methods which use different idealizations of the excavated soil dynamic behavior are compared. The investigated SSI models include i) full SMR models, ii) quarter SMR models, iii) SMR massless foundation models and iv) SMR excavation cavity models. Sensitivity studies address the excavation mesh size and mesh nonuniformity. Both uniform and highly non-uniform soil profiles are considered. Comparative SSI results are obtained in terms of the acceleration transfer function (ATF) amplitudes. Based on the presented results, application guidelines of the SASSI substructuring for deeply embedded structures are provided.

## SASSI FLEXIBLE VOLUME METHODS

In the SASSI Flexible Volume (FV) substructuring only the free-field soil impedances and the free-field motions are needed for defining the seismic load vector. Both free-field soil motions and impedance functions for embedment soil layers are computed fast using accurate frequency-dependent consistent boundaries for the reflected wave propagation in the infinite soil 3D space. An unique feature of the FV substructuring approach, is that the SSI analysis is performed for the structure dynamically coupled with the excavated soil (the soil removed by the embedment). It should be understood that in the context of the FV substructuring, the wave scattering effects are included by the excavated soil motion. The excavated soil acts as a cavity within the soil deposit. If the excavated soil motion is predicted inaccurately, then this could directly affect the wave scattering effects, and further the SSI responses. The SASSI substructuring is based on splitting the overall SSI system in three subsystems (Gutierrez, 2011, Ghiocel et al., 2013). Based on the FV substructuring, different methods were implemented within the SASSI methodology. These methods differ on how accurate they handle the excavated soil dynamic modelling. The "reference" FV

method assumes that all translational degrees of freedom of the excavated soil are considered to be SSI interaction nodes. Basically, the FV method uses the full excavation volume model dofs. This modelling assumption corresponds to the "theoretical exact" SSI modelling for the excavated soil dynamics. The Subtraction Method (SM) and the more robust Modified Subtraction Methods (MSM) are "short cuts" of the FV substructuring. The basic idea of SM and MSM is to reduce the number of the excavated soil SSI interaction nodes for which the soil impedances must be calculated to save significant computational time and memory storage. Basically, SM and MSM use reduced-size dynamic models for the excavation volume. This makes SM and MSM much faster, but also more approximate than the reference FV method. For the excavated soil non-interaction nodes, the seismic load components and the free-field soil impedances are neglected. Thus, the non-interaction node equations do not include the free-field soil impedance and excitation force terms. This could affect severely the accuracy of SSI results in certain situation.

The FV substructuring methods, such as FV, SM and MSM are different by how the excavated soil is modelled. Therefore, these

methods differ in the level of approximation introduced for capturing the excavated soil behaviour under the free-field soil excitation. The difference in the excavated soil modelling introduced by the different selections of the SSI interaction nodes impacts directly on the kinematic SSI (or wave scattering) solution accuracy. The SM assumes that the interaction nodes are defined only by the nodes at the interface of the excavated soil with the surrounding soil deposit. This implies that SM uses correct equations of motion only for part of the excavated soil nodes that are the interaction nodes at the interface of the excavation model with the surrounding soil deposit. For the rest of the excavated soil equations that correspond to the non-interaction nodes, the free-field soil seismic load and impedance terms are neglected. As a result of the approximate SSI modelling for a number of equations of motion in the excavated soil at the non-interaction nodes, the excavated soil motion includes a number of spurious vibration modes. These spurious modes can be excited by the short wavelength components in the mid and high frequency ranges. For softer excavated soils there is a larger number of spurious modes in the mid-high frequency range of engineering interest than for stiffer soils. Thus, the SM solution

depreciates faster for the softer excavated soils and higher frequency seismic excitations. For low frequency inputs, since the wave scattering effects are reduced, the effects of the approximate modelling and prediction of the excavation soil dynamics is much less important, and, therefore, SM is reasonably accurate for such situations.

MSM, in addition to the interaction nodes defined by SM at the FE model-far-field soil interface, includes as interaction nodes also the excavation nodes at the ground surface. Including the surface nodes as interaction nodes greatly improves the excavated soil response accuracy since the scattered surface wave motions are captured much more accurately. It was shown that MSM provides a great increase in the accuracy in comparison with SM. MSM appears an accurate and robust method for typical nuclear islands for the frequency ranges of interest in practical applications (Gutierrez, 2011, Ghiocel et al, 2013). However, for deeply embedded structures such as SMRs, the MSM accuracy breaks down (Ghiocel, 2013, 2014). For deeply embedded structures, additional excavation internal nodes need to be defined as interaction nodes at different depths within the excavation. These internal interaction nodes are able to capture the existence of significant scattered body waves and soil layer interface waves within deep excavation "pools". For getting an appropriate modelling, the additional excavation internal nodes defined as interaction nodes should be defined on continuous horizontal surfaces within the excavation. The number of required layers of internal interaction nodes within excavation depends on the soil column properties. This defines the "Fast Flexible Volume" (FFV) method. The FFV method defines as interaction nodes all the excavation outer surface nodes plus additional horizontal layers of the excavation internal nodes. Thus, the FFV excavation model represents a more refined reduced-order model including internal nodes than the MSM excavation model. The spacing between the internal interaction node layers

is an important parameter for the FFV method.

The wave scattering effects could be also affected by the excavation mesh size and mesh nonuniformity. Next section includes few case studies that address the excavation volume mesh issues for deeply embedded structures.

## CASE STUDIES

In this section different SSI modelling aspects which are specific to deeply embedded structures such as SMRs are investigated through a number of case studies. These SSI modelling aspects of interest include: i) accuracy of different FV substructuring methods, ii) SSI solution sensitivity to excavated soil mesh size and mesh nonuniformity, iii) use of excavation cavity models and massless foundation models to assess wave scattering effects, and iv) use of quarter SSI models instead of full SSI models to validate the SSI solution accuracy. All SSI analyses were performed using the ACS SASSI software (2015).

## Substructuring Methods

Figure 1 shows the SMR massless foundation model that was used for investigating the accuracy of the different FV substructuring methods. The generic SMR foundation model is a shell FE model with an overall size 120ft x 100ft x 100ft (H x L x W). The basement shell and the soil excavation mesh size is 4ft x 8ft x 8ft (4ft vertical and 8ft horizontal). The basement includes 30 embedment soil layers, down to a foundation depth of 120 ft. Figure 2 (right) shows the two geological layer soil profile that was considered. The top soft soil layer with a  $V_s = 1,000$  fps goes down to a depth of 48ft. Below the 48ft depth, the hard soil layer with a  $V_s = 5,000$  fps (outcrop) extends down to an unlimited depth. The seismic input control motion was defined at the top of the hard soil layer considered to be the outcrop. For this study five scenarios of modelling the excavated soil

were considered, as shown in Figure 2 (left). These five modellings were defined using four types of SSI substructuring methods with different selection of interaction nodes (plotted with red lines): i) Flexible Volume (FV) method, as the reference method, ii) Fast Flexible Volume (FFV) method with two different sets of excavation internal interaction nodes, iii) Modified Subtraction Method (MSM) and iv) Extended Subtraction Method (ESM). The FFV method was considered with two modelling options as illustrated in Figure 2 (left): i) FFV-Skip2, for which the excavation internal interaction nodes were selected by repeatedly skipping two consecutive node layers, and ii) FFV-Skip5, for which the excavation internal interaction nodes were selected by repeatedly skipping five consecutive node layers. MSM includes all the excavation volume outer surface nodes as interaction nodes, while ESM (extended subtraction method) includes an additional layer of interaction nodes at the 48ft depth that is at the level of the abrupt change in the embedment soil stiffness. SM was excluded from the illustrated results, since for this deeply embedded SSI problem performs very poorly. Figure 2 (left) at the bottom includes for each of the five SSI modelling scenarios, information on the number of interaction nodes and the SSI analysis runtime in seconds and percentage of the FV method runtime. It should be noted that FFV is 5-10 times faster than FV, while MSM is about 17 times faster than FV. Figure 3 illustrates the accuracy performance of the five SSI modelling scenarios. Selected results show the acceleration transfer function (ATF) amplitudes in horizontal and vertical directions on the SMR foundation at the -32ft depth that is  $\frac{1}{4}$  of the total embedment depth. It should be noted that except FFV-Skip2, all the other excavation "reduced-order models" provide results that deviate from the "reference" FV method. ESM performs the worst, even poorer than MSM. For the SMR problem at hand, only the FFV-Skip2 results match very closely the FV results for the entire frequency range. The

conclusion is valid for any node locations within the SMR foundation. Based on the obtained results, we recommend the use of the FFV-Skip2 for typical SMR problems. The SSI analysis runtime savings are about 80% for FFV-Skip2 in comparison with FV as described in Figure 3.

### Excavation Horizontal Mesh Size

A number of publications on the SASSI methodology recommend unconditionally the use of the same excavated soil mesh size in horizontal and vertical directions. This is an overly restrictive condition that could produce a large penalty on the SSI analysis computational effort. This excavation element size restriction is not justified to be imposed for all practical situations. In many situations, even the excavation horizontal mesh size is 1.5-2.0 times larger than the vertical mesh size, or even larger, the computed SSI responses are still reasonably accurate. Herein, a comparison of SSI results for two different horizontal embedment mesh sizes is presented. The two SMR embedment horizontal meshes are i) 8ft mesh size including 7,938 interaction nodes, shown in Figure 1, and ii) 4ft mesh size including 29,371 interaction nodes, as shown in Figure 4 (left). The soil profile was assumed to be uniform with a  $V_s = 1,000$  fps. Seismic input motion was defined at the ground surface. The comparative computed ATF results in Figure 4 (right) show that the use of a horizontal mesh size of 4ft instead of 8ft, although increases by about 10 times the SSI analysis runtime and by about 4 times the number of interaction nodes and the memory storage, has a negligible impact on the SSI response accuracy. We recommend to SSI analysts to always perform preliminary sensitivity analysis with different excavation horizontal mesh sizes rather than use directly a small mesh size that is equal to the vertical mesh size. The saving for the SSI analysis runtime could be tremendous.

### Excavation Mesh Nonuniformity

Figure 5 (left) shows the SMR SSI model considered for the study. The SMR structure has a size of 200ft x 100ft x 100ft (H x L x W) and an embedment of 140ft depth. The soil profile shown in Figure 5 (right) was assumed to be highly non-uniform with a soil stiffness inversion within the SMR embedment depth. Three embedment mesh scenarios were assumed as illustrated in Figure 6: i) Uniform mesh size, ii) Non-uniform mesh size, and iii) Refined non-uniform mesh size. Figures 7 and 8 show the ATF amplitudes computed for the three mesh scenarios in the horizontal and vertical directions within the SMR model at the foundation level and the ground surface level. The computed SSI responses indicate a close agreement between the three excavation mesh models. Based on the obtained results, the effects of the excavation horizontal mesh nonuniformity on the SSI responses appears less significant.

### Excavation Cavity vs. Foundation Models

The SMR massless foundation model and the two layer soil profile shown in Figures 1 and 2 are used. Both the FV and the FFV-Skip2 methods are applied. The SSI analysis is performed for the SMR massless foundation model (FM) and for its excavation cavity model (ECM) that includes only the excavation volume elements and no structure or foundation elements. The ECM model includes only the excavated soil cavity. Figure 9 shows the SMR foundation model results in terms of the ATF computed in the horizontal and vertical directions at the SMR foundation level for the input motion defined at the outcrop level (top of soil layer 13) and the foundation level (top of soil layer 31), respectively. Figure 10 shows the ECM model results in terms of the ATF computed in horizontal and vertical directions at the SMR foundation level for the input motion defined at the outcrop level (top of soil layer 13). It should be noted that the ATF results in Figure 9 obtained for the SMR FM model indicate that the FV and FFV-Skip2 methods provide

basically identical results for both seismic input level scenarios at the outcrop and foundation levels. However, it should be noted that the ATF results in Figure 10 obtained for the SMR ECM model show a much poorer matching between the two methods, also indicating that both FV and FFV-Skip2 are numerically less stable. The ATF curves for ECM are less smooth. The ATF results in Figures 9 and 10 indicate that the FV and FFV-Skip2 provide identical results for FM that has a good numerical condition, but they provide slightly different results for ECM, with both methods becoming slightly unstable and losing accuracy. The investigation results shown in Figures 9 and 10 indicate that for comparing FFV and FV methods, a SMR massless foundation should be used instead of ECM. If ECM is used, then, the conclusions based on result comparisons could be affected by the poor numerical condition of the excavation model in soft soils. We recommend the use of realistic SMR foundation massless models for such validation studies rather than ECM that could be numerically overly sensitive.

### Quarter SSI Models vs. Full SSI Models

As known, Quarter SSI models provide identical results with Full SSI models for the double symmetric SSI models. However, is not fully true. When the embedded SSI model is numerically sensitive, Quarter SSI models may provide results which are slightly different than Full SSI models. It appears that the symmetric and antisymmetric kinematic boundary conditions imposed to the Quarter SSI models help the numerical stability of sensitive FE models, and, therefore, for such sensitive FE models they behave more stable than the Full SSI models. Figure 11 shows for a fully embedded structure the Full SSI model (left) and the Quarter SSI model (right). Figure 12a shows a comparison for the ATF computed at the top corner of the embedded foundation for the Quarter and Full SSI models using the "reference" FV method. As expected, the ATF results overlap. In contrast,

Figure 12b shows a comparison for the ATF computed at the top corner of the embedded SMR foundation for the Quarter and Full SSI models using the MSM method (with the interaction nodes defined on the outer surface of the excavation volume). The ATF results are different for Quarter and Full SSI models. As shown in Figure 12b, the Quarter SSI model with MSM is more stable than the Full SSI model with MSM. These ATF results raised the question on how reliable are the MSM Quarter SSI model results for checking the numerical accuracy of the MSM Full SSI models. *Based on these results, the use of Quarter SSI models to validate the Full SSI model accuracy might be not always appropriate for MSM, since as shown herein, the MSM Full model could be significantly more unstable than the MSM Quarter model. Thus, the conclusions drawn from the*

*Quarter SSI models related to the applied SSI substructuring method accuracy could be different than the conclusions drawn directly from the Full SSI models.*

**REFERENCES**

*Ghiocel, D.M. (2011). "Flexible Volume, Subtraction and Modified Subtraction Methods: A Series of Case Studies", presented to the Defense Nuclear Facility Safety Board (DNFSB), Washington D.C, March, 30*

*Ghiocel, D.M., Yue, D., Fuyama, H., Kitani, T. and McKenna, M.(2013). "Validation of Modified Subtraction Method for Seismic SSI Analysis of Large-Size Embedded Nuclear Islands", SMiRT22 Division V, San Francisco, California, August 18-23*

*Ghiocel D, M. (2014). SASSI Methodology-Based Sensitivity Studies for Deeply Embedded Structures Such As Small Modular Reactors (SMRs)", U.S. Department of Energy Natural Phenomena Hazards Meeting, SSI Session SSI, Germantown, MD, USA, October 21-22*

<http://www.energy.gov/sites/prod/files/2015/05/f22/DOE-NH-SMR-SSI-Methods-Oct-21-2014.pdf>.

*Ghiocel Predictive Technologies, Inc. (2015). "ACS SASSI - An Advanced Computational Software for 3D Dynamic Analyses Including SSI Effects", ACS SASSI Version 3.0 Manuals, March 31, [http://www.ghiocel-tech.com/engTools/ACS%20SASSI\\_V300\\_Brief\\_Description\\_Dec\\_31\\_2014.pdf](http://www.ghiocel-tech.com/engTools/ACS%20SASSI_V300_Brief_Description_Dec_31_2014.pdf)*

*Gutierrez, B. (2011). "U.S. Department of*

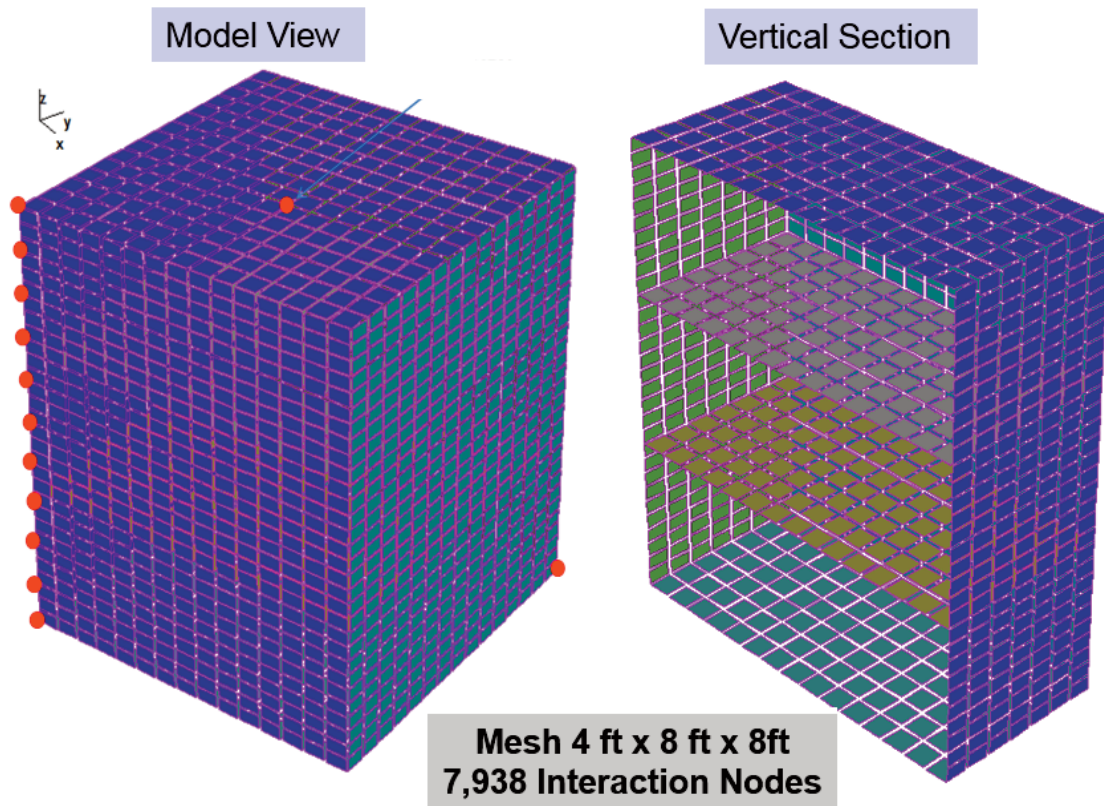


**Figure 1** SMR Massless SSI Model; Outside View (left) and Vertical Section (right)

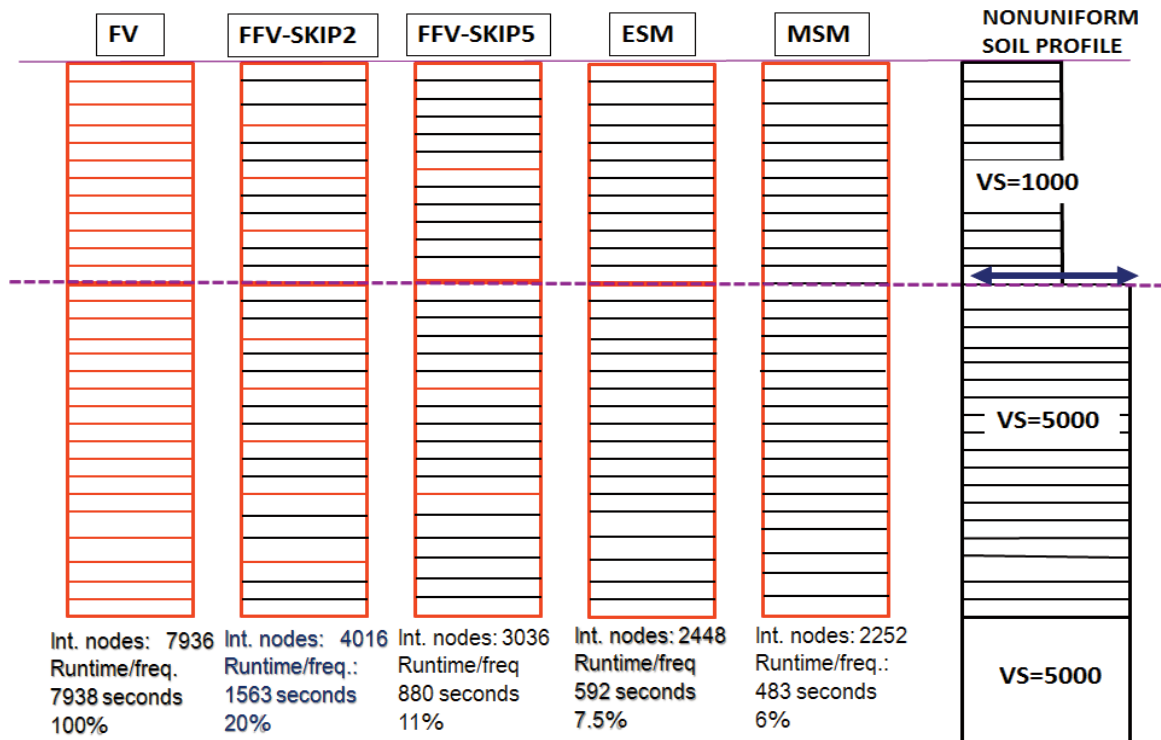


Figure 2 Investigated Cases for Excavated Soil Modelling (left) and Nonuniform Soil Profile (right)

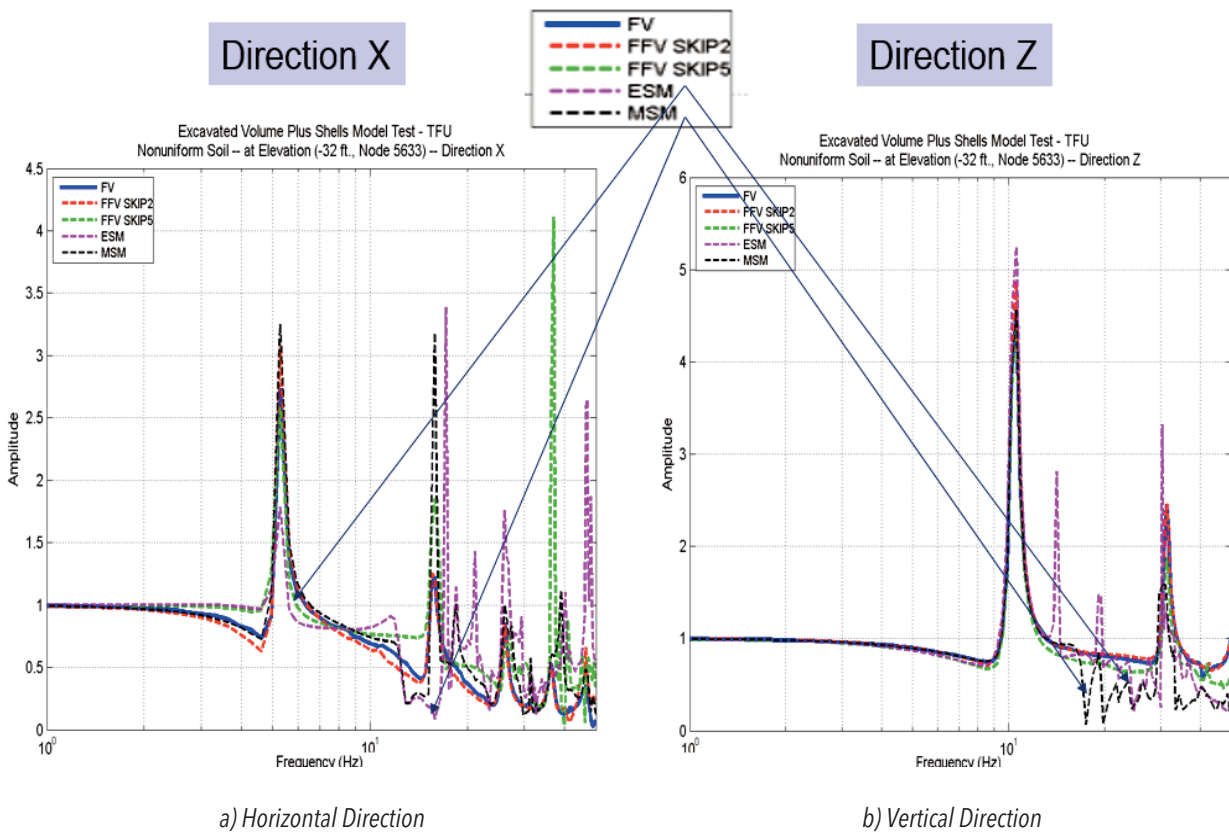
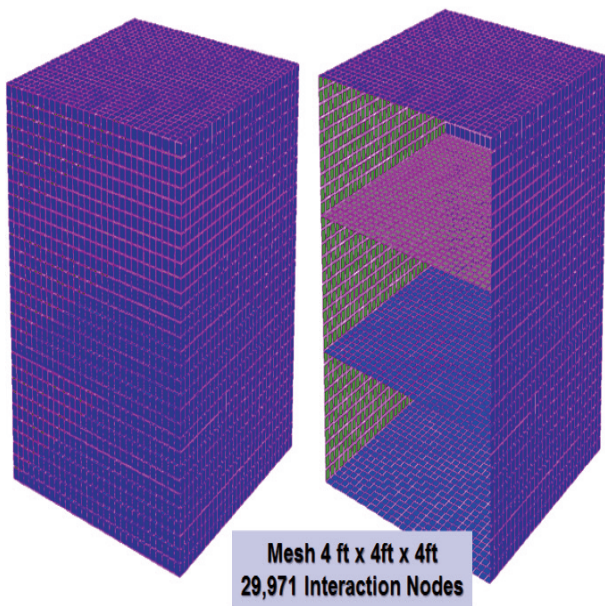
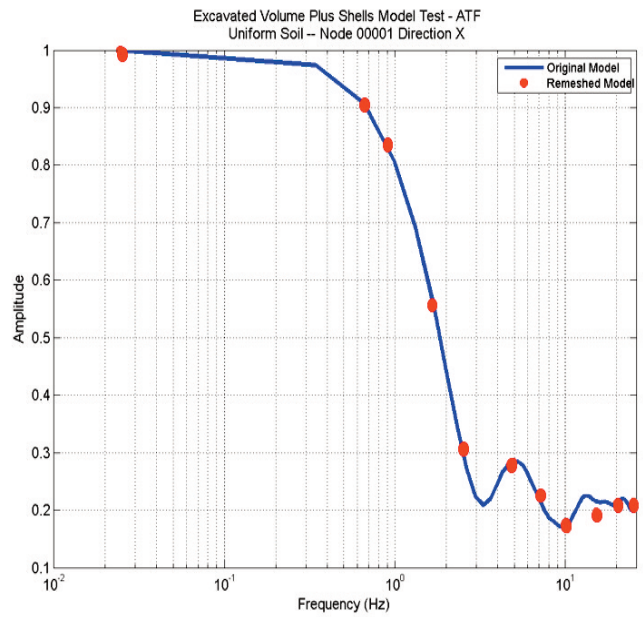


Figure 3 Comparative ATF in SMR at -32 ft Depth Level; Horizontal (left) and Vertical (right)



a) Refined Mesh SMR model



b) Comparative ATF in Horizontal Direction

**Figure 4** Refined Mesh Massless SMR Model (left) and Comparative ATF at SMR Foundation Level for Uniform Soil,  $V_s=1,000$  fps and Ground Surface Seismic Input (right)

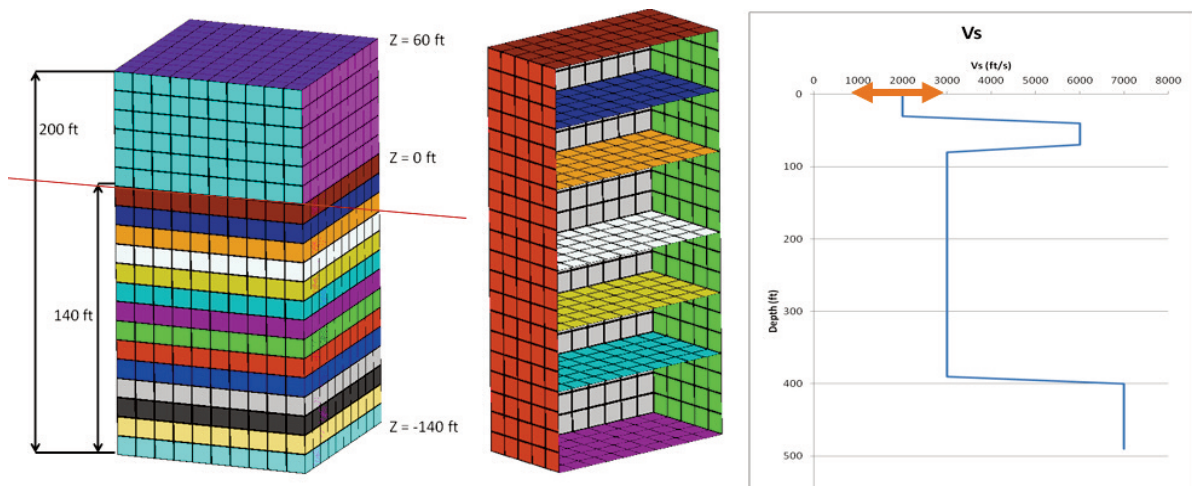


**Figure 5** SMR SSI Model for Excavation Mesh Study (left) with Nonuniform Soil Profile (right)

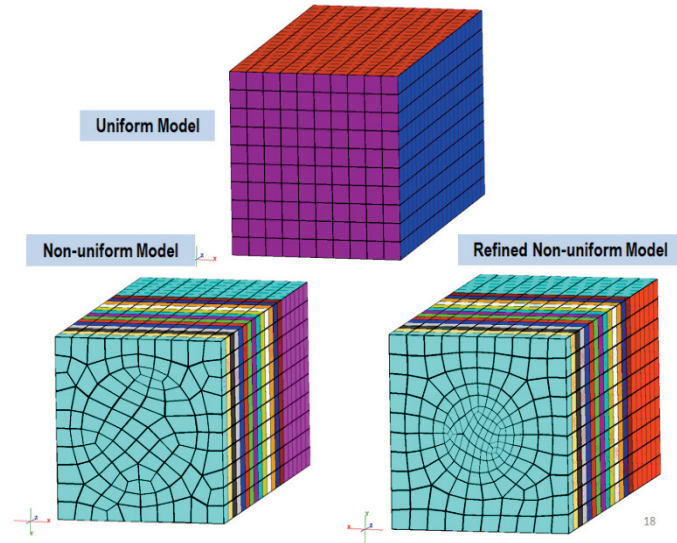


Figure 6 SMR Excavated Soil Mesh Models: i) Uniform, ii) Non-uniform and iii) Refined Non-Uniform

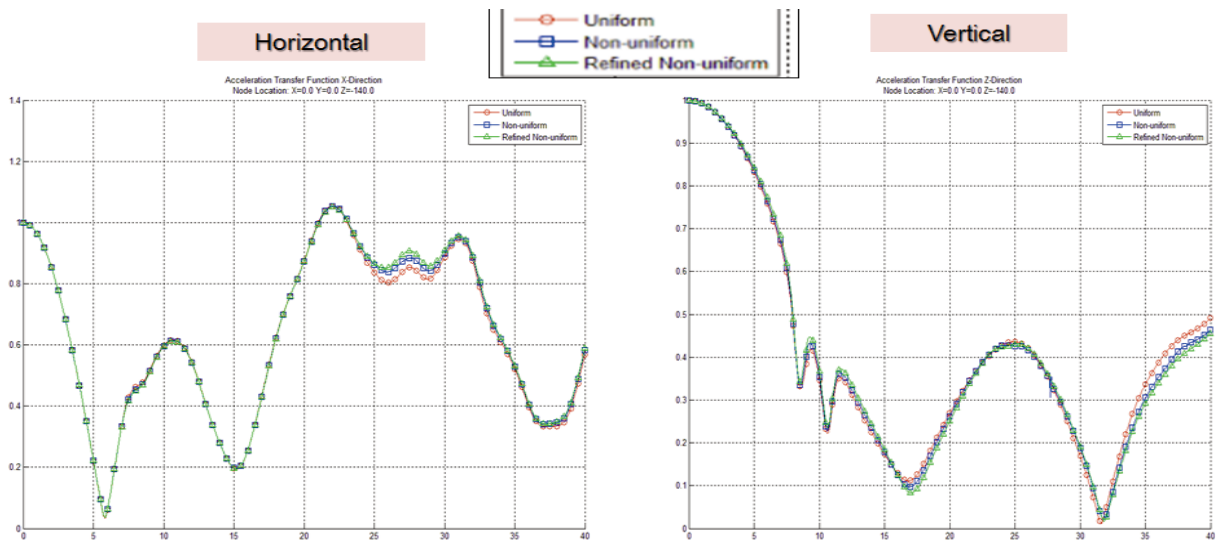


Figure 7 ATF in SMR at Foundation Level for Surface Input; Horizontal (left) and Vertical (right)

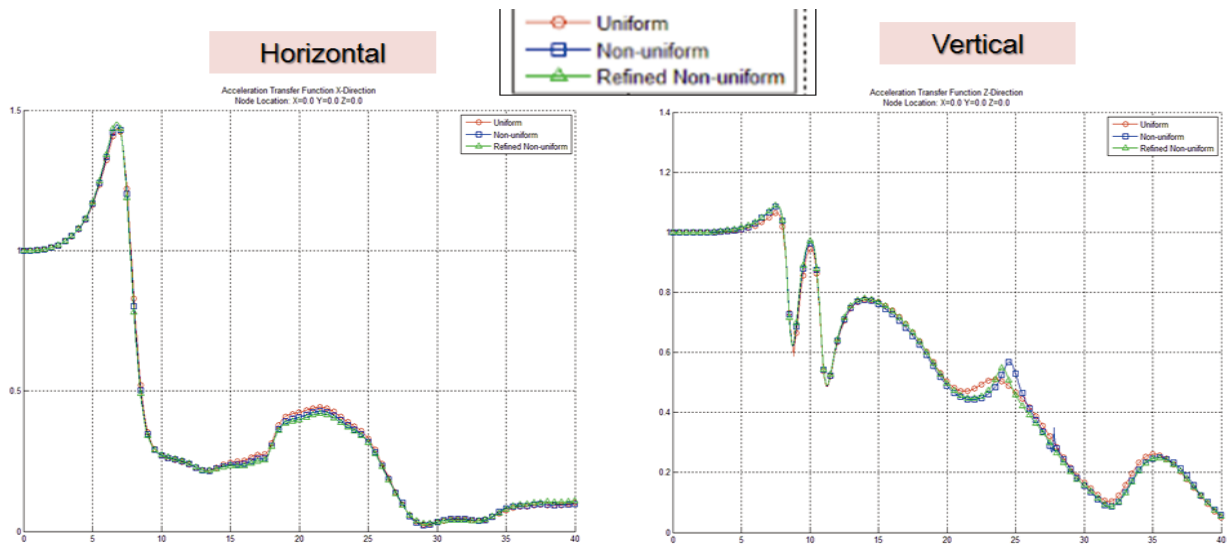
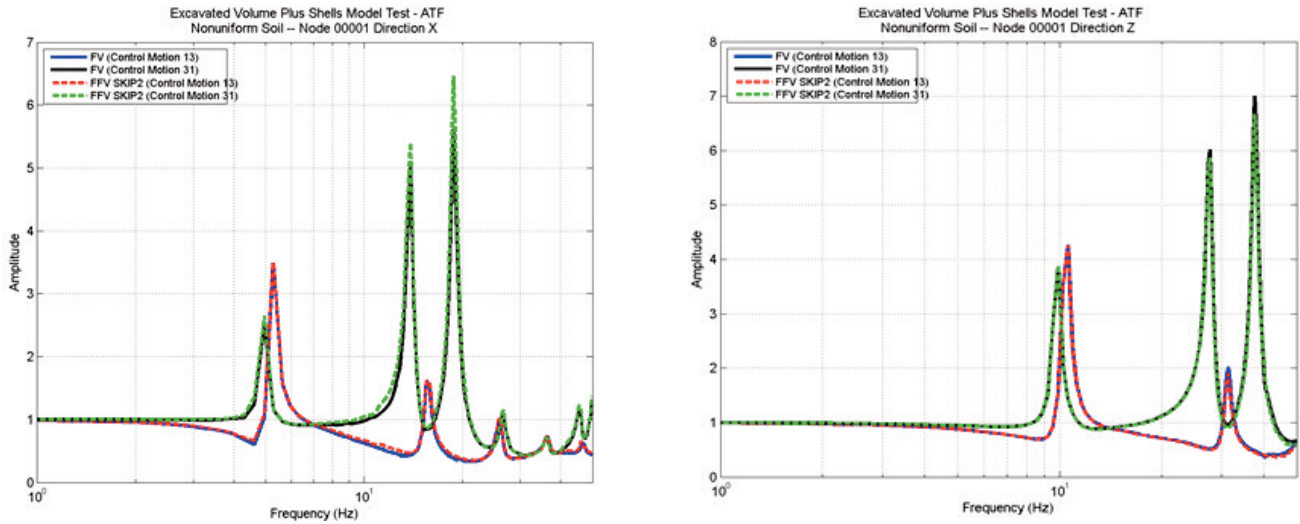
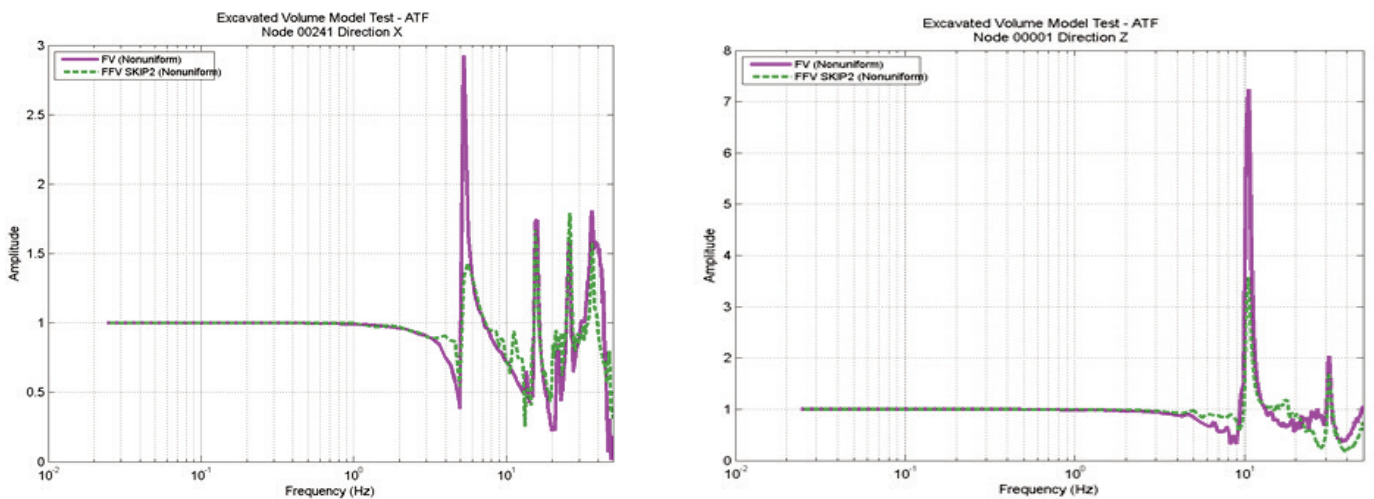


Figure 8 ATF in SMR at Surface Level for Surface Input; Horizontal (left) and Vertical (right)



**Figure 9** ATF for the SMR Foundation Model (FM) Computed at Foundation Level for Nonuniform Soil with Outcrop and Foundation Inputs (Top of Layer 13 and Top of Layer 31)



**Figure 10** ATF for the SMR Excavation Cavity Model (ECM) at Foundation Level for Nonuniform Soil with Outcrop Input (Top of Layer 13)

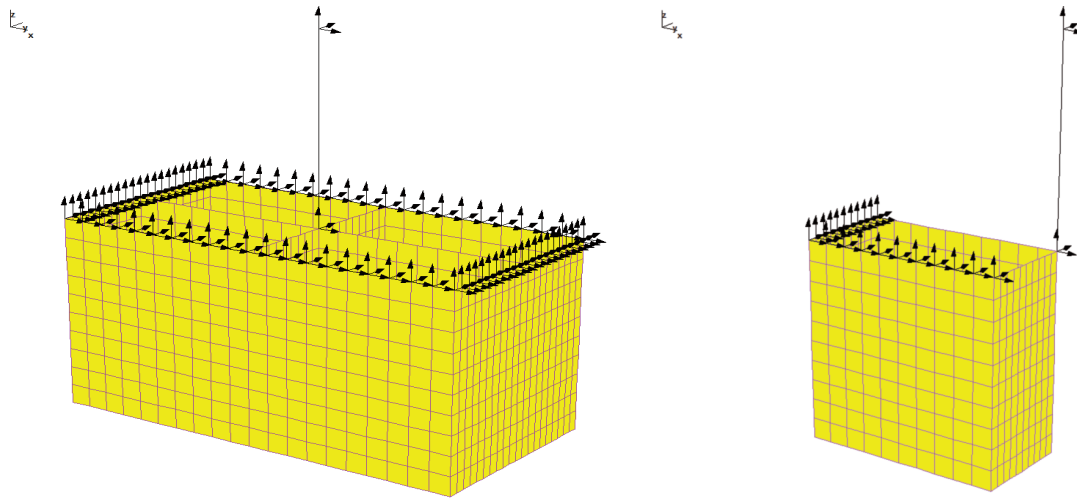
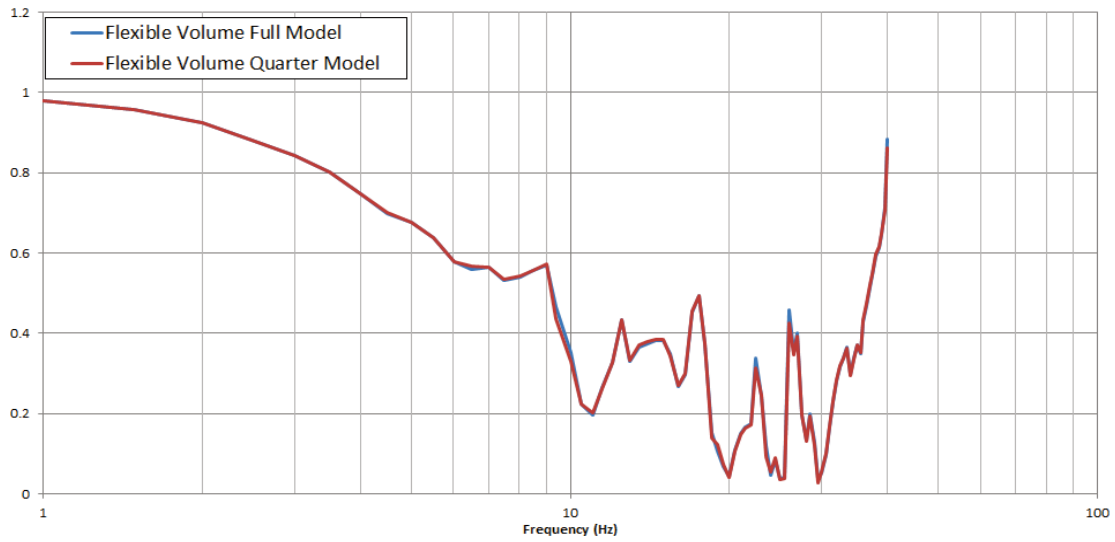
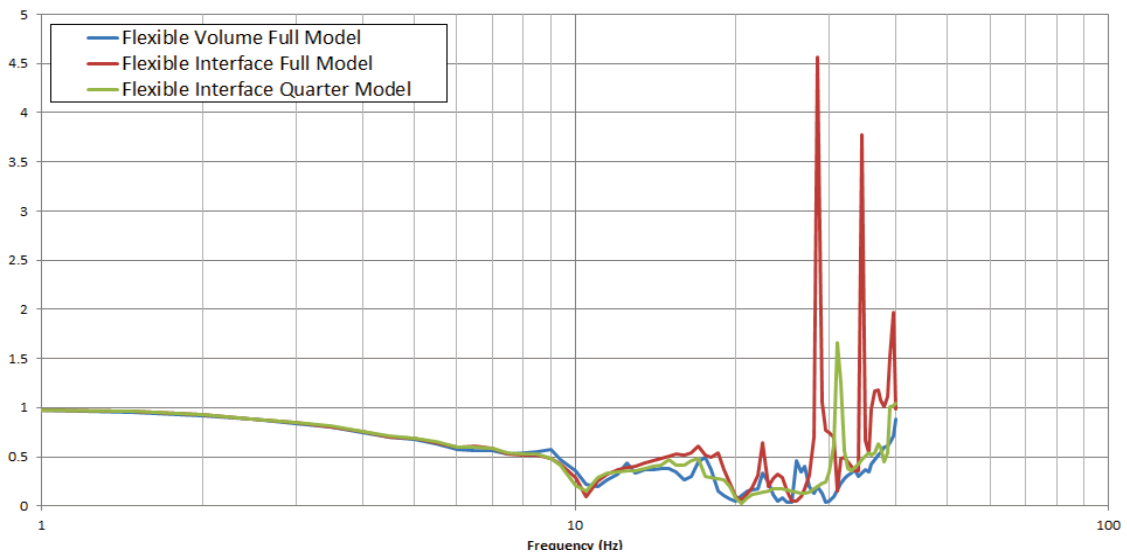


Figure 11 Fully Embedded SSI Model: Full SSI Model (left) and Quarter SSI Model (right)



a) Comparative ATF on SMR Top Corner for Quarter Model and Full Model Using FV



b) Comparative ATF on SMR Top Corner for Quarter Model and Full Model Using MSM (or FI)

Figure 12 ATF at the SMR Shell Top Corner Computed Using the FV and MSM Methods

## COMPARATIVE PROBABILISTIC-DETERMINISTIC SSI STUDIES FOR SURFACE AND EMBEDDED NUCLEAR STRUCTURES ON SOIL AND ROCK SITES

### ABSTRACT

Probabilistic soil-structure interaction (SSI) analysis is capable of capturing in much more detail than deterministic SSI analysis the input uncertainties related to seismic motion, soil layering and structural behaviour. The paper discusses the application of probabilistic SSI analysis to nuclear structures based on the new ASCE 04-15 standard recommendations. Probabilistic and deterministic SSI analyses were comparatively performed for two SSI case studies: i) surface EPRI AP1000 NI stick model and ii) deeply embedded SMR finite-element model. Both soft soil and rock sites were considered. The probabilistic SSI analyses assumed that the spectral shape of the site-specific ground response spectra, the soil stiffness and damping profiles were idealized as random fields. The structural stiffness and damping random variations were modelled as a pair of correlated random variables that depend on the computed structural stress levels. The comparative SSI results include in-structure response spectra (ISRS) at different locations. The probabilistic SSI analysis results for the mean ISRS and 80% non-exceedance probability (NEP) ISRS are compared with the deterministic SSI analysis envelope ISRS computed including the soil variation by three profiles, lower bound (LB), best-estimate (BE) and upper bound (UB). The paper highlights significant modelling limitations in the deterministic SSI analysis.

### BACKGROUND

In the introduction of the revised ASCE 04-2015 standard draft it is stated that the purpose of the analytical methods included in the standard is to provide reasonable levels of conservatism to account for uncertainties. More specifically, in the same section is written that given the seismic design response spectra input, the goal of the standard is based on a set of recommendations to develop seismic deterministic SSI responses that correspond approximately to 80% non-exceedance probability level. For probabilistic seismic SSI analyses, probabilistic responses defined with the 80% non-exceedance probability level (NEP) are considered adequate. In this paper we performed comparative probabilistic-deterministic study for two RB complexes with the intention to confirm the ASCE 04 standard safety goal to achieve 80% non-exceedance probability (NEP) level for deterministic SSI responses, and also to evaluate in more detail the differences between the computed ISRS based on the recommended deterministic SSI and probabilistic SSI approaches.

### PROBABILISTIC SSI METHODOLOGY

The ACS SASSI Option PRO capability for probabilistic SSI analysis uses stochastic simulation based on the Latin Hypercube Sampling (LHS) as recommended by ASCE 04-2015 Standard (Section 5.5). Both probabilistic site response analyses (PSRA) and probabilistic SSI analyses (PSSIA) can be performed highly efficient and accurate. The analyst can also combine deterministic site response analysis (DSRA) with PSSIA, and PSRA with deterministic SSI analysis (DSSIA). The probabilistic site response analysis could include as input, a single UHRS input or a set of deaggregated probabilistic UHRS inputs at the bedrock based on the PSHA results.

Probabilistic modelling include random variabilities due to:

- Response spectral shape model for the seismic input
- Low-strain soil shear wave velocity  $V_s$  and hysteretic damping  $D$  profiles for each soil layer

- Soil layer shear modulus  $G$  and hysteretic damping  $D$  as random functions of soil shear strain
- Equivalent linear values or effective stiffness and structural damping for each group of structural elements and materials depending on stress levels in different parts of structure

Figure 1 shows a generic chart of the PSSIA assuming that the probabilistic seismic input for SSI analysis is defined at the ground surface based on the PSRA simulations.

For the SSI response simulations, the input is represented as an ensemble of input motion sets. The ensemble consists of  $N$  ground acceleration time series sets. Each set consists of two horizontal components and one vertical component. The seismic motion spectral amplitude is assumed to be a lognormally distributed random variable or vector/field. Option PRO includes two probabilistic simulation methods for

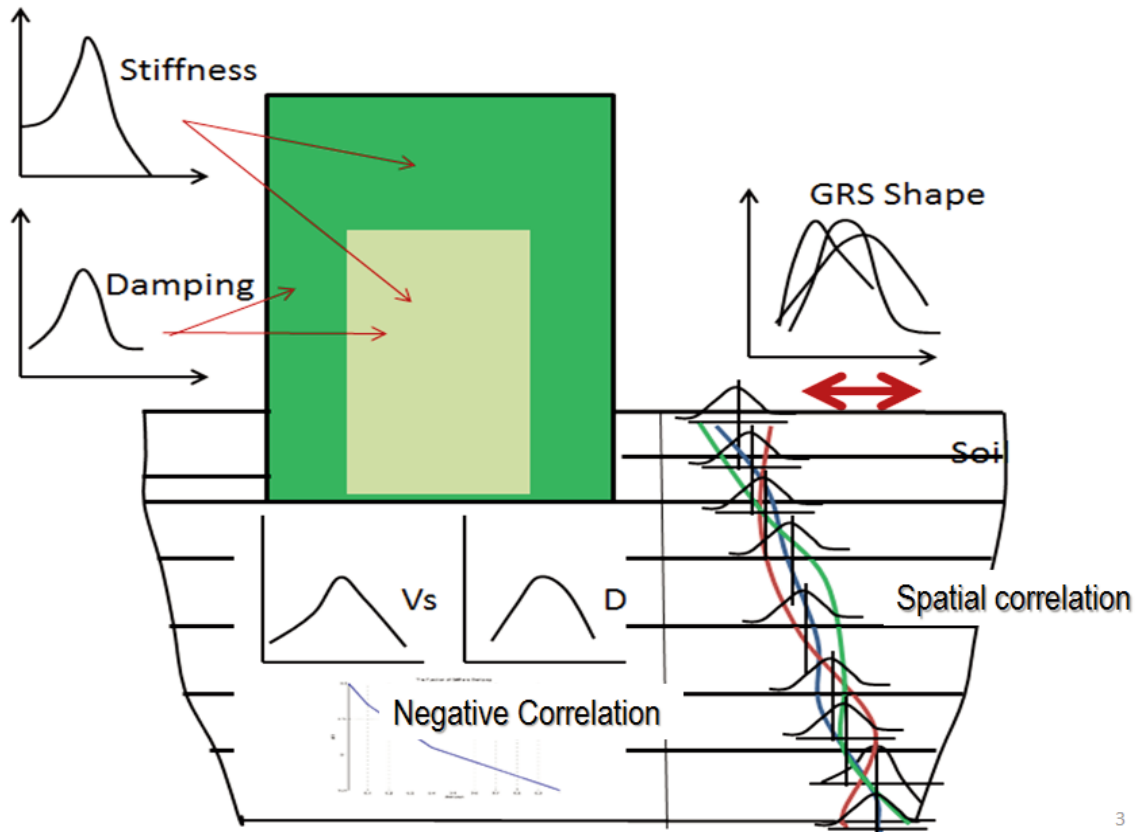


**Figure 1** Probabilistic Input Models for Seismic Motion, Soil Profile and Structure Properties

generating input acceleration time histories that are recommended in ASCE 04-2015 standard (Figure 2): 1) Method 1 that assumes that spectral shape is deterministic, constant shape curve, and 2) Method 2 that assumes that spectral shape is a random, variable shape curve. The low-strain  $V_s$  and  $D$  per soil layer are assumed to be a pair of statistically dependent lognormal random variables. The statistical dependence is due to their joint dependence on the soil shear strain in the layer. In Option PRO, there several options implemented to address the  $V_s$  and  $D$  statistical dependence. Each geological layer including several computational soil layers can be defined having a different, given correlation length. Thus, in general, the soil profiles are made of several segments for which the soil profile spatial correlation with depth is assumed to be constant. The soil profile simulations are based on probability transformed-space KL expansion models (Figure 3). The soil  $V_s$  and  $D$  profiles are assumed to be either i)

normal and lognormal 1D random fields with spatial correlation structures with depth, or ii) a mixture of a short-wavelength normal or lognormal 1D random field with a large-wavelength normal 1D random field. The first modelling option produces ergodic field samples, while the second modelling option produces a non-ergodic field sample since it contains two sources of uncertainties that refer to a slow-amplitude variation and a rapid-amplitude variation as suggested by the Princeton university researchers based on different field measurements (Popescu, 1996). The selection of the soil profile model should be made based on the  $V_s$  field measurements on the site. The soil shear modulus  $G$  and damping  $D$  curves as functions of the soil shear strains in each layers, are modelled as random curves using normal 1D random field models with random samples having slow-variations.

The ACS SASSI Option PRO capability includes a number of seven probabilistic modules. These probabilistic modules are

the ProEQUAKE, ProSOIL, ProSITE, ProHOUSE, ProMOTION, ProSTRESS and ProRESPONSE modules. Out the seven probabilistic profiles, there are six probabilistic modules for simulating the probabilistic SSI inputs and one probabilistic module for computing the probabilistic SSI responses for user-defined different probability levels. Figure 4 shows the generic flowchart that governs the sequence of computational steps for a combined probabilistic site response analysis (PSRA) and probabilistic SSI analysis (PSSIA). Basically, for a full probabilistic analysis, there are three distinct steps to be completed: 1) Generate an ensemble of simulated probabilistic input files using LHS, 2) Run the ensemble of LHS simulated input files to compute the LHS response files, and 3) Post-process statistically the ensemble of the LHS responses. The "N" notation in Figure 4 indicates the number of simulated LHS sample files. It should be noted that PSRA that is plotted with red line and PSSIA with black line.

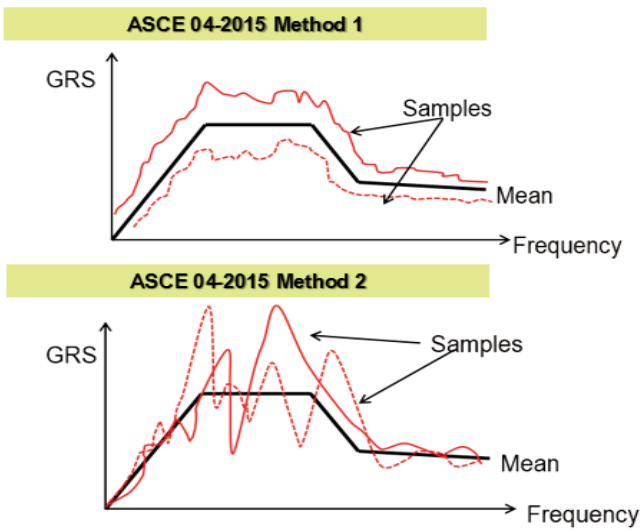


Figure 2 Probabilistic Seismic Input Simulation

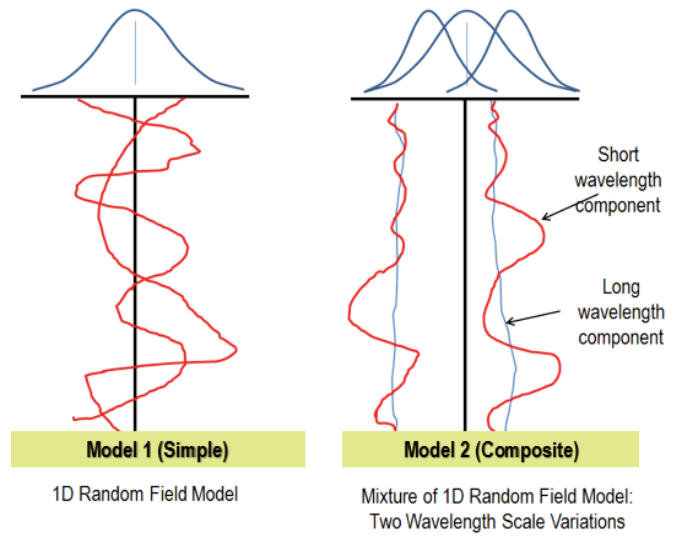


Figure 3 Probabilistic Soil Profile Simulation

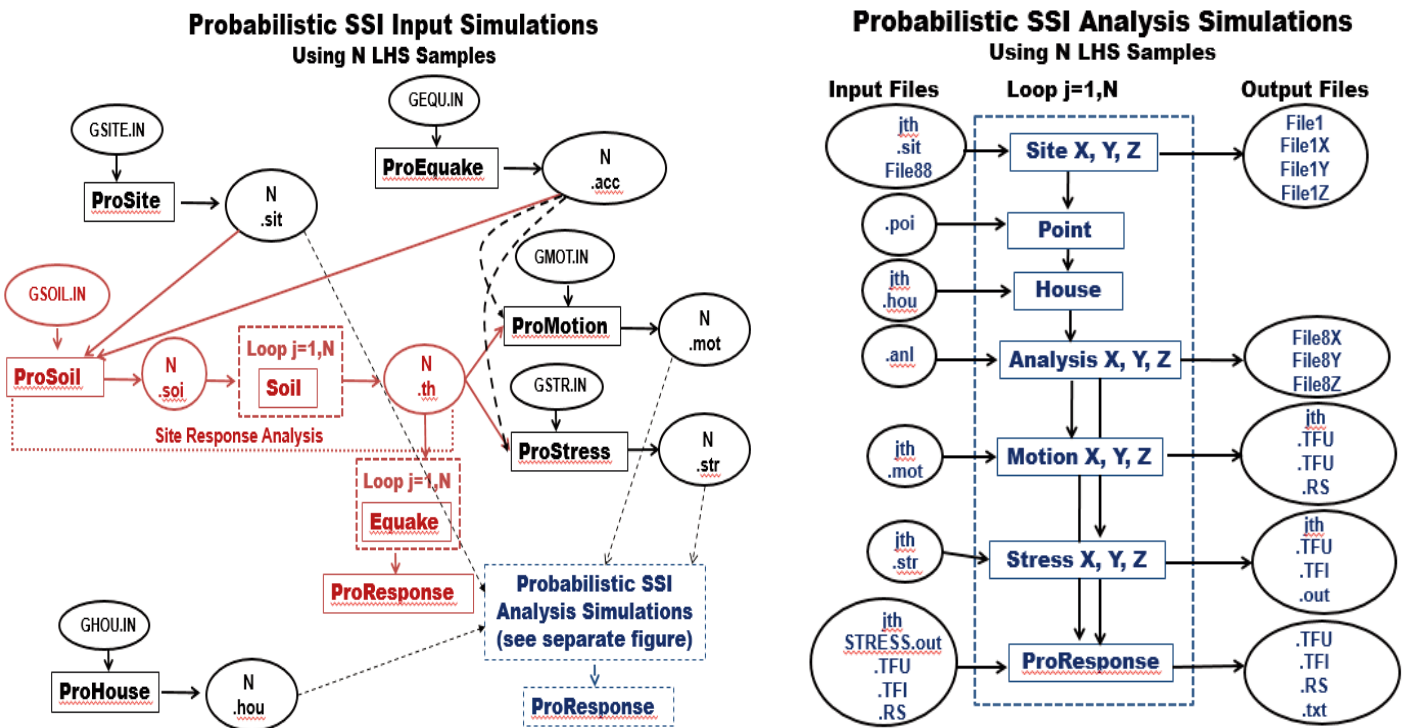
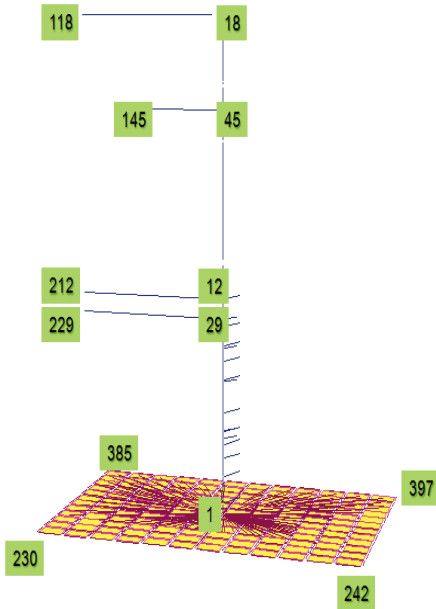


Figure 4 ACS SASSI Option PRO Probabilistic SSI Input Simulation and Analysis Flowchart

**CASE STUDIES**

Two case studies are presented: i) Surface EPRI AP1000 NI stick model with rigid basemat (Figure 5) and ii) Deeply embedded SMR FE model (Figure 6). The SMR embedment depth is 140ft.



**Figure 5** Surface EPRI AP1000 NI Stick

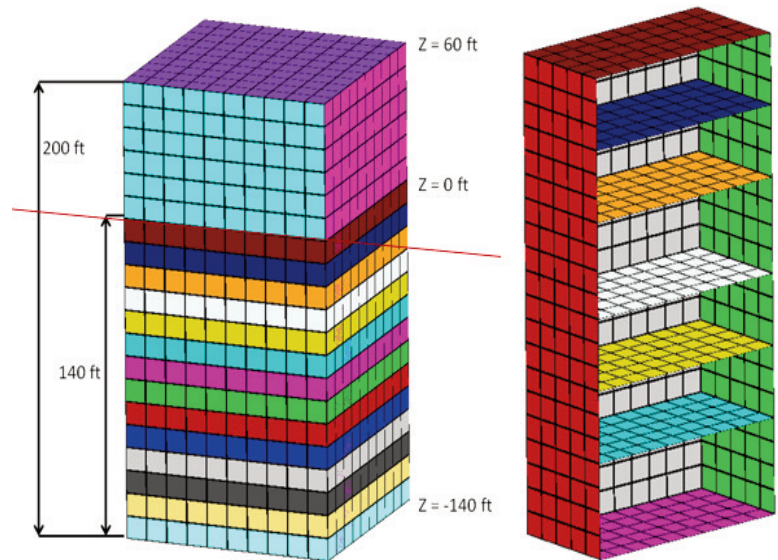


**Figure 6** 140ft Embedded SMR FE Model

**Surface EPRI AP1000 Stick Model**

The EPRI AP1000 stick model foundation size was modified from 150ft x150ft to 150ft x 250ft to reflect more realistically the AP1000 NI foundation area. The probabilistic site-specific seismic input ground response spectra (GRS) were considered to be lognormally distributed random fields along frequency axes. The coefficient of variation was 25% for the soft soil site and 30% for rock site. The correlation structure in frequency that is related to the soil layering filtering effects on incident vertically propagation waves was considered to correspond to a correlation length of 0.7 Hz for the soft soil site and 10 Hz for the rock site. Using the GRS random field model in frequency (Method 2 in ASCE 04-2015), 60 LHS random realizations were simulated for the soil and

rock sites. The statistics of the ensemble of simulations matches closely in statistical sense, as shown in Figure 7 the mean and the mean plus/minus standard deviation GRS curves. For probabilistic modelling of the soil profiles, the soil Vs and the hysteretic damping D were considered as two negatively correlated lognormal random fields as function of depth. The coefficient of variation was 20% for Vs and 30% for damping D. A negative correlation coefficient of -0.60 was assumed between the Vs and hysteretic damping. The spatial correlation length in vertical direction was assumed to be about 20 ft. Figure 8 shows the 60 LHS random realizations for the soil Vs profiles for the soil site (left) and rock site (right). The statistics of the ensemble of simulations matches closely the given input statistics, as

shown in Figure 8 for the mean and the mean plus/minus standard deviation Vs and damping curves. For deterministic SSI analysis the three soil profiles were considered, namely the best-estimate value for the soil shear modulus (BE), lower bound (LB) and as upper bound (UB). The AP1000 stick structural stiffness and damping were defined as two functionally stress-dependent random variables (Ghiocel, 2014). The two inversely dependent random variables were assumed to be lognormal variables with the mean elastic modulus reduction factor of 0.8 and c.o.v. of 0.15 and the mean damping of 7% and c.o.v. of 0.30. For deterministic SSI analysis, the mean GRS input and the uncracked AP1000 stick model (with a full concrete elastic modulus and a damping ratio of 4%) were considered.

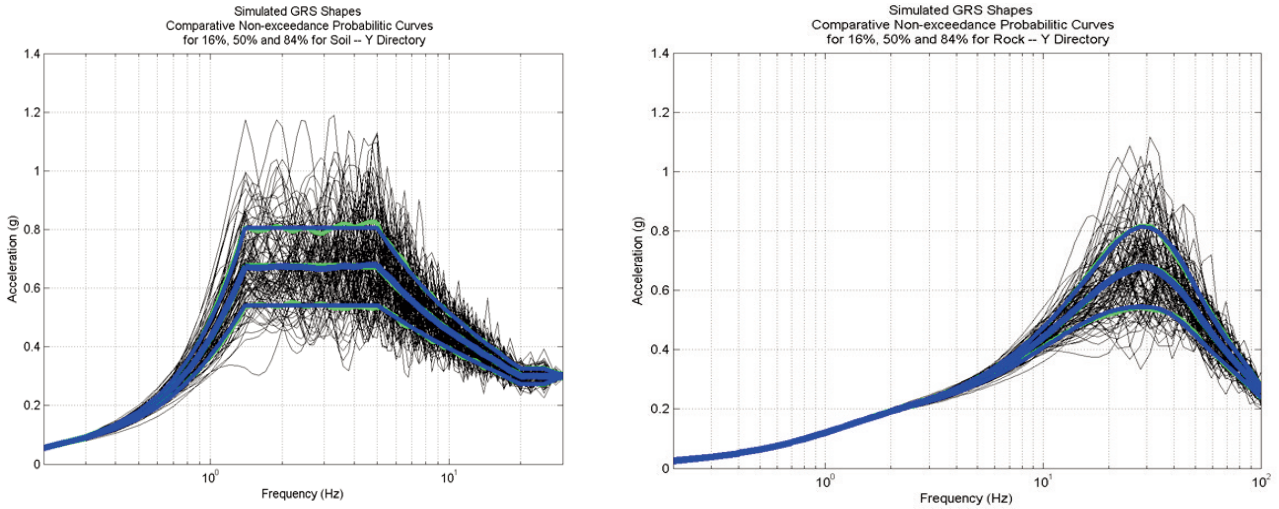


**Figure 7** Probability-Level and Simulated GRS for Soil (left) and Rock (right). Comparisons of Given (green) and Statistically Computed (blue) Mean and Mean +/- Standard Deviation GRS

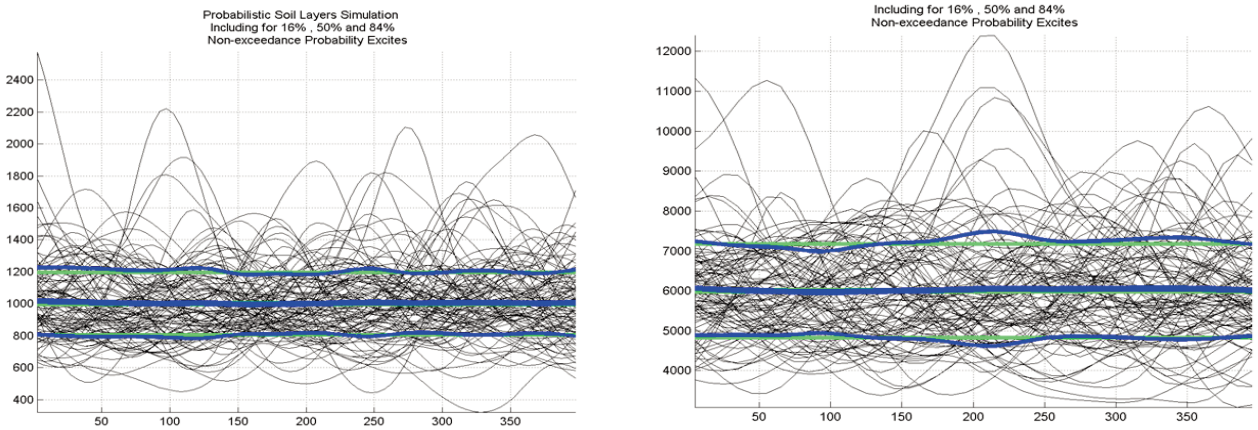


**Figure 8** Probability-Level and Simulated Soil Profiles for Soil (left) and Rock (right). Comparisons of Given (green) and Statistically Computed (blue) Mean and Mean +/- Standard Deviation Soil Profiles

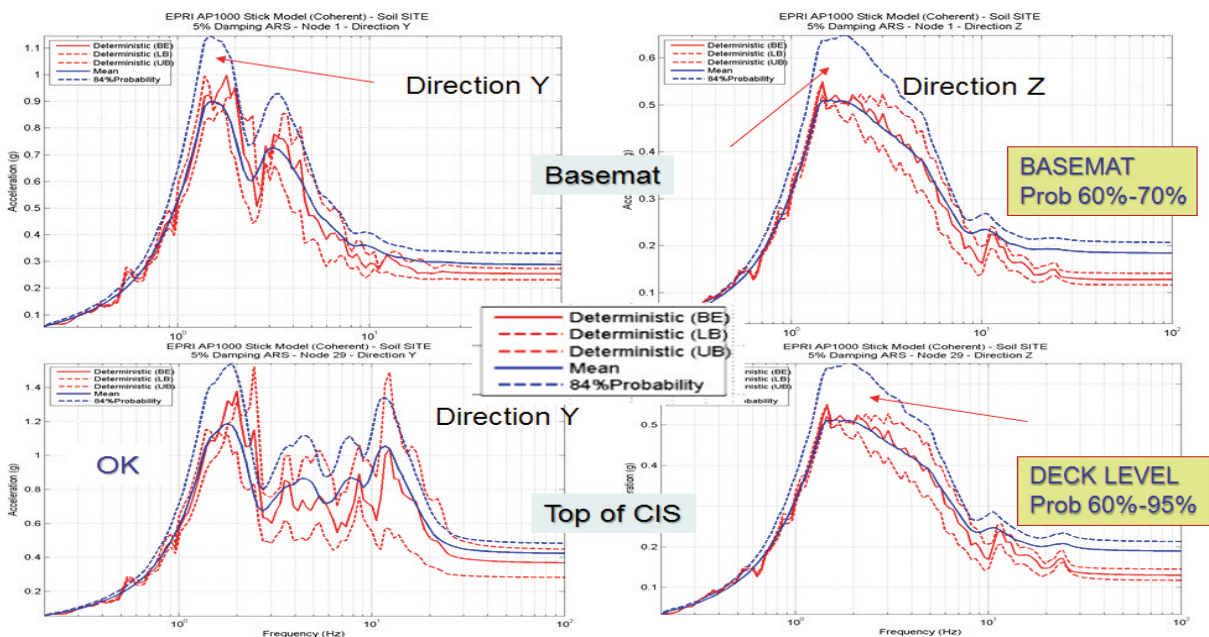


**Figure 9** Deterministic and Probabilistic Mean and 84% NEP ISRS in X and Z Directions for Soil Site

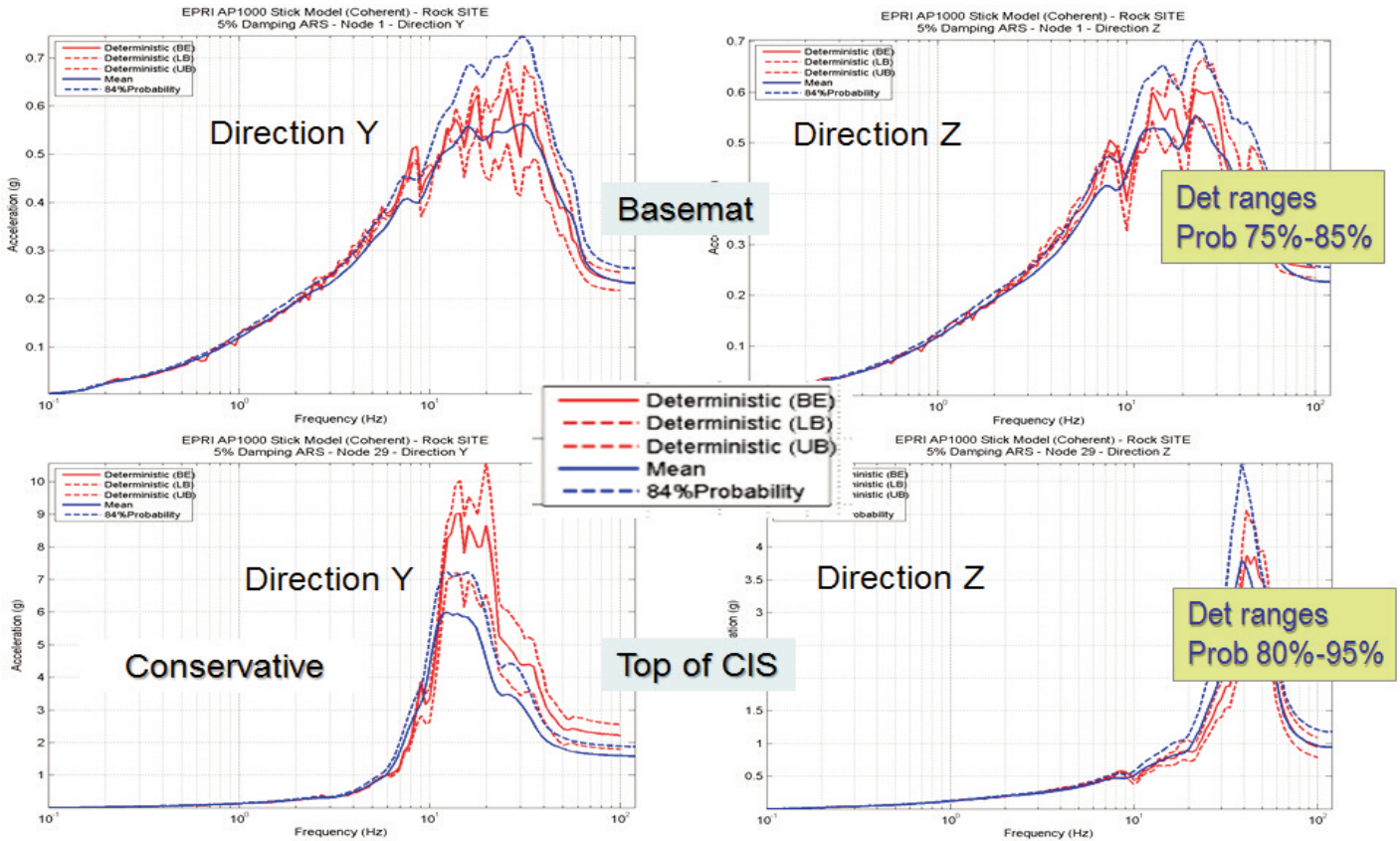


Figure 10 Deterministic and Probabilistic Mean and 84% NEP ISRS in X and Z Directions for Rock Site

Comparative ISRS computed using deterministic and probabilistic SSI analyses for the AP1000 stick sitting on soft soil site and a rock site are shown in Figures 9 and 10. Two locations were selected: i) basemat level, and ii) top of CIS (Containment Internal Structure). The comparisons between the deterministic ISRS and the probabilistic mean and 84% probability-level ISRS indicate that in an overall statistical sense, the ASCE 04 standard performance goal for the 80% non-exceedance probability (NEP) response is accomplished. Typically, the deterministic ISRS, computed as the envelope ISRS for the three deterministic soil profiles, LB, BE and UB soils, is always above mean ISRS, and in the most of the cases between the mean and the 84% NEP ISRS, and in some cases much larger than 84% NEP ISRS. However, there are some specific systematic trends that are discussed hereafter. At the basemat level,

the deterministic ISRS are closer to the mean ISRS response rather than 84% NEP ISRS response, most likely corresponding to 60-70% NEP ISRS responses. For other locations at higher elevations within the AP1000 stick, for the rock site, the computed deterministic ISRS in horizontal direction (envelope of LB, BE and UB soil results) largely overestimates the ISRS amplitude, going up to 95-99% NEP levels, well above the ASCE 04 standard performance goal of 80% NEP level. However, the ISRS comparisons shows some exceptions in both horizontal and vertical directions for which deterministic ISRS are closer to 60-65% NEP ISRS, or much closer to the mean ISRS rather than 80% NEP ISRS. Deterministic SSI response appears to be lower than expected in the vertical direction, especially for the soil site for which 84% NEP ISRS are significantly higher than deterministic ISRS.

**Deeply Embedded SMR Model:**

Figure 6 shows the deeply embedded SMR SSI model. The SMR structure has a size of 200ft x 100ft x 100ft (H x L x W) with an embedment of 140ft depth (Ghiocel, 2014). The soil profile shown in Figure 11 is highly non-uniform with a soil layer stiffness variation inversion within the embedment depth. The seismic control motion was input at the SMR foundation level (FIRS) at 140ft depth (elevation 0ft). For probabilistic analyses the in-column FIRS input motion were computed based on the probabilistic site response analysis using 60 LHS random samples. The statistics and the 60 randomized soil profiles are plotted in Figure 11. The probabilistic seismic input was defined by the UHRS motion simulated at the 500ft depth bedrock. The statistics and the 60 LHS simulations of the UHRS outcrop input are plotted in Figure 12.

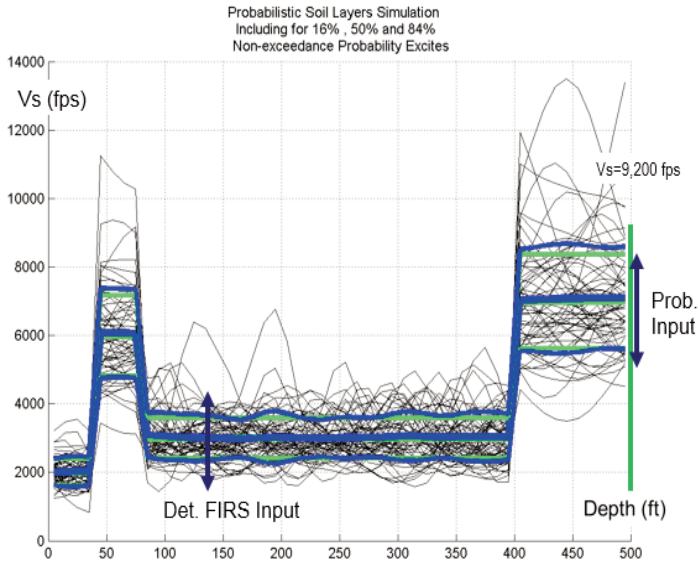


**Figure 11** Probability Level and Simulated Profiles

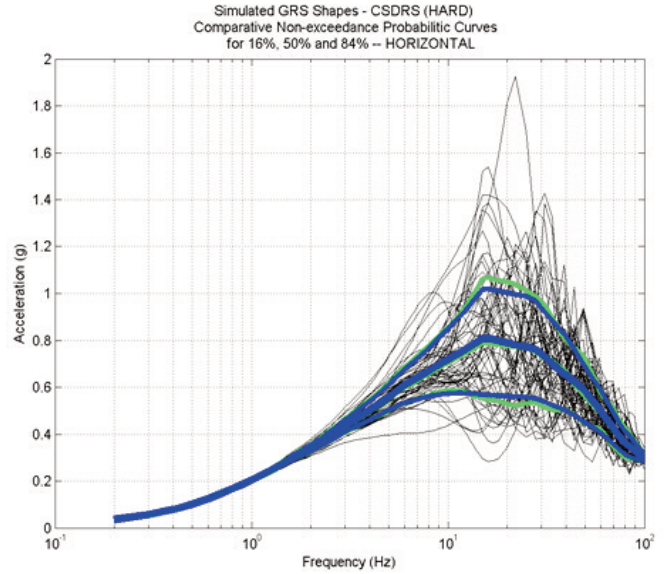


**Figure 12** Probability Level and Simulated UHRS

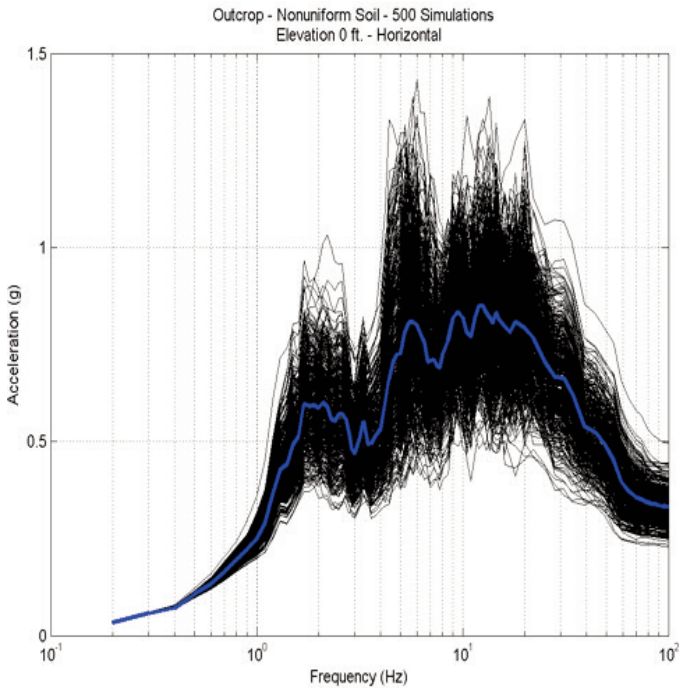


**Figure 13** FIRS Probabilistic Mean and Simulations

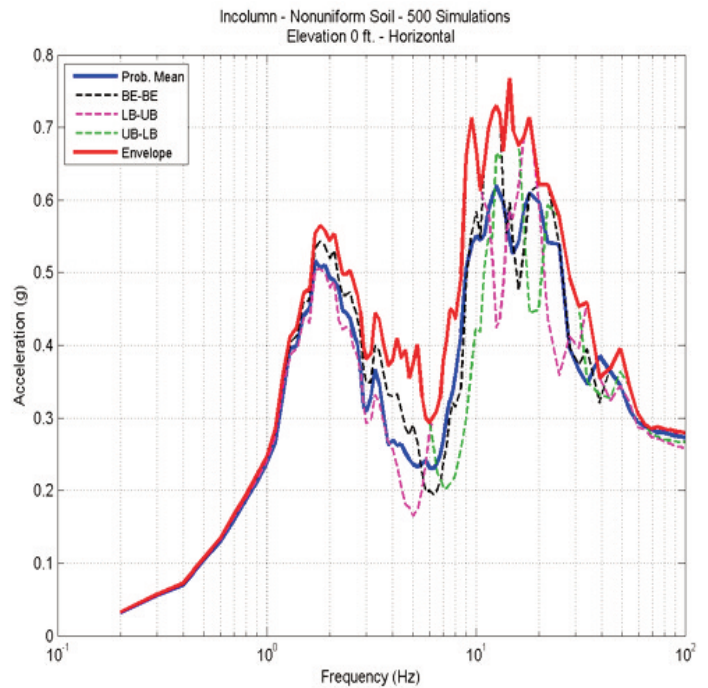


**Figure 14** Probabilistic vs. Deterministic FIRS

The concrete structural stiffness and damping were defined as two negatively correlated random variables. The two random variables were assumed to be lognormal variables with the mean elastic modulus reduction factor of 0.8 and c.o.v. of 0.10 and the mean damping of 6% and c.o.v. of 0.30. A correlation coefficient of -0.80 was assumed. For comparisons, we considered 60 and 500 probabilistic simulations. Figure 15 shows that the

probabilistic mean and 84% NEP ISRS within the SMR structure are basically identical for the 60 and the 500 LHS random samples. Figures 13 shows the probabilistic mean and simulations of the outcrop FIRS at 140ft depth. A comparison between the probabilistic mean in-column FIRS and the deterministic in-column FIRS for the LB, BE and UB soil profiles determined based on the probabilistic site response simulations is shown in Figure 14.

Figure 14 indicates that the deterministic FIRS envelope is larger than the probabilistic mean FIRS as required by the new ASCE 04-2015 standard. It should be noted that the probabilistic SSI input simulations are based on the probabilistic site response simulations. The probabilistic in-column FIRS motions used for probabilistic SSI analysis simulations were computed by the probabilistic site response analysis using the full soil column.

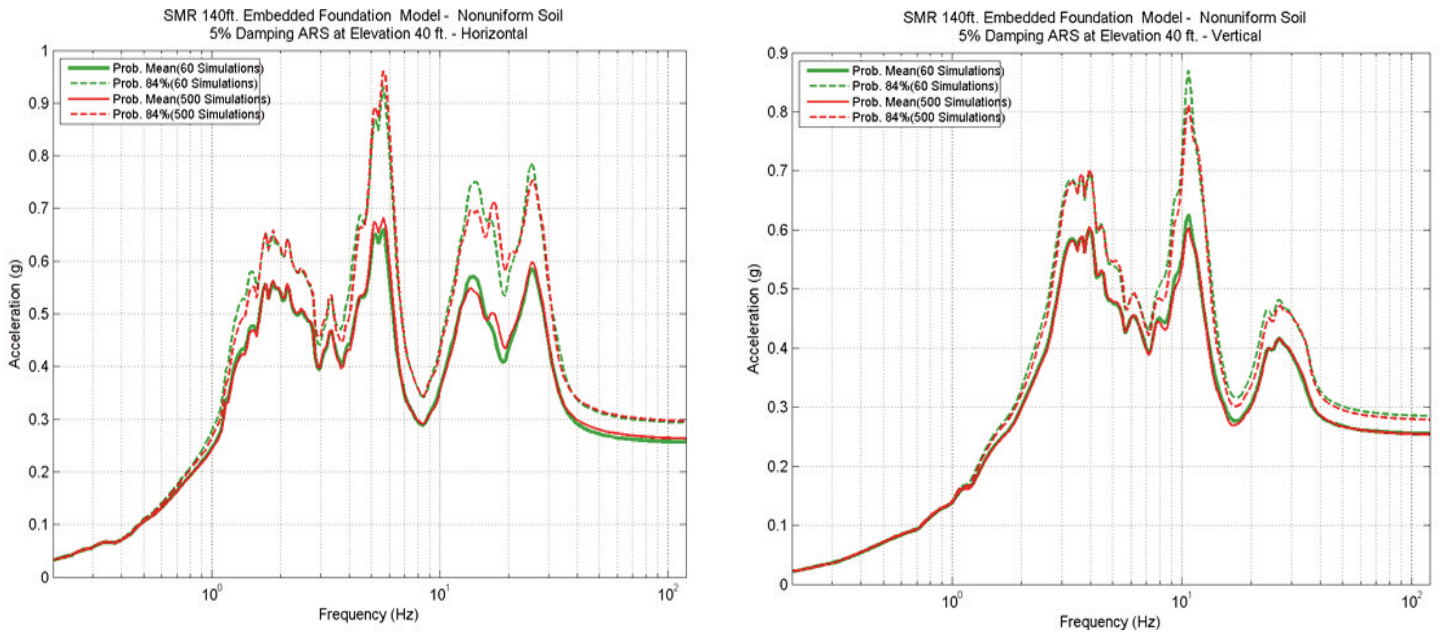


**Figure 15** Comparative Mean and 84% NEP ISRS in Horizontal and Vertical Directions Computed at 100ft Depth (Elevation 40ft above Foundation Level) for the 60 and 500 LHS Simulations

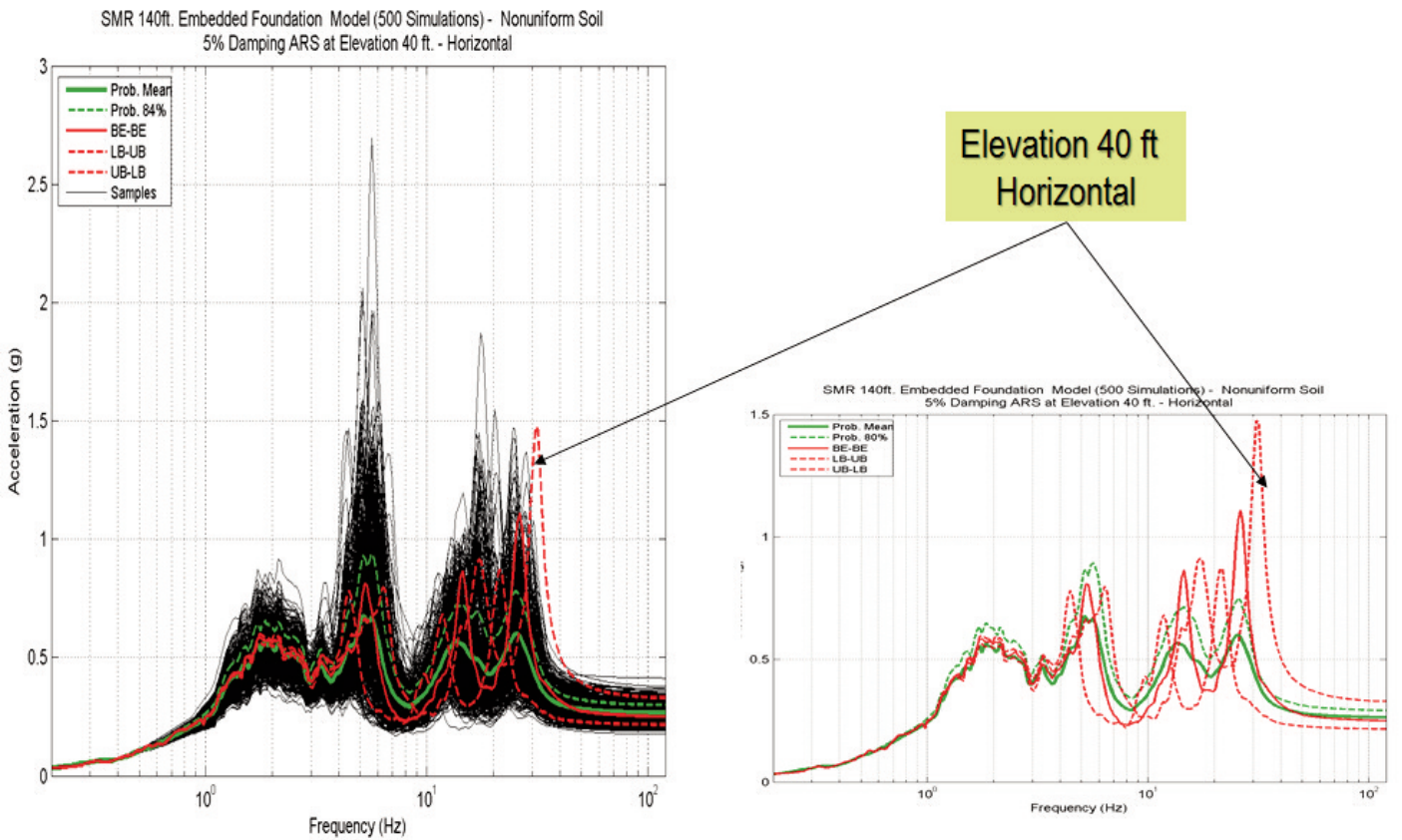


**Figure 16** Deterministic LB, BE, UB ISRS and Probabilistic Mean and 84% NEP ISRS at 40ft Elevation

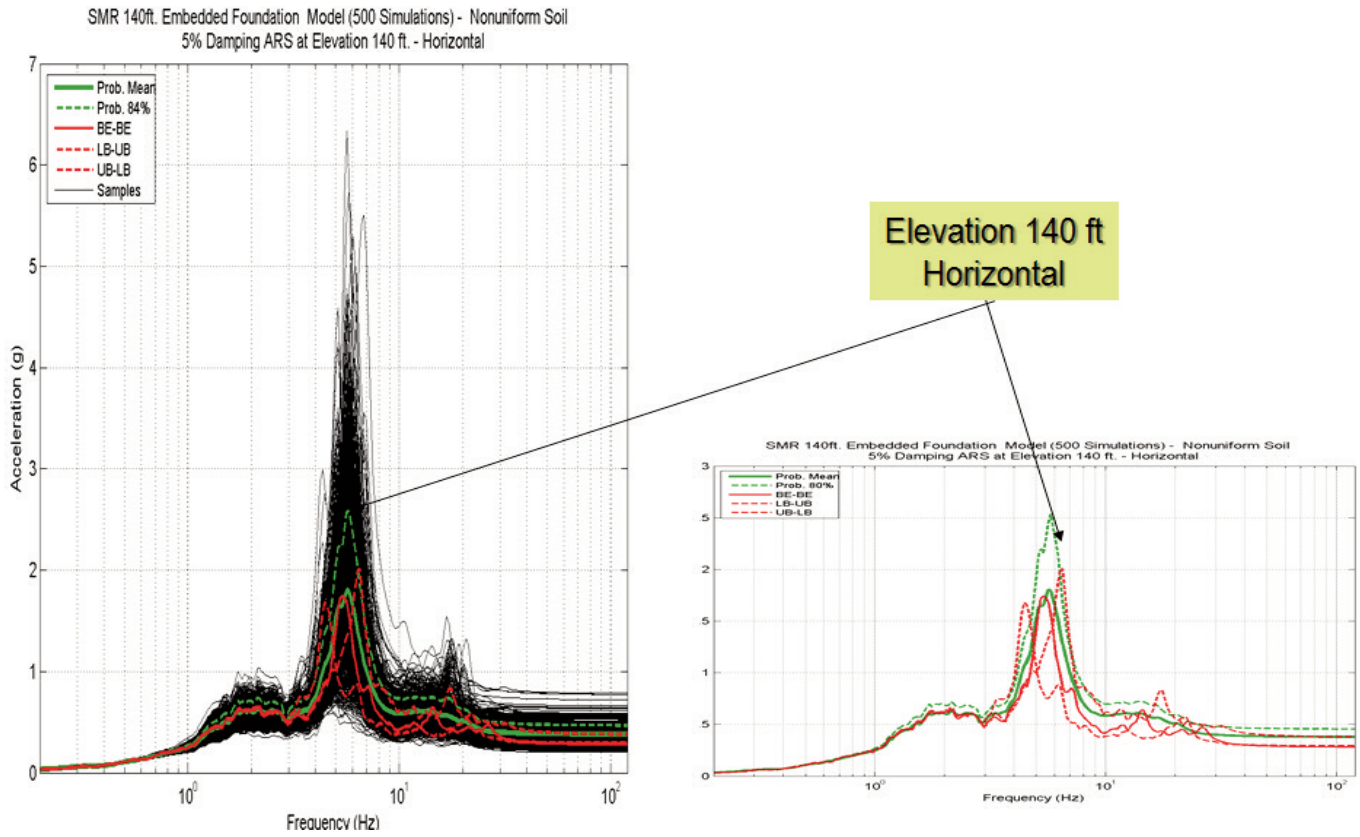


**Figure 17** Deterministic LB, BE, UB ISRS and Probabilistic Mean and 84% NEP ISRS at 140ft Elevation

As expected, the SSI response of the deeply embedded SMR is more sensitive to the soil property variations than the surface AP1000 stick model. The kinematic SSI effects are major for the deeply embedded model and only negligible for the surface model. Figures 16 and 17 show comparisons of the deterministic ISRS for the LB, BE and UB soils, (red lines) and probabilistic mean and 80% NEP ISRS (green lines) at 40ft and 140ft elevations. The left plots include the 500 ISRS random samples. These ISRS comparisons are for two selected situations that illustrate limitations of the deterministic SSI analysis. Figure 16 illustrates that in the high-frequency range, above 10 Hz, the deterministic ISRS, especially for the UB soil, has a much larger spectral peak amplitude than the probabilistic mean or 80% NEP ISRS (see right plots). The difference is larger than 100%. By looking at the Figure 16 ISRS plots (see left plots) that include the prob-

abilistic simulated ISRS, it becomes obvious that the deterministic UB response represents a very biased result that appears to be outside of the range soil profile variations. This is due the fact that producing a randomized soil profile that is similar to the UB soil profile for which all soil layers are being simultaneously stiffer at the 84% NEP level, has a very low likelihood or, in other words, the UB soil profile corresponds to a small occurrence probability within the random sample space. It is evident that the deterministic SSI analysis has no way of considering the low occurrence probability associated to a randomized soil profile that is identical with the UB soil profile. In deterministic SSI analysis, the UB soil profile has an implicit occurrence probability of unity since it corresponds to a sure event. This appears to be a penalty of the deterministic SSI analysis on the economic aspects of the nuclear structure design. Figure 17 shows a reverse situation in

which the deterministic ISRS are well below the probabilistic 80% NEP ISRS (see right plots). For random samples, as indicated in Figure 17 (see left plots), the computed ISRS could be much larger, by 100-150%, than the deterministic envelope ISRS (for LB, BE and UB soils). The probabilistic 80% NEP ISRS dominant peak at @ 6 Hz is about 25-30% larger than the deterministic ISRS peak at @ 6 Hz. This apparent deficiency of the deterministic SSI analysis is due to the simplistic way in which the soil stiffness variation is considered by only three discrete values that correspond to the LB, BE and UB soil profiles. In reality, the soil stiffness variation includes a continuum spectrum of values. There is a myriad of possible random combinations of the input variations that could amplify largely the SSI response. This appears to be a penalty of the deterministic SSI analysis on the safety aspects of the nuclear structure design.

## CONCLUSIONS

The paper compares ISRS results obtained using deterministic and probabilistic SSI analyses in accordance with the recommendations of the new ASCE 04-2015 standard. Serious modelling limitations of the current deterministic SSI approach are highlighted. The differences between deterministic SSI and probabilistic SSI analyses appear to be much larger for deeply embedded structures, such as SMR, which are quite sensi-

tive to the soil motion and layer property variations.

## REFERENCES

*Ghiocel D, M. (2014).* Comparative Probabilistic-Deterministic Studies and RVT-based SASSI Analyses of Nuclear Structures for Soil and Rock Sites", U.S. Department of Energy, DOE Natural Phenomena Hazards Meeting, Session on "Soil-Structure Interaction", Germantown, MD, USA, October 21-22

<http://www.energy.gov/sites/prod/files/2015/05/f22/DOE-NH-Probabilistic-Deterministic-SSI-Oct-21-2014.pdf>

*Ghiocel Predictive Technologies, Inc. (2015).* "ACS SASSI - An Advanced Computational Software for 3D Dynamic Analyses Including SSI Effects", ACS SASSI Version 3.0 Manuals, March 31, [http://www.ghiocel-tech.com/enggTools/ACS%20SASSI\\_V300\\_Brief\\_Description\\_Dec\\_31\\_2014.pdf](http://www.ghiocel-tech.com/enggTools/ACS%20SASSI_V300_Brief_Description_Dec_31_2014.pdf)

## FAST NONLINEAR SEISMIC SSI ANALYSIS USING A HYBRID TIME-COMPLEX FREQUENCY APPROACH FOR LOW-RISE NUCLEAR CONCRETE SHEARWALL BUILDINGS

### ABSTRACT

The paper presents a highly efficient nonlinear SSI approach based on a hybrid time-complex frequency approach using an iterative procedure. The hybrid approach uses a piece-wise equivalent-linearization for computing the FEA solution in complex frequency. The local linearized hysteretic models are calibrated based on the "true" nonlinear concrete wall behaviour in time domain. Sophisticated shear deformation hysteretic models with pinching were implemented. Comparative results of the hybrid approach and the true nonlinear time-integration approach showed very good matching. The hybrid approach is applicable to nonlinear SSI analysis for i) design level for correctly including the concrete cracking in structures as a function of stress levels in accordance to the new ASCE 04-2015 standard (Sections 3.2.2 and 3.3.2) and the USNRC SRP requirements, and ii) beyond design level in accordance with the ASCE 43-2005 recommendations, to properly compute the inelastic absorption factors for structural fragility analyses. The paper presents a validation case study of a typical low-rise shearwall nuclear structure for which the hybrid approach results are compared with the "true" nonlinear time-integration approach results. Nonlinear SSI analyses performed for rigid rock and soft soil sites demonstrate the capabilities of the hybrid approach. The nonlinear SSI hybrid approach is also much faster and robust than the "true" nonlinear SSI time-integration approach.

### INTRODUCTION

The fast nonlinear SSI approach uses an iterative equivalent linear procedure in complex frequency domain to solve repeatedly the linearized SSI system FEA solution. The nonlinear concrete hysteretic response is computed using wall panels defined as "macro shell elements". For each shearwall panel, the hysteretic shear force is computed in time domain using the nodal panel SSI displacements. The nodal displacements are applied as boundary conditions to the nonlinear concrete wall panels. The iterative approach is fast convergent in only few iterations. For typical nuclear applications, the nonlinear SSI analysis in complex frequency via the proposed hybrid approach is tens to hundreds times faster than the nonlinear SSI analysis in time domain. In addition to the computational speed aspect, the complex

frequency nonlinear SSI approach via local equivalent linearization is much simpler to apply and much more numerically robust than the time domain nonlinear SSI approaches that need very small integration time steps to avoid noisy results, as also recognized by many researchers including the MIT researchers (Kausel and Assimaki, 2002). The engineering literature includes various hysteretic models for the idealization of the reinforced concrete shearwall behaviour. For the low-rise shearwall buildings that are of interest for nuclear buildings, from various hysteretic models, we selected the Cheng-Mertz hysteretic model (Cheng and Mertz, 1989) that was used over years in a number of studies for the DOE and ASCE standards. Figure 1 shows the Cheng-Mertz hysteretic models for the shear and bending behaviour in the low-rise shearwalls. The figure includes a comparison between

experimental testing and numerical simulation using Cheng-Mertz hysteretic of a shearwall panel (Chen and Mertz, 1989). Figure 2 shows a comparison of the Chen-Mertz models for Shear (CMS) and Bending (CMB) against the popular Takeda model for a shearwall panel assuming that all models have the same backbone curve and displacement history inputs. Figure 2 shows the hysteretic loop response comparisons for two material backbone (BBC) curves with different concrete cracking thresholds. The cracking threshold point is plotted on BBC with a black dot. Thus, for low cracking thresholds the CMS hysteretic loops are pinched, while the CMB and Takeda loops are not. Thus, for BBC with low cracking thresholds for which pinching occurs, the CMB and Takeda models may dissipate more energy than CMS that is capable of capturing well pinching effects.

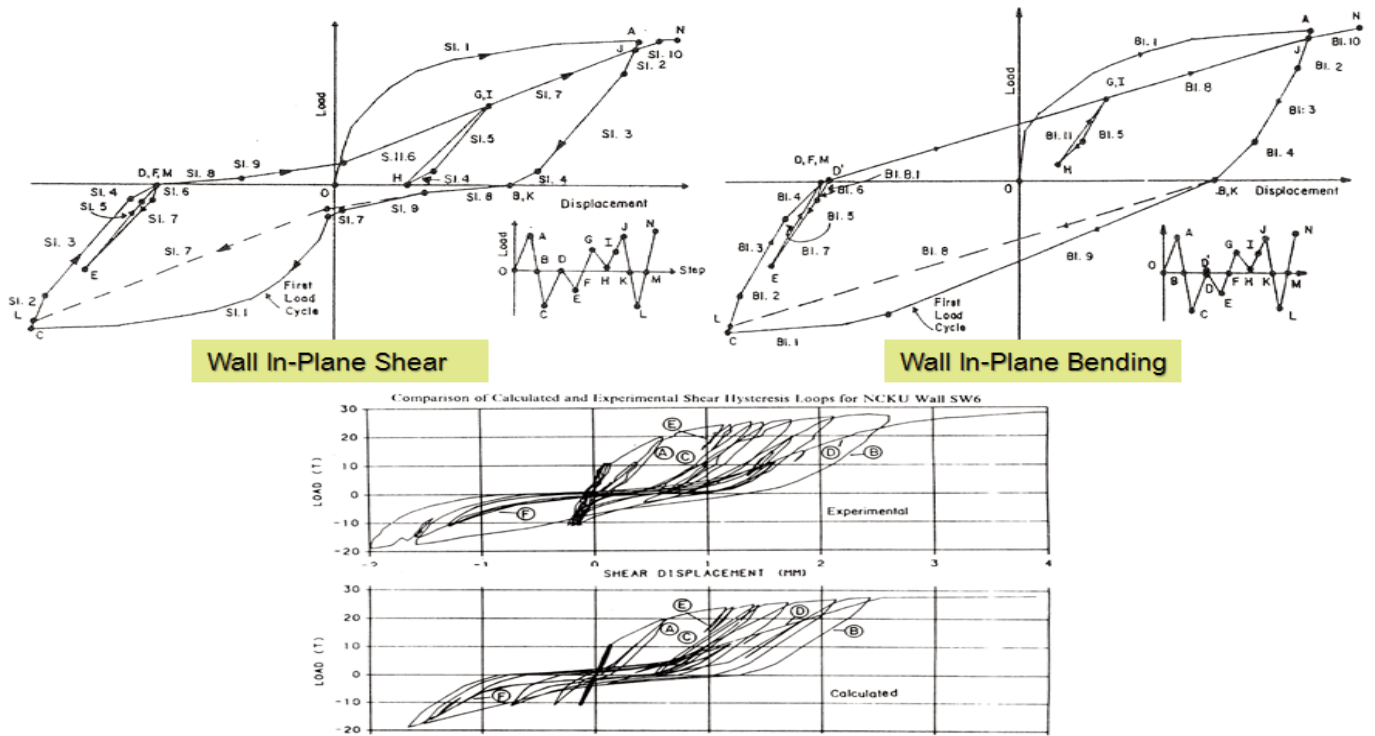


Figure 1 Chen-Mertz Hysteretic Models for Shear Deformation (CMS) and Bending Deformation (CMB)

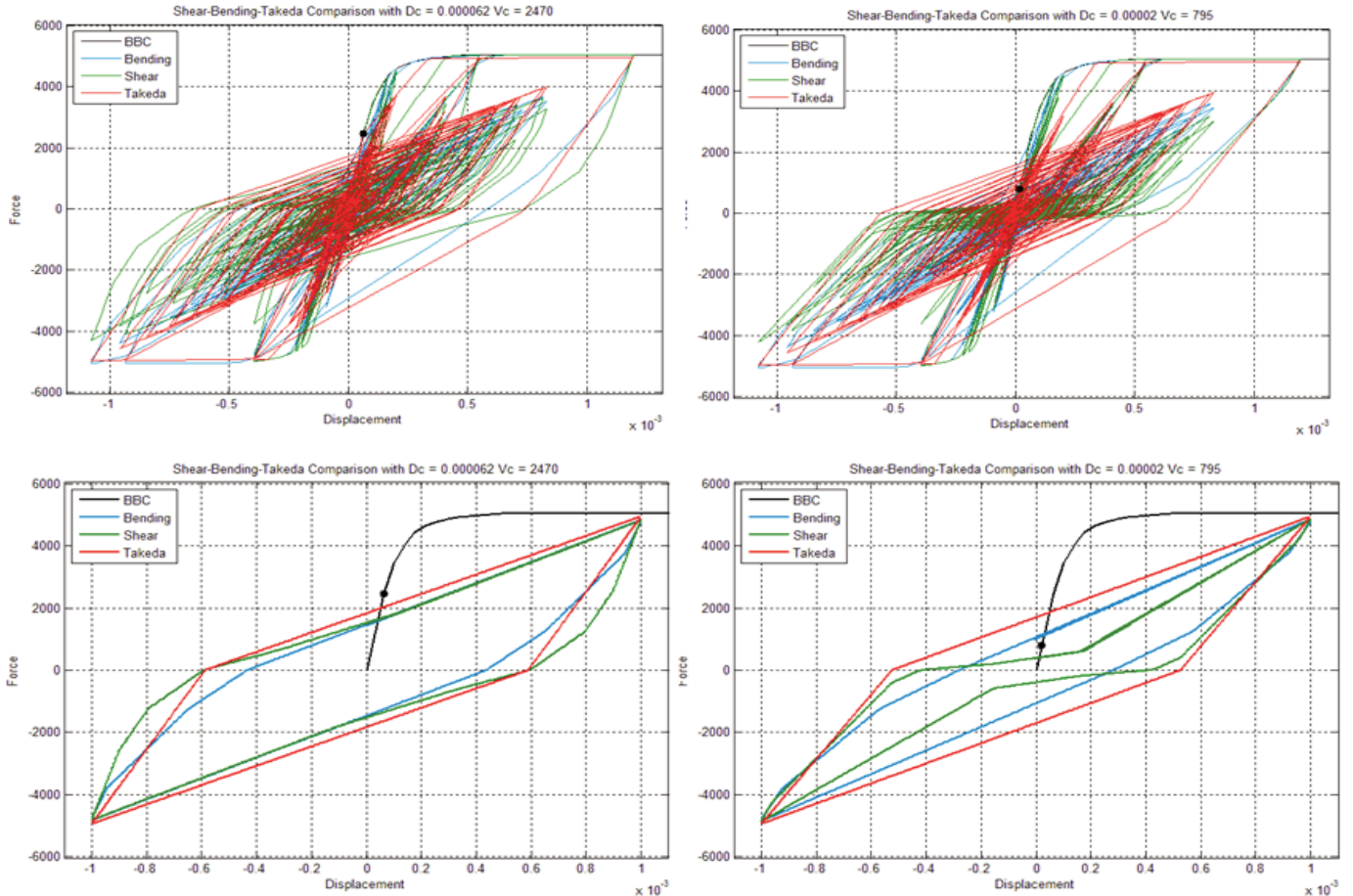
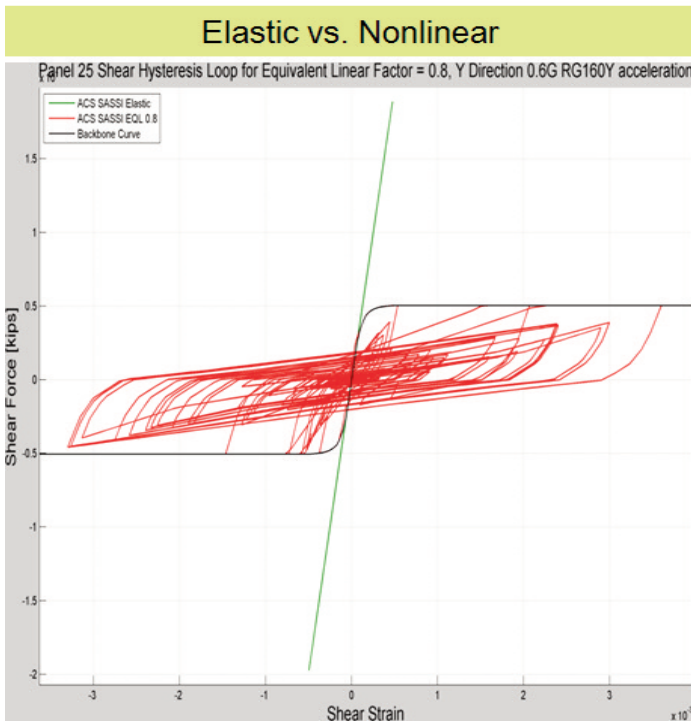
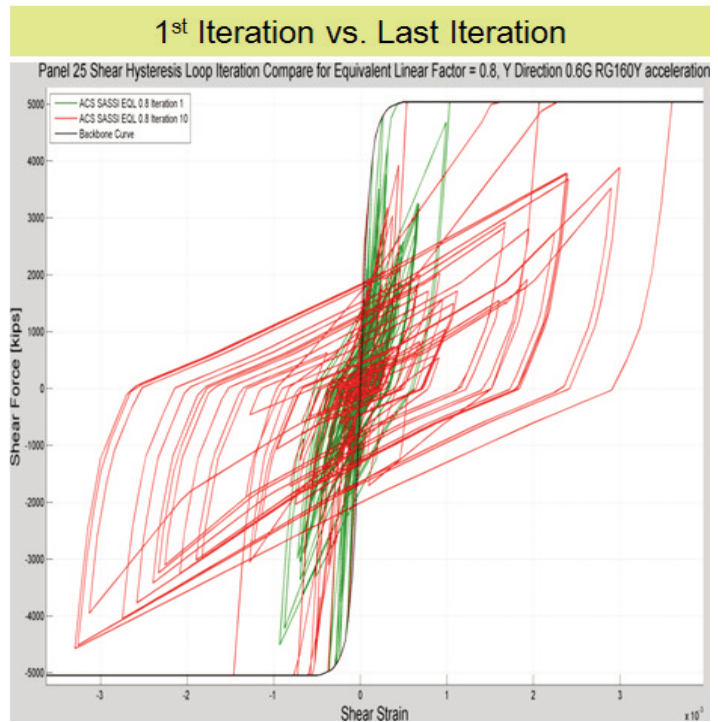


Figure 2 Comparison of CMS, CMB and Takeda Hysteretic Model Responses for Same Inputs



**Figure 3** Linear versus Nonlinear Behavior



**Figure 4** 1<sup>st</sup> versus Last Nonlinear Iteration

The nonlinear SSI analysis hybrid approach as implemented in the ACS SASSI Option NON software (2015) includes the following computational steps:

1) For the initial iteration, perform the linear SSI analysis using the elastic material stiffness and damping properties for all shearwall panels

2) Compute the concrete shearwall panel shear force responses in time domain that are further used to calibrate the local panel linearized hysteretic models in complex frequency

3) Perform a new SSI analysis iteration using reanalysis (restart analysis) in the complex frequency domain

using the hysteretic models computed in Step 2 for all selected panels

4) Check convergence of the nonlinear SSI response after new SSI iteration, and go back to Step 2 if convergence is not achieved. Otherwise stop.

A typical nonlinear SSI analysis result using the hybrid approach is shown in Figure 3 (for Panel 25 in Figure 6). The plots in Figure 3 show a comparison of a concrete shearwall panel hysteretic behavior computed for the linear elastic structure before the first SSI iteration and for the nonlinear structure after the last SSI iteration, for a beyond-design earthquake that is twice than the design earthquake. The green line shows the linear elastic shear force-displacement variation, while the red line shows the nonlinear shear force-displacement variation in the last iteration. The computed inelastic response of the concrete wall panel appears to be close to structure collapse. The

computed ductility factors with respect to yielding appear to be about 8-10 (since no clear yielding point defined in BBC), the maximum normalized story drifts (shear strain) about 0.004 and the computed inelastic absorption reduction factor about 3.50. Figure 4 shows a comparison between the nonlinear hysteretic loops computed after the 1st SSI iteration and after the last iteration for the same panel for the beyond-design earthquake. The 1st SSI iteration results are far from the converged results. Additional 5 SSI iterations (SSI reanalyses) were required for the nonlinear result convergence. These results alert against published papers that recommend for nonlinear SSI analysis the

use of a cascaded SSI approach with no SSI iterations.

**VALIDATION CASE STUDY**

A case study of a typical low-rise shearwall nuclear plant structure (Figure 5) is shown to demonstrate the application of the nonlinear SSI approach in complex frequency. The nonlinear hysteretic behaviour is determined based on the computed panel drifts and the shear forces, assuming a Cheng-Mertz shear (CMS) deformation model. The computed story drifts exclude the panel rigid body rotations coming from the SSI rocking modes that do not produce any stresses in the panel.

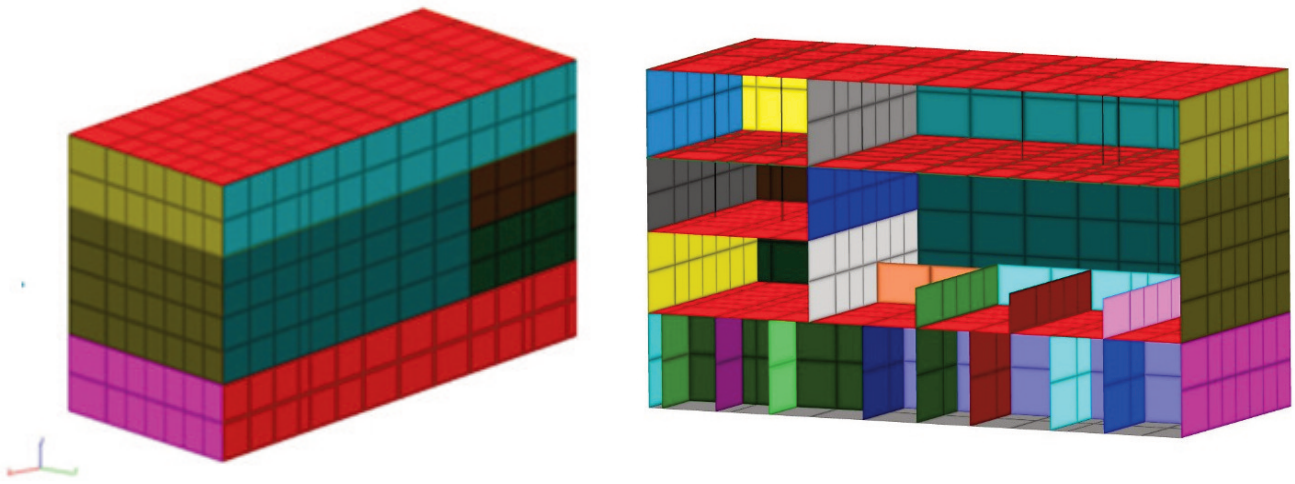


**Figure 5** Low-Rise Concrete Shearwall Building; Outside View (left) and Section View (right)

The first step in the nonlinear SSI analysis as implemented in ACS SASSI is to create the concrete wall panels (macro shell elements) with nonlinear behaviour. Using the SUBMODELER GUI module specialized commands, such as Wallfr, Panelize, MergeGroup and SplitGroups, the structural walls can be effectively partitioned per floors. The entire model preparation process is almost automatic, so that it takes only a couple of hours to finalize a complex nonlinear FEA

model. Figures 5 and 6 show the split of the investigated shearwall structure in various nonlinear wall panels.

An aspect of key importance for the nonlinear analysis input are the constitutive force-displacement curves or the backbone curves (BBC) for each structural wall panel. In ACS SASSI, using the SUBMODELER module BBC command, the constitutive curves can be

generated very rapidly. A key parameter of the BBC curves is the shear capacity value for the shearwall panel. Various options for computing shear capacity for flanged and non-flanged concrete walls were implemented in accordance with the new ASCE 43-2015 draft recommendations are based on the experimental shearwall panel testing database at the University of New York at Buffalo (Gulec and Whittaker, 2009).

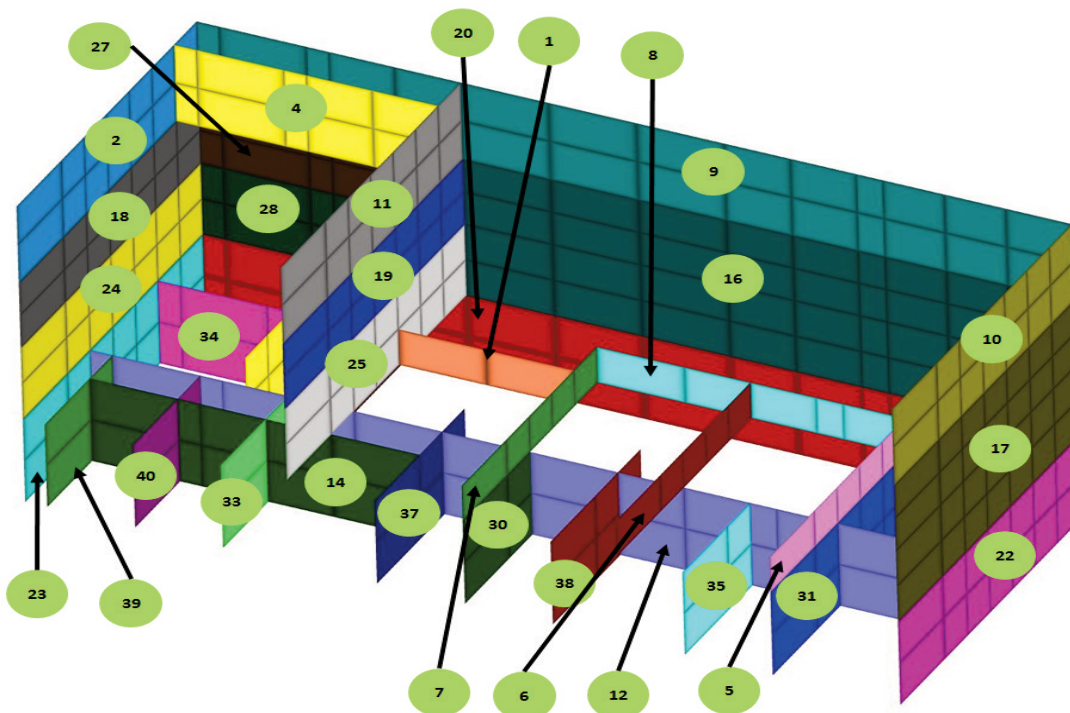


**Figure 6** Shearwall Building View With 40 Wall Panels Used for Nonlinear Structure Analysis

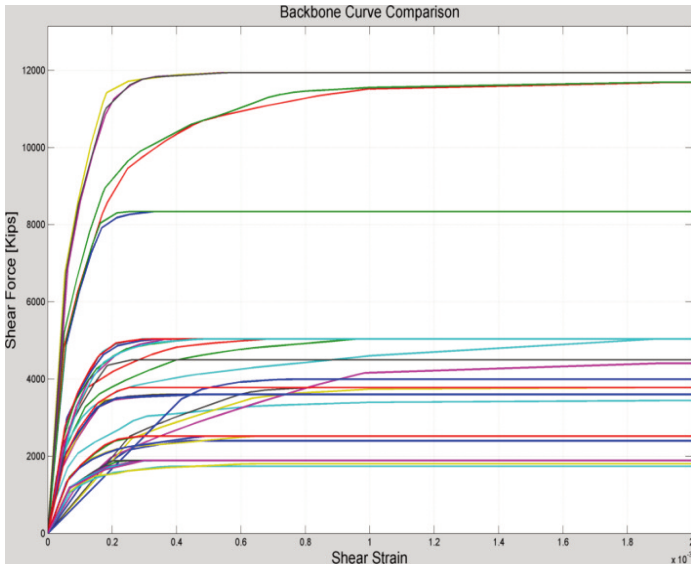


**Figure 7** The BBC for Shearwall Panels

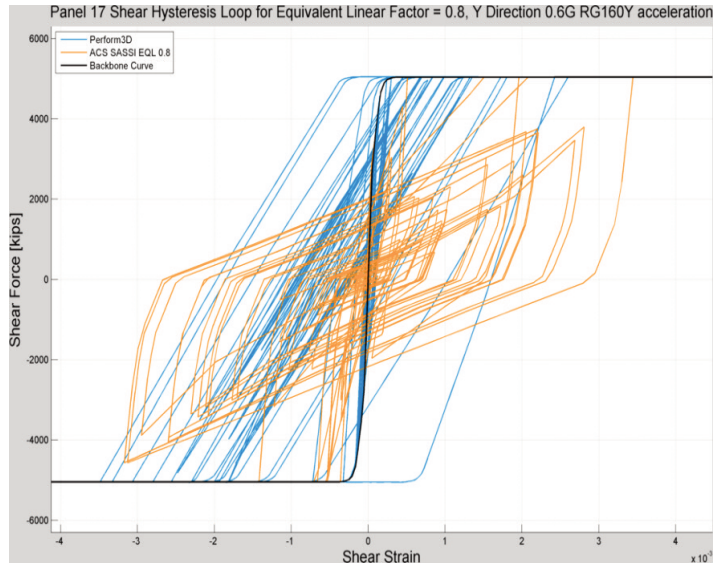
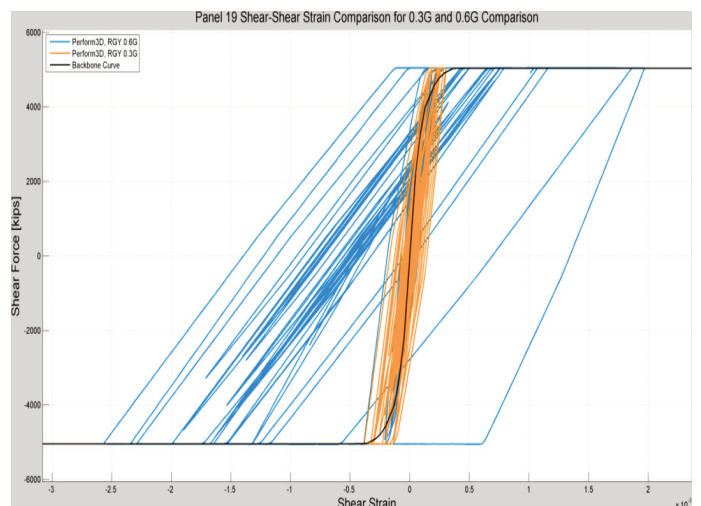
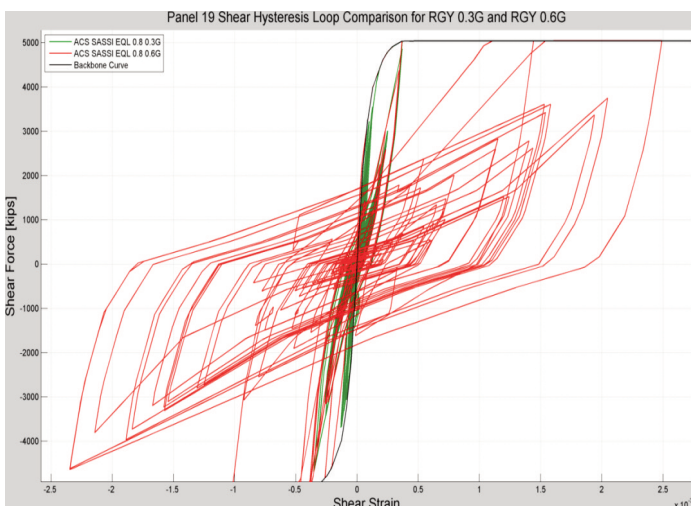


**Figure 8** Comparison of Hysteretic Models

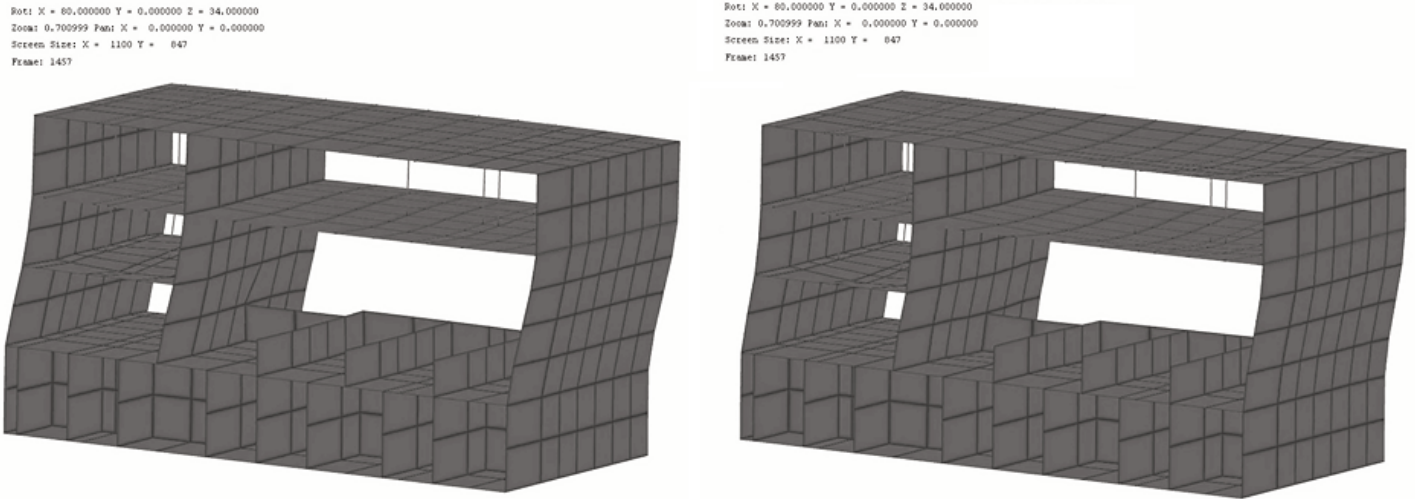
The hybrid approach, as implemented in ACS SASSI, was validated for the low-rise shearwall structure in Figures 5 and 6 against the “true” nonlinear time-history analysis, as implemented in the specialized PERFORM3D software (trademark of Computer Structures, Inc.). The two FEA computer codes were applied to the fixed-base model of the low-rise shearwall structure for the same analysis inputs. Using PERFORM3D a nonlinear pushover analysis was performed to create the BBC for the entire structure and the BBC for each wall panel, as illustrated in Figure 7. The input acceleration time histories were simulated based on the RG

1.60 design spectrum anchored at 0.30g and 0.60g ZPGA. However, the shear force hysteretic models were different. For the ACS SASSI analysis we used the Cheng-Mertz (CMS) model, while for PERFORM3D analysis we selected the fiber model applicable to the low-rise shearwall panels. Figure 8 shows the two model hysteretic loops for the same story drift history. The Cheng-Mertz shear model (brown line in Figure 8) appears to be more refined since degrades the loading-unloading stiffness as a result of the concrete degradation, and also captures accurately the pinching effects characteristic to shear deformation models

(origin oriented type). The fiber model (blue line in Figure 8) shows no stiffness degradation and low energy dissipation for the small amplitude cycles with no trace of pinching. Comparisons between ACS SASSI results and PERFORM3D were done for both 0.30g and 0.60g ZPGA earthquake levels. The convergence of the iterative hybrid approach was achieved in 4-5 SSI iterations for 0.30g input and 6-7 SSI iterations for 0.60g input. This 5 to 7 number of iterations implies a nonlinear SSI analysis runtime of about 2-3 times of the linear elastic SSI analysis runtime, if the appropriate SSI analysis restart options are selected.



**Figure 9** Panel 17 Hysteretic Loops Computed for 0.30g and 0.60g Using ACS SASSI Cheng-Mertz Model (left) After Final Iteration and PERFORM3D Fiber Model (right)



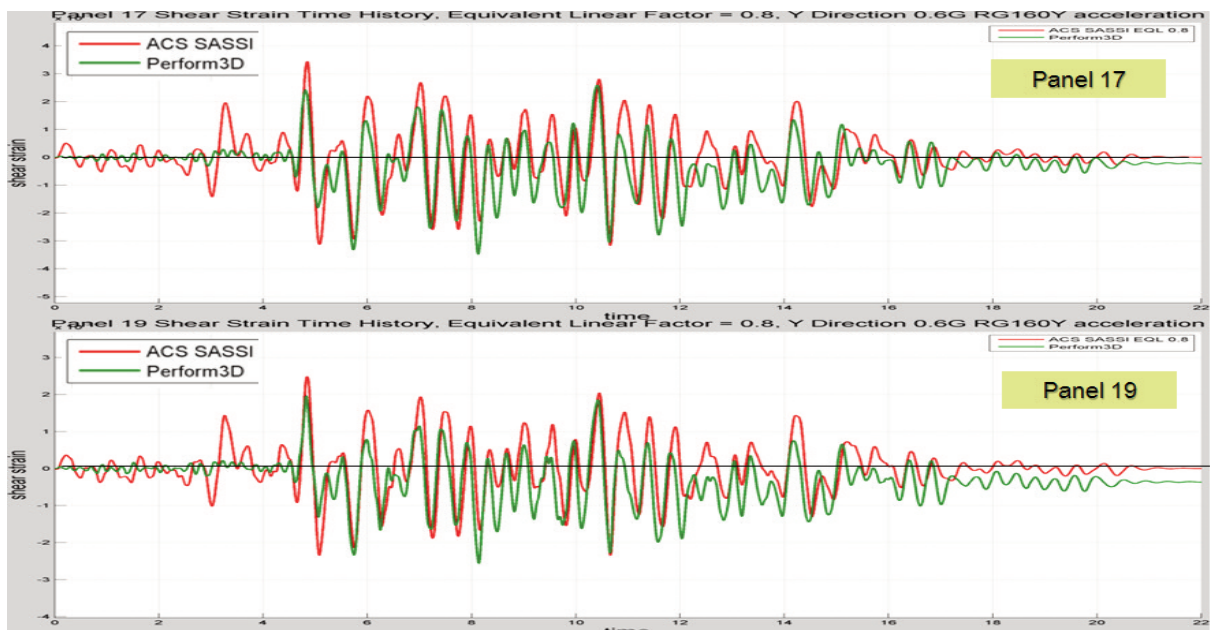
**Figure 10** Structural Deformation Computed at the 7.285 Sec. Time for 0.60g Seismic Input for ACS SASSI Option NON (left) and PERFORM3D (right)

Figure 9 shows the hysteretic loops for Panel 17 (see Figure 6 for the panel location) using the two FEA codes for the 0.30g and 0.60g seismic inputs. The maximum absolute value of the normalized inelastic story drifts (shear strain) was 0.0025 for both the hybrid approach and true nonlinear time approach.

Figure 10 shows the deformation of the nonlinear structure computed using the two FEA codes for the fixed-base models, ACS SASSI (left) and PERFORM3D (right) at the

same time moment, specifically at 7.285 seconds of the 0.60g earthquake duration. For a more detailed comparison that includes side-to-side structural animations for a part of the duration of the 0.60g input (twice than design input), see [http://www.ghiocel-tech.com/enggTools/ACS\\_SASSI\\_vs\\_Perform3D\\_Nonlinear\\_Response\\_for\\_Rigid\\_Foundation\\_0.6g\\_Acc.avi](http://www.ghiocel-tech.com/enggTools/ACS_SASSI_vs_Perform3D_Nonlinear_Response_for_Rigid_Foundation_0.6g_Acc.avi). These side-by-side animations illustrate a very good matching between the two FEA codes results.

Figure 11 shows a comparison of the computed inelastic story drift histories in Panels 17 and 19 (see Figure 6 for their locations) for the 0.60g seismic input. The matching between the ACS SASSI iterative solution (red) and PERFORM3D nonlinear time history solution (green) is also very good. The SSI motion phasing is very well captured by the hybrid approach. The main difference between the two FEA solutions, is the shift to negative values that occurs for the time-domain solution that indicates a permanent story drift.



**Figure 11** Story Drifts for Panels 17 and 19 Computed Using ACS SASSI Iterative Approach and PERFORM3D Time-Domain Integration Approach

The shear force inelastic reduction factors computed for each panel for the 0.30g and 0.60g earthquakes in the Y-direction (transverse) using ACS SASSI (colored line) and PERFORM3D (black line) are plotted in

Figure 12. The iterative SSI runs were done for three effective strain reduction factor (SRF) values of 0.60, 0.80 and 1.0. The differences in results for the three SRF input values are negligible. The matching between

the computed inelastic factors was very good. Please note that the X-direction (longitudinal) panels have zero inelastic factors (negligible shear forces) since seismic input is only in Y-direction.

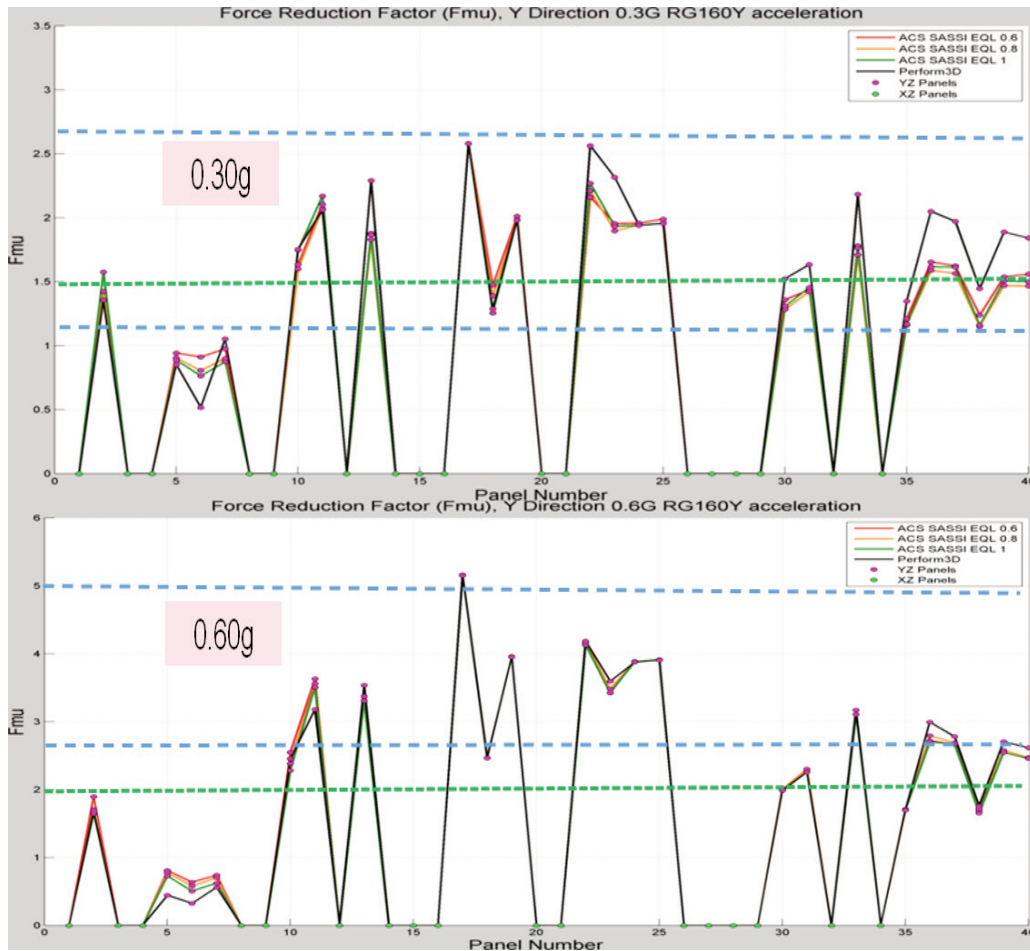


**Figure 12** Shear Force Inelastic Absorption Factors for 0.30g and 0.60g Y-Direction Seismic Inputs Using ACS SASSI Hybrid Approach (color) and PERFORM3D Nonlinear Time Integration Approach (black)

Figure 12 also compares the computed inelastic absorption factors with the values provided by the ASCE 43-05 standard (horizontal green dotted line) for the low-rise shearwall buildings for the limit state C (reduced yielding) for 0.30g input and limit state A (ultimate, close to collapse) for 0.60g input, respectively. On the same plots, we also included the results published by Ibarra and Chowdhury (horizontal blue dotted line) for the median and 5% non-exceedance probability values of the inelastic absorption

reduction factors based on a Southwest Research Institute (SwRI) study for stiff concrete structures (Ibarra and Chowdhury, 2006).

An additional comparison between the ACS SASSI iterative approach and PERFORM3D time integration approach was done in terms of the computed in-structure acceleration response spectra (ARS) for 0.60g in Y-direction. Figure 13 shows the ISRS computed at lower and higher elevation locations. Again,

there is a good matching of the nonlinear analysis results of the two FEA codes.

It should be noted that the SRF values of 0.8 and 1.0 provide the best ARS matching with the nonlinear time domain results up to a frequency of 20 Hz. For higher frequencies than 20 Hz, computed ARS using PERFORM3D are much larger than linear elastic ARS. The PERFORM3D acceleration histories include large numerical noise above the 20 Hz frequency.

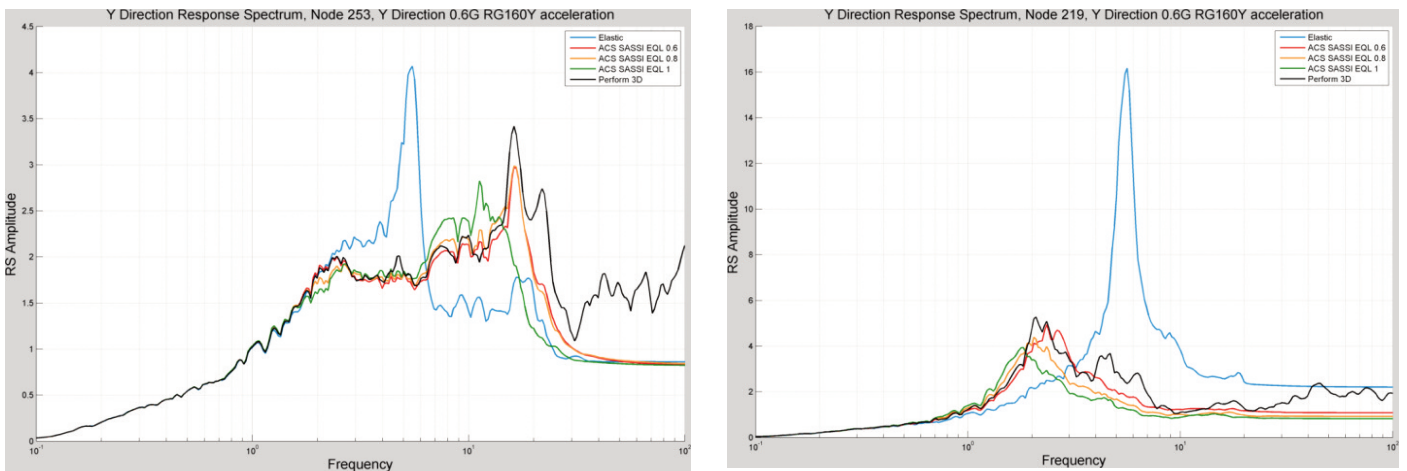


**Figure 13** Elastic (blue line) vs. Inelastic ARS Computed for 0.60g Seismic Input Using ACS SASSI (3 SRF values: 0.6 red, 0.8 orange and 1.0 green) and PERFORM3D (black)

**SSI ANALYSIS CASE STUDIES FOR ROCK AND SOIL SITES**

For the limited space remaining in this paper, we would like to illustrate the application of the

ACS SASSI hybrid approach to the nonlinear SSI analysis of the nuclear shearwall building for a hard-rock site ( $V_s$  of 8000 fps) and a soft-soil site soil ( $V_s$  of 1000 fps). Comparative results in

terms of the wall panel ductilities (computed with respect to the cracking threshold) and the shear force inelastic factors for the 0.30g and 0.60g earthquake levels are provided in Table 1.

Panel	Rock Site				Soil Site			
	0.3g		0.6g		0.3g		0.6g	
	$\mu^*$	$F\mu$	$\mu^*$	$F\mu$	$\mu^*$	$F\mu$	$\mu^*$	$F\mu$
2	1.25	1.40	3.70	1.66	1.01	0.94	2.13	1.34
3	1.27	1.31	2.24	2.07	1.27	0.95	2.16	1.50
9	1.28	1.21	2.24	1.92	1.30	0.93	2.31	1.44
10	1.97	1.63	5.58	2.35	2.40	1.07	10.80	1.50
11	6.20	2.03	15.91	3.43	6.29	1.47	16.27	2.47
13	3.14	1.81	6.91	3.27	2.85	1.60	8.18	2.75
17	12.71	2.51	61.80	5.03	10.97	1.66	65.76	3.33
18	2.66	1.38	37.62	2.43	1.89	1.01	24.83	1.50
19	7.40	1.95	50.01	3.88	6.22	1.38	41.31	2.68
22	3.22	2.17	6.61	4.07	3.00	1.36	10.46	2.52
23	4.27	1.88	9.34	3.39	2.86	1.43	7.65	2.32
24	9.85	1.92	64.26	3.84	3.71	1.24	52.54	2.40
25	9.55	1.92	56.04	3.84	5.64	1.42	50.37	2.79
30	1.92	1.27	4.90	2.02	0.97	1.02	2.84	1.31
31	2.25	1.39	5.63	2.26	2.37	1.33	8.74	2.22
33	2.73	1.69	6.02	3.09	1.61	1.41	3.52	2.19
35	1.60	1.14	4.35	1.70	0.99	1.00	3.80	1.24
36	2.94	1.57	6.72	2.67	2.28	1.35	7.14	2.09
37	2.49	1.54	5.69	2.67	1.95	1.41	4.64	2.20
38	1.82	1.13	4.93	1.67	1.67	1.28	4.77	1.83
39	2.36	1.45	5.28	2.53	0.95	0.96	2.23	1.37
40	2.44	1.45	5.61	2.45	1.11	1.13	2.68	1.65
Average	3.88	1.63	16.88	2.83	2.88	1.24	15.23	2.03
Max	12.71	2.51	64.26	5.03	10.97	1.66	65.76	3.33

Note \* : The ductility ratio are computed with respect to cracking strain

**Table 1** Computed Panel Ductilities (wrt cracking) and Inelastic Factors for Rock and Soil Sites

It should be noted that the wall panel inelastic factors for the soil site were 0.65-1.10 of the inelastic factors for the hard-rock site. The average and maximum inelastic factors were for the 0.30g earthquake 1.64 and 2.51 for the hard-rock site, and 1.24 and 1.66 for the soil site. For the 0.60g earthquake, the same quantities were 2.83 and 5.03 for the hard-rock site, and 2.03 and 3.33 for the soil site, respectively. The maximum inelastic factors shown in Table 1 were compared with those computed at SwRI (Ibarra and Chowdhury, 2006) for the concrete limit states C (1.5 times yielding deformation) and A (8 times yielding deformation) computed for stiff concrete structures, such as nuclear structures, with no SSI effects included. The median inelastic absorption factor values computed by Ibarra and Chowdhury were about 2.60 for limit C and 5.00 for limit A. These values compare extremely well with the inelastic factors computed using ACS SASSI for the hard-rock site in the most damaged walls that were 2.51 for limit C (for 0.30g input) and 5.03 for limit A (for 0.60g input). The differences were less than 5%.

The nonlinear SSI analysis results show significant coupling between the nonlinear structural behaviour and the SSI foundation motion. This is an important modelling aspect. The inelastic structural deformations could change severely the amplitude and frequency content of the SSI foundation rocking motion. The influence is larger for soil sites. A comparison of the SSI structural motion animations for the linear elastic structure (uncracked) and the nonlinear concrete structure is shown at

[http://www.ghioce-tech.com/enggTools/ACS\\_SASSI\\_Elastic\\_vs\\_Nonlinear\\_Response\\_For\\_Soil\\_Foundation\\_0.6g\\_Acc.avi](http://www.ghioce-tech.com/enggTools/ACS_SASSI_Elastic_vs_Nonlinear_Response_For_Soil_Foundation_0.6g_Acc.avi). The structural animations are obtained for the 0.60g earthquake and the soil site. The structural animations indicate clearly that the assumption that the SSI foundation motion is not influenced by the structural nonlinear behaviour, as some researchers wrote in their recent papers, is completely wrong.

## CONCLUDING REMARKS

The presented results validate the proposed nonlinear SSI hybrid approach against the "true" nonlinear time integration approach. The nonlinear SSI hybrid approach results were also compared favourably with the results obtained by the SwRI research studies on the nonlinear behaviour of stiff concrete structures, such as nuclear structures. The nonlinear SSI hybrid approach based on an iterative linearized FEA solution in complex frequency appears to be tens to hundreds of times faster than the "true" nonlinear SSI analysis based on the time-integration approach for identical computer platforms. In addition, the hybrid approach is much more robust than the time-domain nonlinear approaches using the direct integration that are often overly noisy and overly sensitive to small input parameter variations.

## REFERENCES

*Cheng, Y.F. and Mertz, G. (1989).* "Inelastic Seismic Response of Reinforced Concrete Low-Rise Shear Walls of Building Structures", University of Missouri-Rolla, Dept. of Civil Engineering, CE 89-30

*Ghioce Predictive Technologies, Inc. (2015).* "ACS SASSI - An Advanced Computational Software for 3D Dynamic Analyses Including SSI Effects", ACS SASSI Version 3.0 User Manuals, Revision 3, March 31, [http://www.ghioce-tech.com/publications/ACS%20SASSI\\_V300\\_Brief\\_Description\\_Dec\\_31\\_2014.pdf](http://www.ghioce-tech.com/publications/ACS%20SASSI_V300_Brief_Description_Dec_31_2014.pdf)

*Gulec and Whittaker, A. and B. Stojadinovic. (2009).* "Peak shear strength of squat reinforced concrete walls with boundary barbell or flanges," ACI Structural Journal, Vol. 106, No. 3, pp. 368-377.

*Kausel, E. and Assimaki, D. (2002).* "Seismic Simulation of Inelastic Soils Via Frequency-Dependent Moduli and Damping", ASCE Journal of Engineering Mechanics, Vol. 128, No.1, January

*Ibarra, L. and Chowdhury, A. (2006).* "Inelastic Absorption Energy Factors for Short Period Deteriorating SDOF Systems", 1st ECEES, Geneva, Switzerland, September 3-8, Paper 429

## SEISMIC MOTION INCOHERENCY EFFECTS ON SOIL-STRUCTURE INTERACTION (SSI) AND STRUCTURE-SOIL-STRUCTURE INTERACTION (SSSI) FOR NUCLEAR STRUCTURES

### ABSTRACT

The paper investigates the effects of motion incoherency (3D random wave propagation) on seismic responses of nuclear structures with a focus on the seismic SSSI analysis. Basic theoretical aspects are briefly reviewed. Two NPP case studies are investigated. The incoherency effects are computed for both the single, standalone structure SSI models and the multiple structure SSSI models. The paper considers both rock and soil sites. The incoherent analyses were performed using stochastic simulation. Comparative SSI and SSSI responses include acceleration in-structure response spectra (ISRS), structural forces and moments. It is shown that the motion incoherency could amplify significantly SSSI effects for the soil sites. The seismic SSSI effects could impact significantly on the ISRS, soil pressures and bending moments in basement walls and slabs.

### MODELING OF SEISMIC MOTION INCOHERENCY

The 1D seismic wave propagation assumption has been accepted in the nuclear engineering practice over the last few decades. Based on the 1D or vertically propagation assumption, the coherent motion at the ground surface is described by a "rigid body" motion in horizontal plane for which all the soil point motions under the foundation footprint have identical motions. In contrast to simplified representation of seismic wave field by coherent motion, the incoherent motion is a more accurate representation of the seismic random wave field that realistically includes the 3D seismic wave propagation aspects. Incoherent motions implicitly incorporate randomly inclined body waves and surface waves since they are developed based on real data from the dense array statistical earthquake records. Incoherent motions represent realistic 3D wave motion simulations based on the stochastic models which are developed from real record databases (Figure 1). Thus, incoherent motions include a much more

realistic idealization of seismic ground motion than coherent motions. To capture this spatial variability of the ground motion, an adequate stochastic field model is required. Assuming that the spatial variation of the ground motion at different locations could be defined by a homogeneous/stationary Gaussian stochastic field, then, the spatial variability is completely defined by its coherency spectrum or coherence function.

#### Incoherent Free-Field Motion

The coherent free-field motion at any interaction node dof k,  $U_k^{g,c}(\omega)$  is computed by  $U_k^{g,c}(\omega) = H_k^{g,c}(\omega)U_0^g(\omega)$  (1) where  $H_k^{g,c}(\omega)$  is the (deterministic) complex coherent ground transfer function vector at interface nodes and  $U_0^g(\omega)$  is the complex Fourier transform of the control motion. Similarly, the incoherent free-field motion at any interaction node dof k, is computed by:  $U_k^{g,i}(\omega) = \tilde{H}_k^{g,i}(\omega)U_0^g(\omega)$  (2) where  $\tilde{H}_k^{g,i}(\omega)$  is the (stochastic) incoherent ground transfer function vector at interaction node dofs

and  $U_0^g(\omega)$  is the complex Fourier transform of the control motion. The main difference between coherent and incoherent free-field transfer function vectors is that  $H_k^{g,c}(\omega)$  is deterministic quantity while  $\tilde{H}_k^{g,i}(\omega)$  is a stochastic quantity (the tilde represents a stochastic quantity). The quantity includes deterministic effects due to the vertically propagating body waves adjusted to incorporate the stochastic motion spatial variation effects in the horizontal plane. Thus, the incoherent free-field transfer function at any interaction node can be defined by:  $\tilde{H}_k^{g,i}(\omega) = S_k(\omega)H_k^{g,c}(\omega)$  (3) where  $S_k(\omega)$  is a frequency-dependent quantity that includes the effects of the stochastic spatial variation of free-field motion at any interaction node dof k due to incoherency. In fact, in the numerical implementation based on the complex frequency approach,  $S_k(\omega)$  represents the complex Fourier transform of relative spatial random variation of the motion amplitude at the interaction node dof k due to incoherency. Since these relative spatial variations are

random,  $S_k(\omega)$  is stochastic in nature. The stochastic  $S_k(\omega)$  can be computed for each interaction node dof k using the *spectral factorization* of coherency matrix computed for all SSI interaction nodes. For any interaction node dof k, the stochastic spatial motion variability transfer function  $H_k^{\theta,i}(\omega)$  in complex frequency domain is described by the product of the stochastic eigen-series expansion of the spatial incoherent field times the deterministic coherent ground motion complex transfer function:

$$H_k^{\theta,i}(\omega) = [\sum_{j=1}^M \Phi_{j,k}(\omega)\lambda_j(\omega)\eta_{\theta_j}(\omega)]H_k^{e,c}(\omega) \quad (4)$$

where  $\lambda_j(\omega)$  and  $\Phi_{j,k}(\omega)$  are the j-th eigenvalue and the j-th eigenvector component at interaction node k. The factor  $\eta_{\theta_j}(\omega)$  is the random phase component associated with the j-th eigenvector that is given by  $\eta_{\theta_j}(\omega) = \exp(i\theta_j)$  in which the random phase angles are assumed to be uniformly distributed over the unit circle.

**Incoherent SSI Response Calculations**

For incoherent motion input, the complex Fourier SSI response at any structural dof i,

$U_i^{s,i}(\omega)$ , is computed similarly by the superposition of the effects produced by the application of the incoherent motion input at each interaction node dof k:

$$U_i^{s,i}(\omega) = \sum_{k=1}^N H_{i,k}^{s,i}(\omega)U_k^{e,i}(\omega) = \sum_{k=1}^N H_{i,k}^{s,i}(\omega)[\sum_{j=1}^M \Phi_{j,k}(\omega)\lambda_j(\omega)\eta_{\theta_j}(\omega)]H_k^{e,c}(\omega)U_0^e(\omega) \quad (5)$$

Based on the approximation of the above equation, various incoherent SSI prediction approaches, from refined stochastic approaches to simple deterministic approaches, were implemented.

The number of coherency matrix eigenvectors or incoherent spatial modes depends on the eigen-series convergence. The higher the foundation flexibility is and the higher the frequency of interest is, the larger number of incoherent modes is (see Figure 2). For the "rigid" basemats, the higher-order incoherent modes are filtered out due to the kinematic SSI. However, for elastic foundations, the higher-order

modes are not filtered out, and therefore, they should be included in the SSI analysis. If only a limited number of incoherent spatial modes are used, then, the incoherent SSI response could be highly inaccurate (Ghiocel, 2014). Figure 3 shows the vertical ISRS computed at the basemat of a typical NI complex using the SRSS approach (Short, Hardy, Merz and Johnson, 2007) with 20 and 40 incoherent modes, respec-

tively. The ISRS results indicate an underestimation of the ISRS peak amplitude of up to 65% for 20 incoherent modes and up to 25% for 40 incoherent modes in comparison with the mean ISRS computed using the reference stochastic simulation approach. In vertical direction, all foundations appears to be flexible due to the reduced stiffness of their baselabs for the out-of-plane bending.

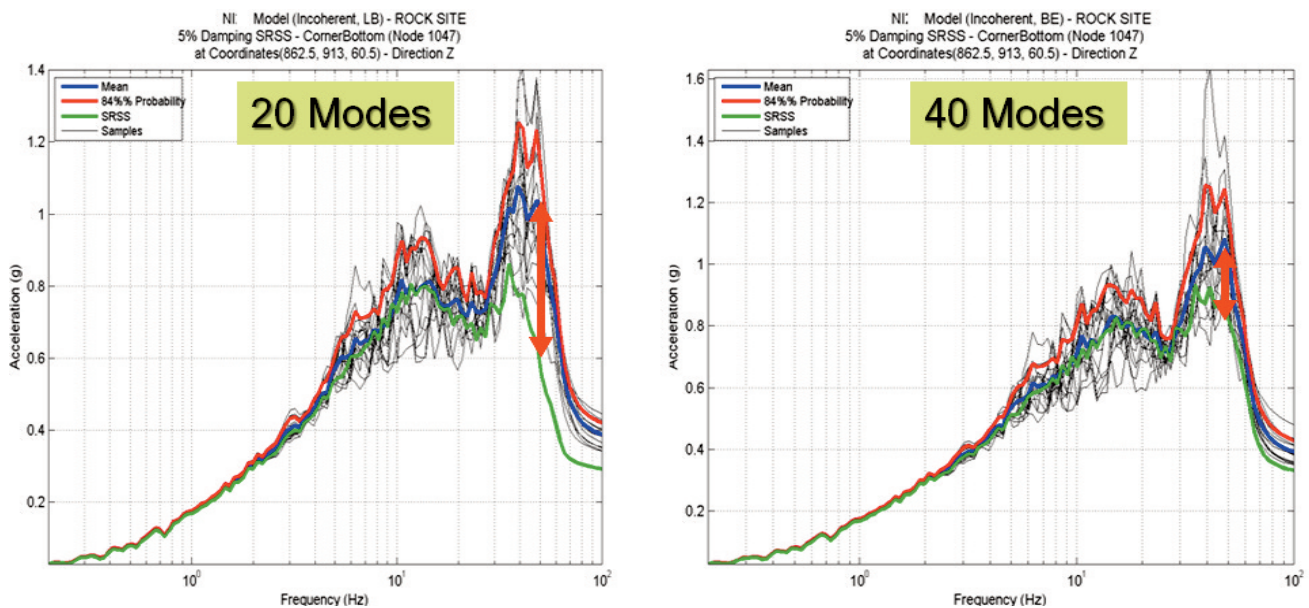


**Figure 3** Effect of Number of Incoherent Modes on the ISRS Computation Using SRSS Approach

In US, EPRI investigated different incoherent SSI approaches for their application to the new nuclear power plant design within the United States (Short, Hardy, Merz and Johnson, 2007). Stochastic approach is based on simulating incoherent motion field random realizations. Using Stochastic Simulation (Simulation Mean in EPRI studies) algorithm, a set of incoherent motion random samples are generated at the SSI interaction nodes. For each incoherent motion sample, an incoherent SSI analysis is performed. The mean SSI response is obtained by statistical averaging of SSI response random samples. Deterministic approaches used were based on using simple superposition rules of random incoherent mode effects, such as the Algebraic Sum (AS in 2007 EPRI studies) or the Square-Root of the Sum of Square (SRSS in 2007 EPRI studies), to approximate the

mean incoherent SSI motion. To limit the computational efforts, SRSS is typically used with a reduced number of incoherent modes, and, therefore, applicable only to very-very stiff foundations. It should be noted that the EPRI validated incoherent SSI approaches are based on the simplification assumption that the incoherent complex motion phases are zero, or very close to zero, and therefore they are neglected. From a physical modeling point of view this not true, but, this makes the EPRI validated approaches be conservative with respect to the incoherent ISRS response computation. The zero-phase assumption produces a slightly conservative solution for simple stick SSI models as the AP1000 stick SSI model used in the 2007 EPRI validation studies (Short, Hardy, Merz and Johnson, 2007). More recent EDF studies (Zentner and Devesa, 2011) also used a deterministic SSI

approach based on the zero-phase assumption that was implemented in the Code\_Aster software, which is theoretically equivalent to the AS approach in the EPRI studies. However, the zero-phase assumption can provide sometimes a biased solution, especially for large-size elastic foundation models (Ghiocel, 2014). A significant practical limitation of the EPRI zero-phase approaches is that the SSI response time histories are not usable for multiple time-history analysis of the secondary systems. The cross-correlation between SSI motions at different locations are largely affected by zeroing the SSI motion phases. In the ACS SASSI code (2015), on purpose, if the complex response phase-adjustment is selected, then no acceleration or relative displacement time-history can be computed. This is to protect analyst from obtaining inaccurate results.

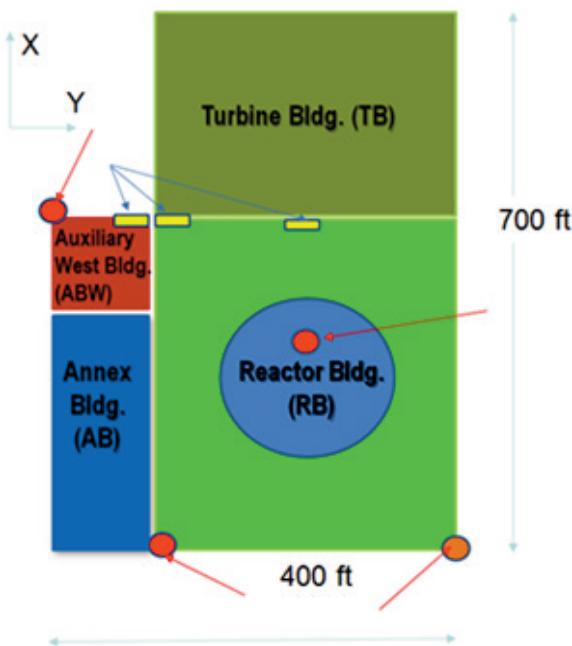


Figure 4 SSSI Model 1 of RB-TB-AB-ABW

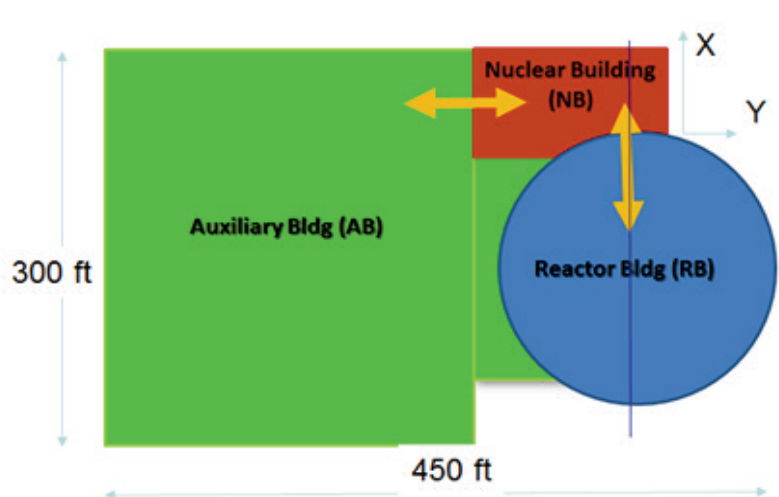


Figure 5 SSSI Model 2 of RB-AB-NB

**CASE STUDIES**

In this paper two incoherent SSSI analysis case studies. Both standalone SSI and SSSI FE models were considered. The two SSSI models include different NPP layouts as shown in Figures 4 and 5. The SSSI Model 1 includes four nuclear buildings, Reactor Building complex, Turbine Building complex and two Annex Buildings (RB, TB, AB and ABW) over a horizontal area of about 400ft x 700ft. The SSSI Model 2, includes three nuclear buildings, Reactor Building structure, Auxiliary Building and another Nuclear Building (RB, AB and NB) over a horizontal area of about 300ft x 450ft. It should be noted that in the SSSI Model 1 all buildings are surface or shallowly embedded. In contrast, in the SSSI Model 2, the RB structure is deeply embedded, while AB and NB structures are only shallowly embedded. For all coherent and incoherent SSI and SSSI analyses the ACS SASSI software (2015) was used.

**SSSI Model 1 RB-TB-AB-ABW:**

This SSSI model was used for two soil site conditions, named "Soil" and "Rock", which are shown in Figures 6 and 7. The incoherent SSSI analysis used the 2007 Abrahamson generic coherency function models for soil and rock sites. The seismic input ZPGA was 0.30g for the Soil site and 0.50g for Rock site as illustrated by the spectral plots in Figure 6. Figures 8 and 9 show the coherent and incoherent 5% damping ISRS computed at the top of the ABW structure for the standalone SSI model and the SSSI coupled model for both the Rock site (Figure 8) and Soil site (Figure 9). As expected, for the Rock site the SSSI effects are minimal, while the incoherency effects are significant. However, for the Soil site, in Y-direction, the SSSI effects show that basically the dynamic behaviour of the ABW structure is totally changed due to the adjacent RB complex. The ABW ISRS peak at 4 Hz is

split in two peaks at slightly lower and higher frequencies due to the SSSI coupling with the RB complex. Also, the incoherency effects amplify the coherent SSSI ISRS peak amplitude at @ 6 Hz by about 25-30%. In the vertical Z-direction, the SSSI effects are also quite visible. Figure 10 shows the effects of motion incoherency on the SSSI effects of the RB complex. The plots show the ISRS computed at a critical location at the top of the Internal Structure (IS). As expected, for the Rock site (upper plots) the SSSI effects are minimal, while the incoherency effects are significant. However, for the Soil site (lower plots), in the Y-direction, the SSSI effects show that basically the dynamic behaviour of the RB complex structure is significantly changed @ 6 Hz frequency. The new ISRS peak at @ 6 Hz in Figure 10 occurs for incoherent SSSI and does not exist for coherent SSSI. The new ISRS peak is due to the fact that the

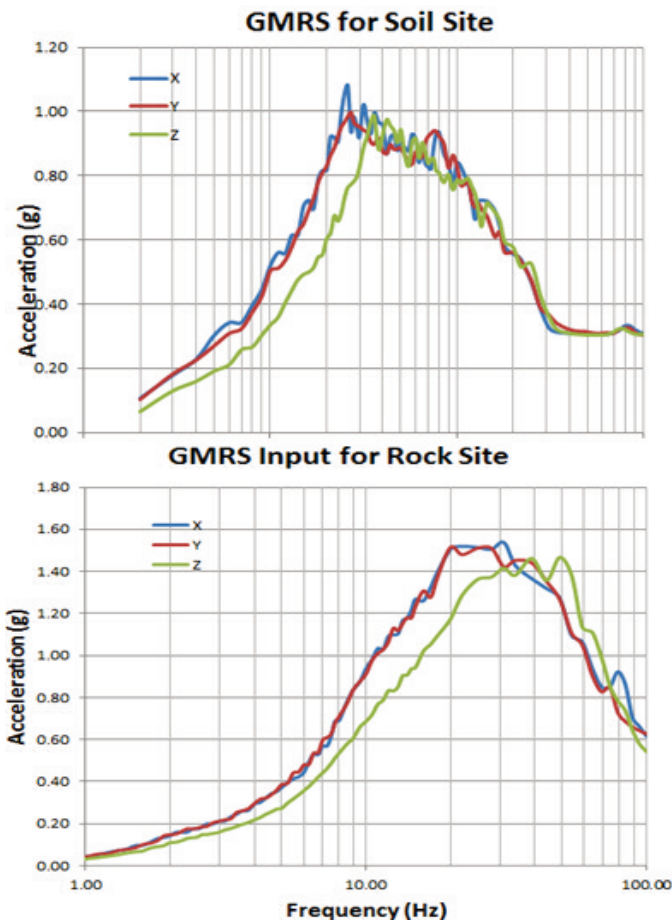


Figure 6 Site-Specific GMRS Inputs

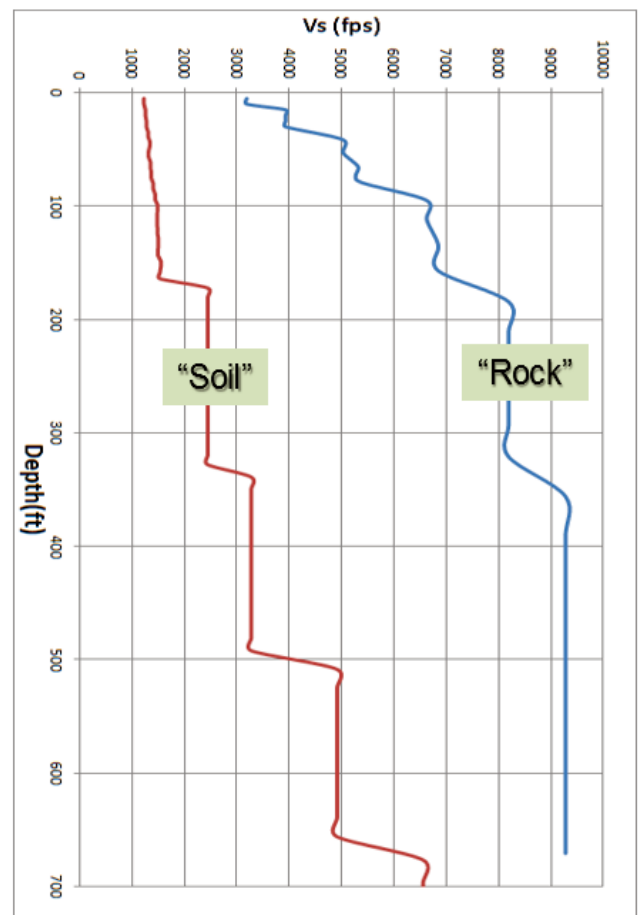
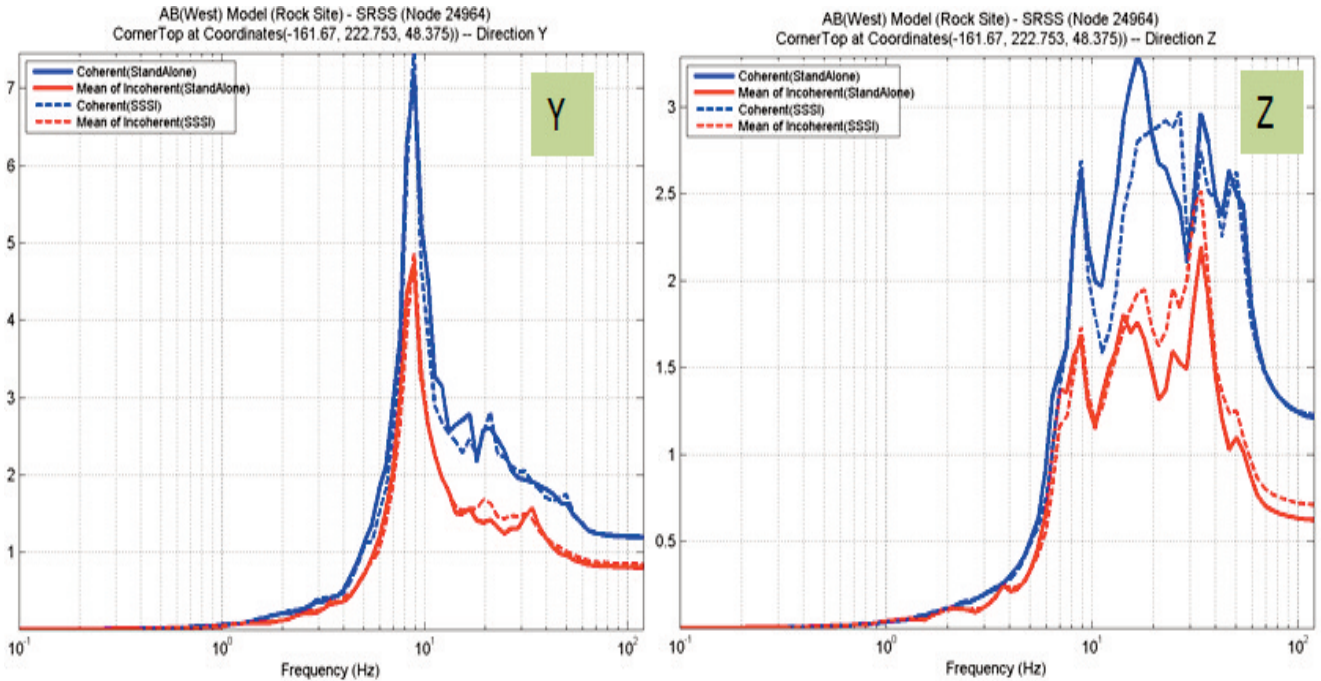


Figure 7 Vs Soil Profiles and Rock Site Conditions



**Figure 8** Coherent and (Mean) Incoherent ISRS Based on ABW SSI and SSSI Models for Rock Site

incoherent motion excites some of the RB structure local and antisymmetric vibration modes which are “dormant” under coherent

SSSI. The incoherent SSSI ISRS peak amplitude at @ 6 Hz is about 100% higher than the coherent SSSI ISRS amplitude at same

frequency. *This is an important practical aspect for the NPP seismic SSI analysis that is not fully recognized at this time.*

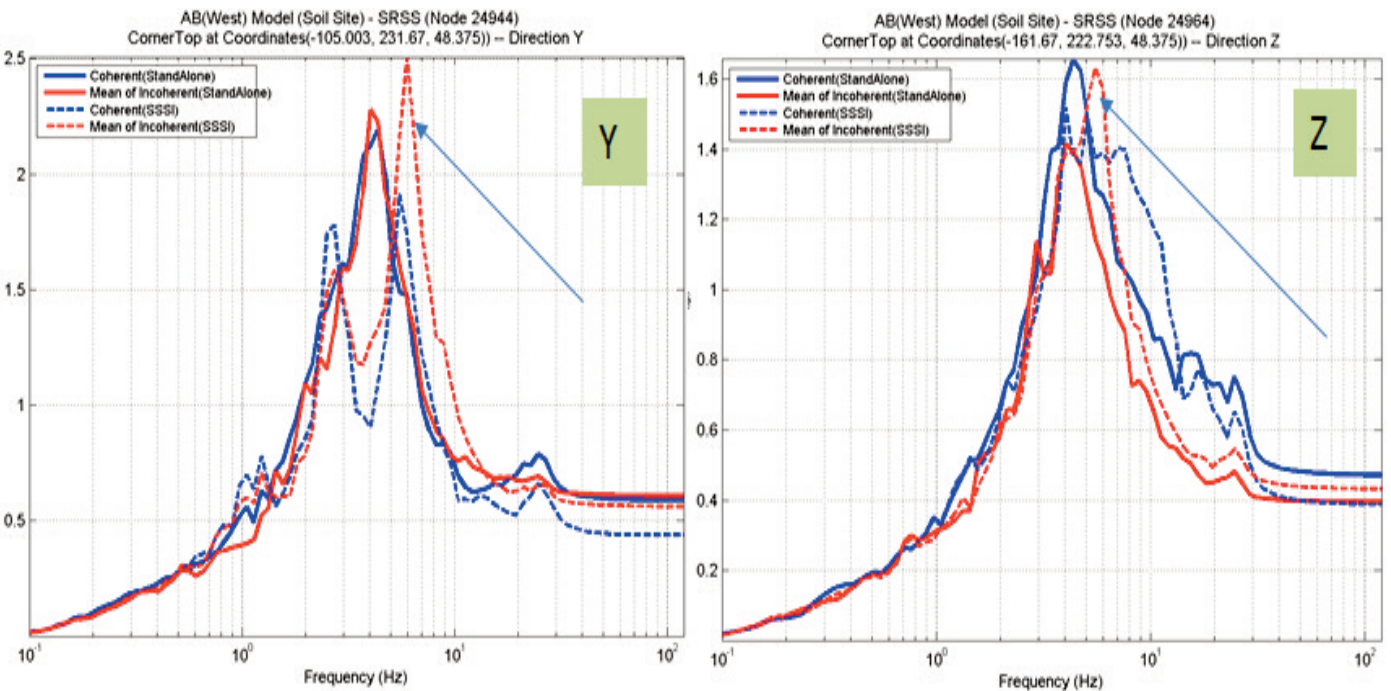


**Figure 9** Coherent and (Mean) Incoherent ISRS Based on ABW SSI and SSSI Models for Soil Site

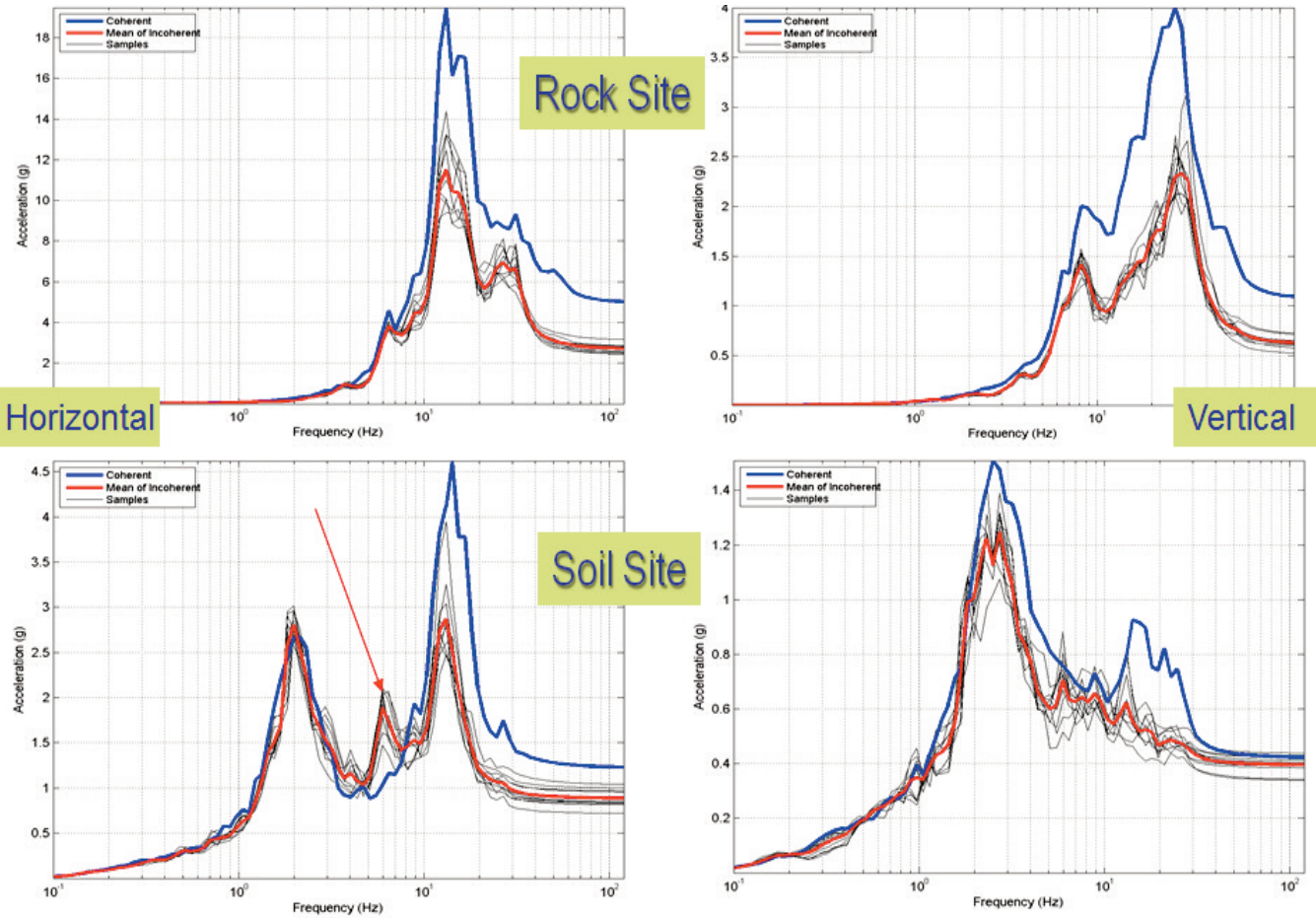


**Figure 10** Coherent and (Mean) Incoherent ISRS Based on RB SSSI Models for Rock and Soil

Figures 11 and 12 show the out-of-plane (o-p) bending moments in the ABW and RB complex walls computed in the vicinity of the neighboring building based on the SSSI analyses. The coherent o-p bending moments

are plotted with blue color, while the (mean) incoherent o-p bending moments are plotted with brown color. Figure 11 shows that for the Rock site for the incoherent SSSI there is an increase of the o-p moments for the

embedment part of the walls, and a reduction above ground level. However, for the Soil site, the o-p moment increases due to motion incoherency are extremely large, well above 100%.

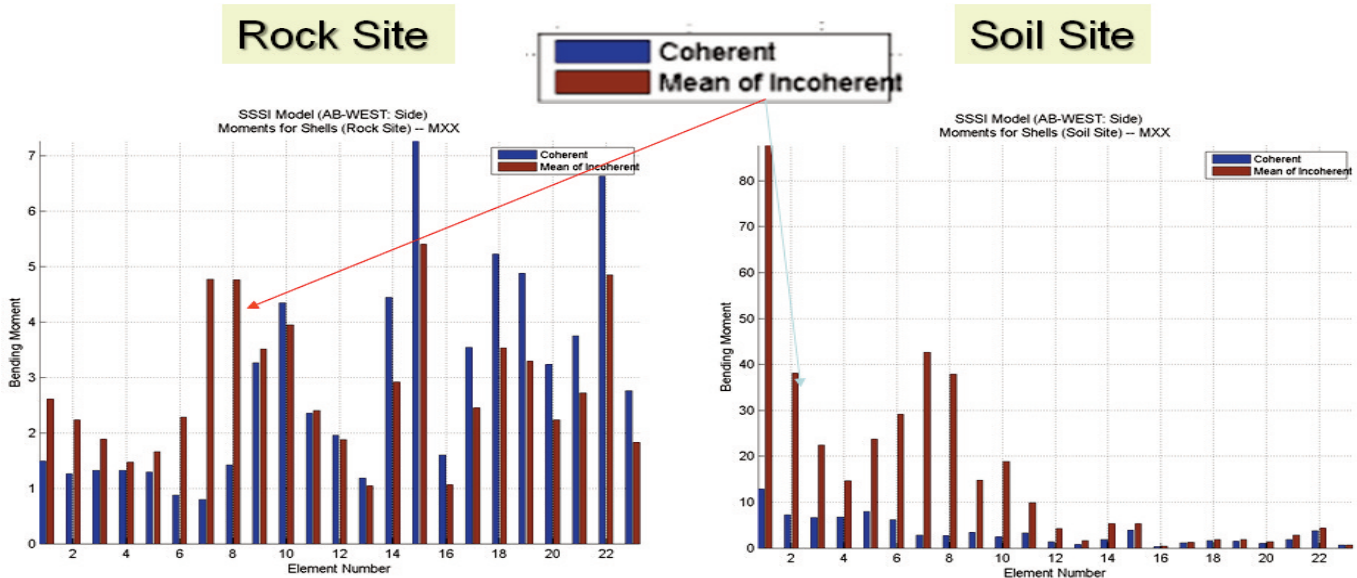


**Figure 11** Out-of-Plane Moments in ABW Walls in Vicinity of RB Complex (From Foundation to Roof)

Figure 12 indicates that for the RB walls, for the Soil site, the incoherent SSSI effects are much larger than the coherent

SSSI effects. *This important aspect was often overlooked in the past due to the lack of*

*sufficient reliable and efficient computational SSI modelling and analysis capabilities.*

**SSSI Model 2 RB-AB-NB:**

The investigated case study is for site with a deep soil profile having the soil Vs values varying in the 800-1500 fps range for the top 500ft depth. The seismic input motion is based on a site-specific FIRS input at the basement of the RB structure at the depth of about 50ft. The NB and AB have shallower embedments of about 20ft

depth. The site-specific in-column FIRS motions to be used for SSI and SSSI analyses were obtained based on site response analysis with the outcrop FIRS motion as input. Figure 13 shows a comparison between the 5% damping ISRS computed at the top of the NB structure based on standalone SSI and SSSI analyses for coherent inputs. It

should be noted that the SSSI NB ISRS are reduced in X-direction due to the NB base motion constraint produced by the presence of the adjacent deeply embedded RB structure, and amplified in the Y-direction due to the influence of the torsional motion of the large-size AB structure with very stiff basement that has significant mass eccentricities.

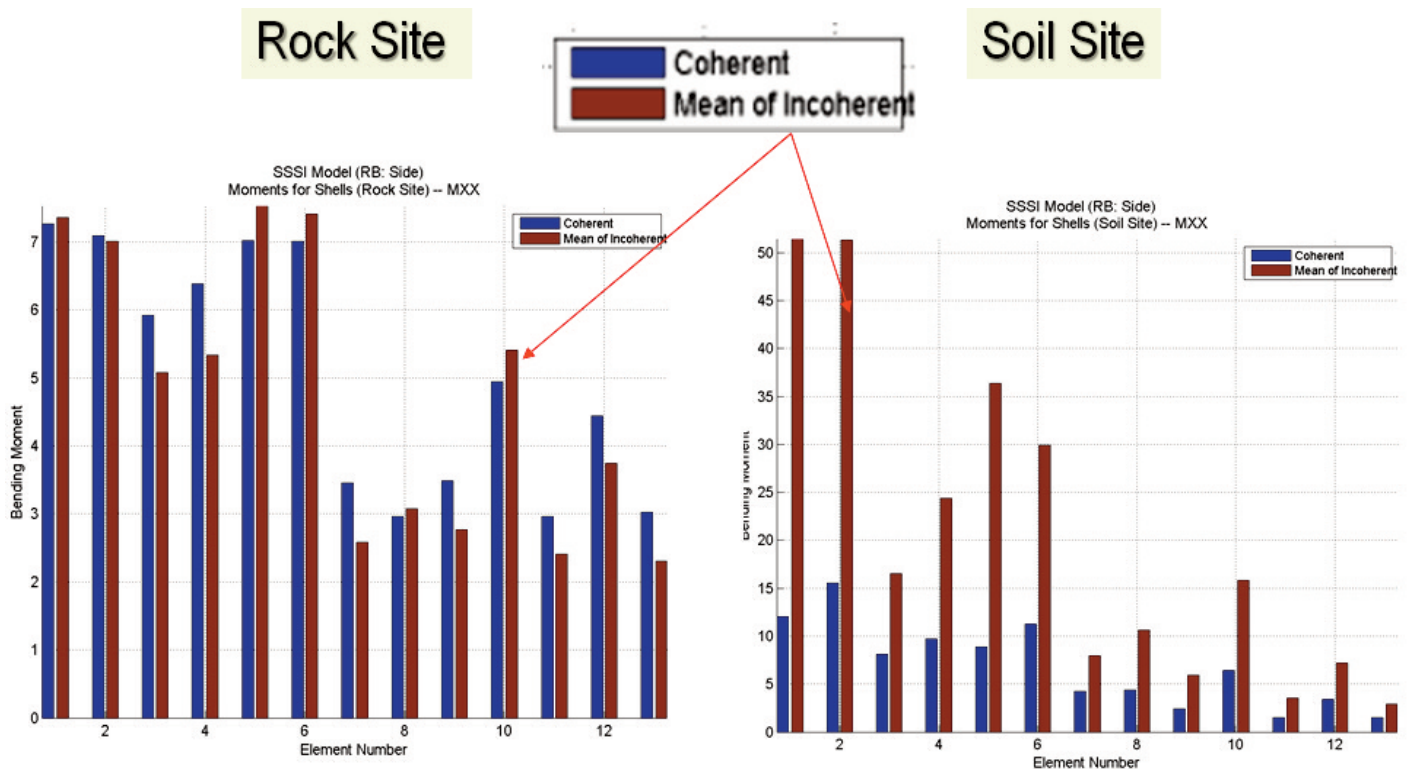


**Figure 12** Out-of-Plane Moments in RB Walls in Vicinity of ABW (From Foundation to Roof)

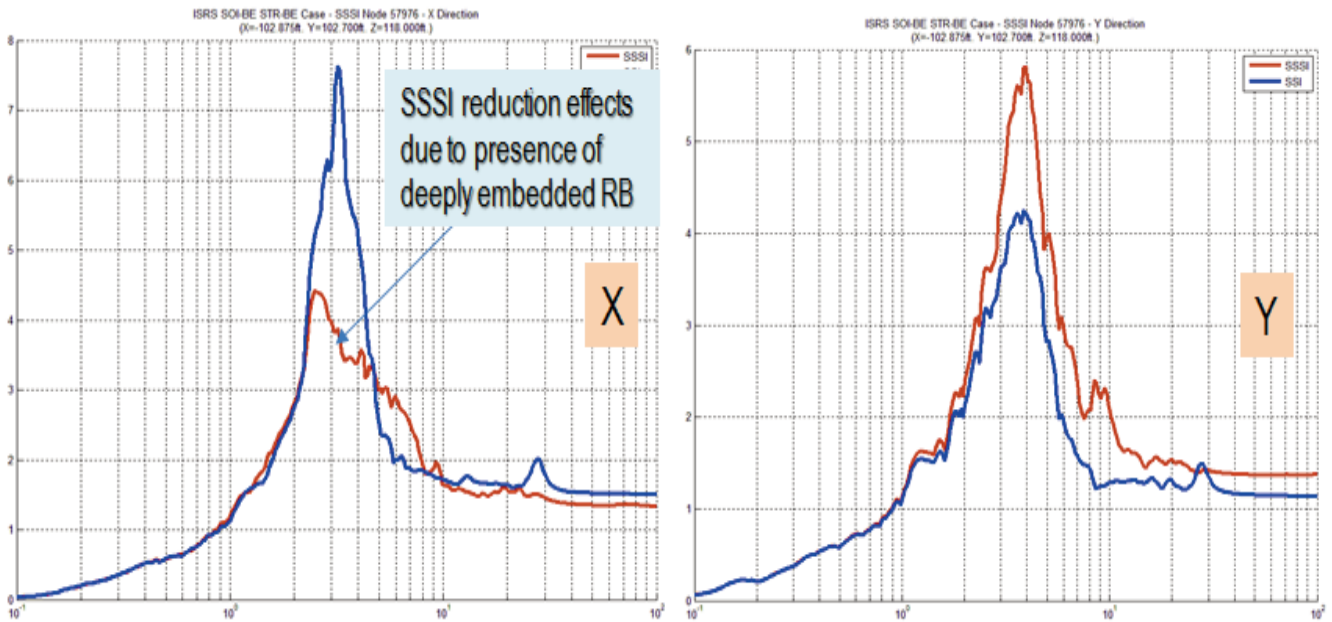


**Figure 13** Horizontal ISRS for NB Standalone SSI Model (blue line) and SSSI Model (red line)

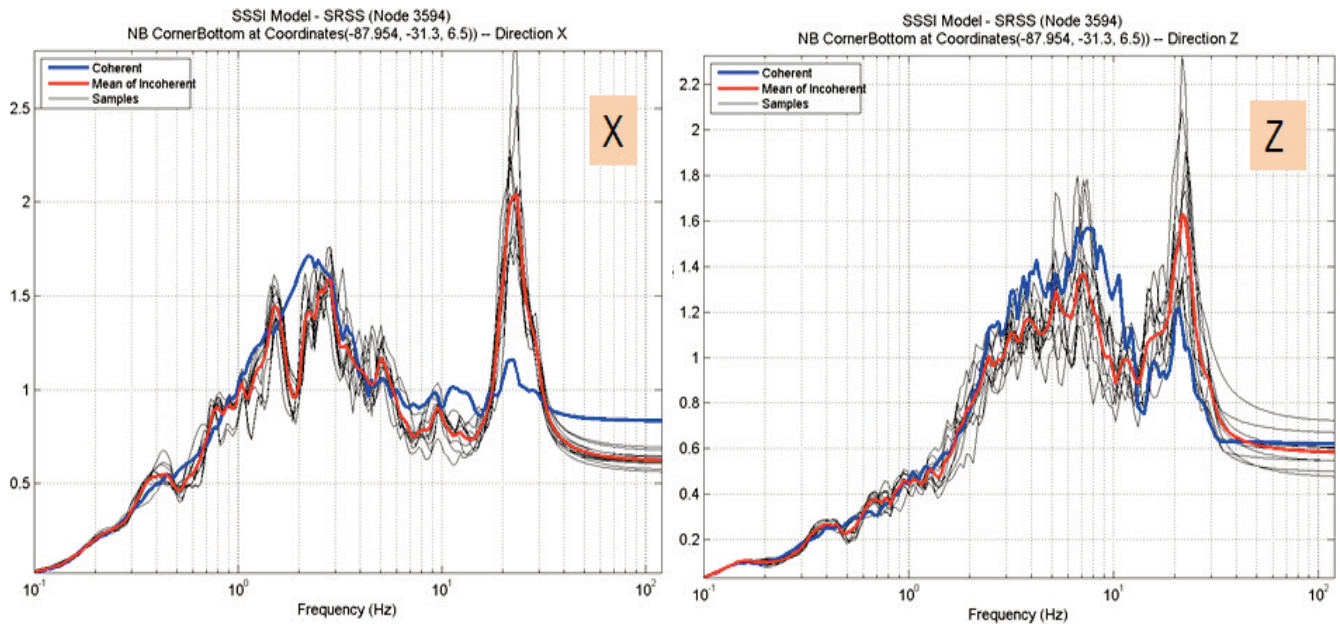


**Figure 14** Horizontal and Vertical Coherent ISRS (blue) and (Mean) Incoherent ISRS (red) for NB SSSI Model at Basemat Corner near RB Foundation

Figure 14 shows a comparison of the coherent ISRS and incoherent ISRS computed from the SSSI analysis at the NB basemat corner near the RB foundation. The incoherent SSSI effects

were the largest for this ISRS location. The high-frequency SSSI mode at @ 20.0 Hz that was “dormant” for the coherent SSSI analysis is largely amplified, about 100%, for the

incoherent SSSI analysis. The dynamic coupling between the NB structure and RB structure is significantly excited by the incoherent motion.

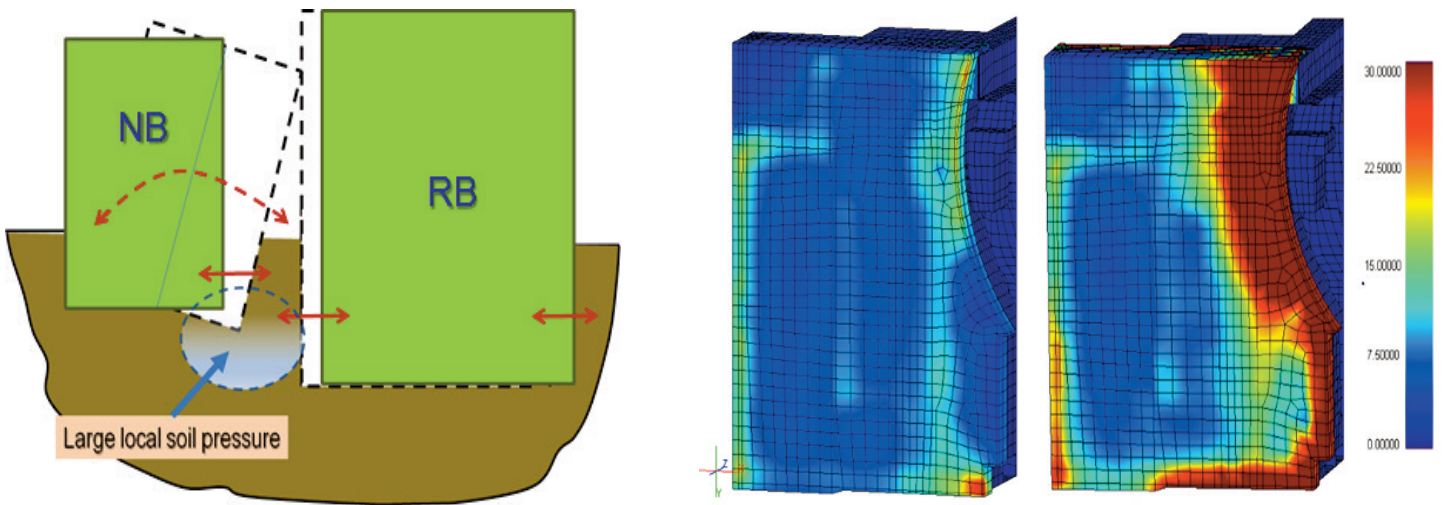


**Figure 15** Seismic Soil Pressures on NB Baseslab for Standalone SSI Model (left) and SSSI (right)

The seismic soil pressures on the NB baseslab computed based the standalone SSI and SSSI analysis are shown in Figure 15. The seismic pressure contour plots show large soil pressure amplifications at

the edge of the NB baseslab close to the RB foundation. The RB foundation restricts the motion of the NB foundation. For such situation, it is possible that the surrounding soil nonlinear local behavior might play a

significant role on SSSI effects, especially for incoherent motions that could produce larger amplification of scattered waves. Additional ACS SASSI nonlinear analyses are underway.

**CONCLUSIONS**

The paper investigates the seismic motion incoherency effects on the SSI and SSSI responses using a state-of-the-art stochastic FEA modeling via stochastic simulation. It is shown the motion incoherency could play a significant role for SSSI effects, especially for soft soil sites by largely amplifying the ISRS and the basement soil pressures (and bending moments).

**REFERENCES**

Ghiocel D, M. (2014). "Effects of Seismic Motion Incoherency on SSI and SSSI

Responses of Nuclear Structures for Different Soil Site Conditions", U.S. Department of Energy, DOE Natural Phenomena Hazards Meeting, Session on "Soil-Structure Interaction", Germantown, MD, USA, October 21-22 <http://www.energy.gov/sites/prod/files/2015/05/f22/DOE-NH-Motion-Incoherency-SSI-SSSI-Oct-21-2014.pdf>

Ghiocel Predictive Technologies, Inc. (2015). "ACS SASSI - An Advanced Computational Software for 3D Dynamic Analyses Including SSI

Effects", ACS SASSI Version 3.0 Manuals, March 31, [http://www.ghiocel-tech.com/enggTools/ACS%20SASSI\\_V300\\_Brief\\_Description\\_Dec\\_31\\_2014.pdf](http://www.ghiocel-tech.com/enggTools/ACS%20SASSI_V300_Brief_Description_Dec_31_2014.pdf)

Short, S.A., G.S. Hardy, K.L. Merz, and J.J. Johnson (2007). "Validation of CLASSI and SASSI to Treat Seismic Wave Incoherence in SSI Analysis of Nuclear Power Plant Structures", Electric Power Research Institute, Palo Alto, CA and US Department of Energy, Germantown, MD, Report No. TR-1015111, November

## RANDOM VIBRATION THEORY (RVT) BASED SSSI ANALYSIS FOR NUCLEAR STRUCTURES FOUNDED ON SOIL AND ROCK SITES

### ABSTRACT

The RVT SSI approach is based on the random vibration theory (RVT) applicable to linear time-invariant dynamic systems excited by Gaussian processes. The advantages of RVT are related to the analysts' convenience for not using input acceleration time histories for the SSI analysis. The RVT SSI approach uses the direct analytical relationship between the power spectral density (PSD) functions and the response spectra (RS). Three different analytical formulations for the PSD-RS transformation were considered. The three analytical formulations were implemented using the acceleration, velocity and displacement ground response spectra as inputs. The RVT SSI analysis results include two case studies: i) the EPRI AP1000 NI stick model and ii) a deeply embedded SMR FE shell model. The in-structure response spectra (ISRS) computed using the RVT SSI analysis were compared with the "reference" ISRS computed by traditional SSI analysis using input acceleration time histories. The "reference" ISRS were computed using either deterministic SSI or probabilistic SSI with randomized seismic inputs based on the recommendations of the new ASCE 04-2015 standard. Both rock and soil sites are considered. It is shown that the RVT SSI analysis results are quite sensitive depending on the particularity of the analytical approach used for computing the RS from the PSD functions. Conclusions and guidelines on the application of the RVT SSI approach are provided.

### RANDOM VIBRATION THEORY SSI APPROACH

The random vibration theory (RVT) approach uses the analytical relationship between the power spectral density functions and the response spectra. The RVT approach is based on the linear random vibration theory applicable to linear time-invariant dynamic systems excited by Gaussian stationary processes. For such systems, the dynamic responses are also Gaussian processes. The RVT approach has the advantage that computes the SSI response of a deterministic SSI system using directly the ground response spectra (GRS) input without the need of developing compatible input acceleration time histories. Herein, the RVT approach is applied in conjunction with the SSI methodology based on complex frequency response method where the input and outputs are defined by their power spectral density functions (PSD). Assuming that the seismic input and SSI response motions are realizations of a Gaussian stationary process, the RVT approach computes directly the ISRS any location within the structure from the PSD functions

associated to the SSI response motions. To compute RS from PSD, the maximum of the stochastic response is determined by solving the "first-passage problem" of a single-degree of freedom (SDOF) oscillator under a Gaussian process input motion that represents the SSI response motion at the selected location. The implemented RVT SSI approaches include several options related to the PSD-RS transformation. These options are related to the stochastic approximation models used for computing the maximum SSI response of a SDOF system over a time period  $T$ , i.e. during the earthquake intense motion time interval. The maximum SSI response of the SDOF system that represents the RS amplitude can be expressed by using peak factors that are applied to the stochastic motion standard deviation (RMS). These quantities depend on the duration  $T$ , the mean crossing rate of the motion and probability level associated to the maximum response ("first passage problem"). The "first passage problem" consists of computing the maximum value of the stochastic response for a given motion duration,  $T$ . The motion duration  $T$  should correspond to the

stationary, intense part of the motion that can be defined as the time for the accumulated energy of the input motion to increase from 5% to 75% of its total energy (Arias Intensity). The basic RVT relationship applicable to the RVT SSI analysis in frequency domain relates the SDOF oscillator response motion PSD  $S_x(\omega)$  at location of interest to the input ground motion PSD  $S_u(\omega)$ :

$$S_x(\omega) = |H_{SSI}(\omega)|^2 |H_o(\omega)|^2 S_u(\omega) \quad (1)$$

The maximum extreme amplitude valued of the SDOF system motion represents the RS amplitude. The RVT SSI analysis flowchart for computing acceleration response spectra (ARS) at a selected location is shown in Figure 1. The input is the input ground response spectra (GRS) and the end output is the ARS at the location of interest within structure. There are three major computational steps: 1) Compute the input GPSD from input GRS, 2) Compute SSI response PSD by convolving the input GPSD computed in Step 1 with the square amplitudes of the SSI system and the SDOF system transfer functions, consistent with equation 1, and 3) Compute the response ARS at given location based on the SSI response PSD computed in Step 2.

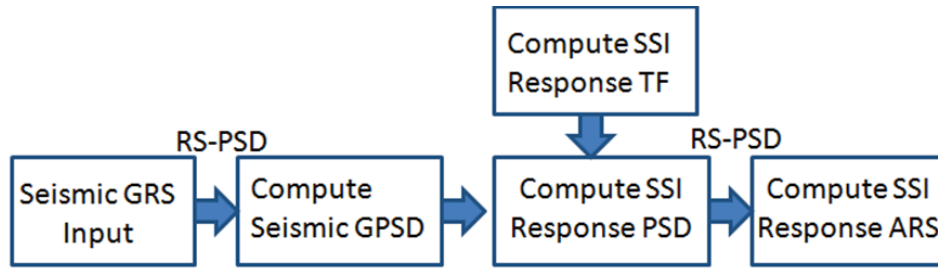


Figure 1 RVT-based Flowchart for ISRS Computations

To compute the ARS that is the maximum acceleration response of the SDOF mounted on the structure,  $X_{\max,P}$ , for a given non-exceedance probability  $P$ , first, the response peak factor  $p_P$  that corresponds to the given probability level  $P$  should be computed, and then, applied to the standard deviation,  $\sigma_X$ , of the Gaussian process  $X$ :

$$X_{\max,P} = p_P \sigma_X \quad (2)$$

There are also approaches that use mean peak factors, not probability level peak factors. To compute the mean maximum response,  $\bar{X}_{\max}$ , the mean response peak factor  $p$  and the standard deviation  $\sigma_X$  of the process  $X$  need to be determined. Then, mean maximum response is computed simply  $\bar{X}_{\max} = p \sigma_X$  (3) where

$$\sigma_X^2 = \int_{-\infty}^{\infty} S_X(\omega) d\omega \text{ in which } S_X(\omega) \text{ is the PSD of the}$$

stochastic response.

Similarly, using a peak factor  $q$ , the standard deviation of maximum response  $\sigma_{X_{\max}}$  can be computed by

$$\sigma_{X_{\max}} = q \sigma_X \quad (4)$$

Herein, three analytical formulations were used to compute the response peak factors:

1) **MK or MK-UK Approach:** Maharaj Kaul-Unruh-Kana formulation uses the response peak factor given the non-exceedance probability  $P$  (Unruh and Kana, 1981):

$$p = \left[ -2 \ln \left( \left( -\frac{\pi}{\omega_0 T} \right) \ln(P) \right) \right]^{1/2} \quad (5)$$

where  $\omega_0$  is the circular frequency of interest for maximum response computation. It should be noted that the MK-UK formulation provides directly the probability-level maximum response for a given non-exceedance probability  $P$ .

2) **AD Approach:** Alan Davenport formulation (AD) uses peak factors,  $p$  for the mean of the maximum response (Davenport, 1964) and  $q$  for the standard deviation the maximum response (Igusa and Der Kiureghian, 1983):

$$p = \sqrt{2 \ln(v_0 T)} + \frac{0.5772}{\sqrt{2 \ln(v_0 T)}} \quad (6)$$

$$q = \frac{1.2}{\sqrt{2 \ln(v_0 T)}} - \left[ \frac{5.4}{13 + (2 \ln(v_0 T))^{3.2}} \right] \quad (7)$$

where the mean crossing rate is defined by  $v_0 = \frac{1}{\pi} \sqrt{\frac{\lambda_0}{\lambda_2}}$

in which  $\lambda_0 = \sigma_X^2 = \int_{-\infty}^{\infty} S_X(\omega) d\omega$  and

$$\lambda_2 = \sigma_{\dot{X}}^2 = \int_{-\infty}^{\infty} \omega^2 S_X(\omega) d\omega.$$

3) **AD-DK Approach.** Alan Davenport-Der Kiureghian formulation (AD-DK) uses peak factors,  $p$  for the mean of the maximum response corrected for the motion spectral shape and  $q$  for the standard deviation the maximum response (Igusa and Der Kiureghian, 1983):

$$p = \sqrt{2 \ln(v_e T)} + \frac{0.5772}{\sqrt{2 \ln(v_e T)}} \quad (8)$$

$$q = \frac{1.2}{\sqrt{2 \ln(v_e T)}} - \left[ \frac{5.4}{13 + (2 \ln(v_e T))^{3.2}} \right] \quad (9)$$

$$\text{where } v_e T = \begin{cases} \max(2.1, 2\delta v_0 T) & ; 0 < \delta \leq 0.1 \\ (1.63\delta^{0.45} - 0.38)v_0 T & ; 0.1 < \delta < 0.69 \\ v_0 T & ; 0.69 \leq \delta < 1 \end{cases} \quad (10)$$

in which the frequency content shape factor is  $\delta = \sqrt{1 - \frac{\lambda_1^2}{\lambda_0 \lambda_2}}$

in which  $\lambda_1 = \int_{-\infty}^{\infty} \omega S_X(\omega) d\omega$

## CASE STUDIES

The RVT-based SSI analysis results include two case studies: i) the surface EPRI AP1000 NI stick model and ii) a deeply embedded SMR shell FE model. Both rock and soft soil site conditions were considered.

### Surface EPRI AP1000 Stick Model:

The surface EPRI AP1000 SSI stick model was considered with a deep soft soil site ( $V_s = 1,000$  fps) and a uniform rock site ( $V_s = 6,000$  fps). Herein, the mean ISRS computed using the RVT SSI approach and probabilistic SSI approach. The probabilistic SSI approach was based on 30 randomized LHS simulations of the seismic input as recommended by the ASCE 04-2015 standard (Section 5.5). The site-specific GRS spectral shapes were randomized as described in a separate paper (Ghiocel, 2015). No random variability was assumed for soil profile or structural properties (assumed with uncracked concrete and 4% damping). Figures 2 and 3 show the 5% damping ISRS computed at two locations, at basemat and higher elevations, within the AP1000 NI stick using the Acceleration Method for the rock and soil site, respectively. The RVT ISRS were computed using i) a

single RVT run for the mean GRS input, and ii) 30 RVT runs for the 30 LHS randomized spectral shape samples of the GRS input. Figure 2 results, obtained for the rock site, show that mean ISRS computed using RVT compare quite reasonably with the "reference" mean ISRS computed using the 30 LHS randomized GRS input samples. It should be noted that for the higher elevation location the mean RVT ISRS are 15-20% different than the reference mean ISRS. The MK-UK and AD provide higher ISRS peaks, while AD-DK provides lower ISRS peaks than the reference ISRS. Figure 3 results, obtained for the soft soil site, show that mean ISRS computed using RVT are slightly lower, by up to 10-15%, than the reference mean ISRS. The most accurate results are obtained for MK-UK and AD using 30 RVT runs for the 30 GRS input samples rather than a single RVT run for the mean GRS input. It should also be noted that in the high frequency range the RVT ISRS are always higher by 20-30% than the reference mean ISRS.

Figures 4 and 5 repeat the same SSI results as in Figures 2 and 3 using the Displacement Method. The ISRS

comparisons for the rock and soil sites in Figures 4 and 5 show identical with the ISRS shown in Figures 2 and 3, with the exception of the mean ISRS peaks at 9 Hz and 13 Hz for the higher elevation location which are fully truncated by the RVT approach for the soil site. This ISRS peak truncation of the 3rd and 4th ISRS peak at the higher elevation location appears as a surprise, given the good behaviour of the RVT Displacement Method for the other frequency ranges and the computed RVT ISRS at the basemat level. The RVT Displacement Method follows the detailed algorithm description provided in the paper referenced by the new ASCE 04-2015 standard for the RVT SSI approach. Thus, the Figures 4 and 5 results indicates that for the soft soil sites the RVT Displacement Methods may fail to predict correctly some ISRS peaks in the mid frequency range. It was observed that the artificial ISRS peak truncation in the Displacement Method happens not always, and only for ISRS that have more than one single dominant spectral peak. It happens most likely to the higher frequency ISRS peaks. For some other case studies the ISRS were OK, especially for surface models.

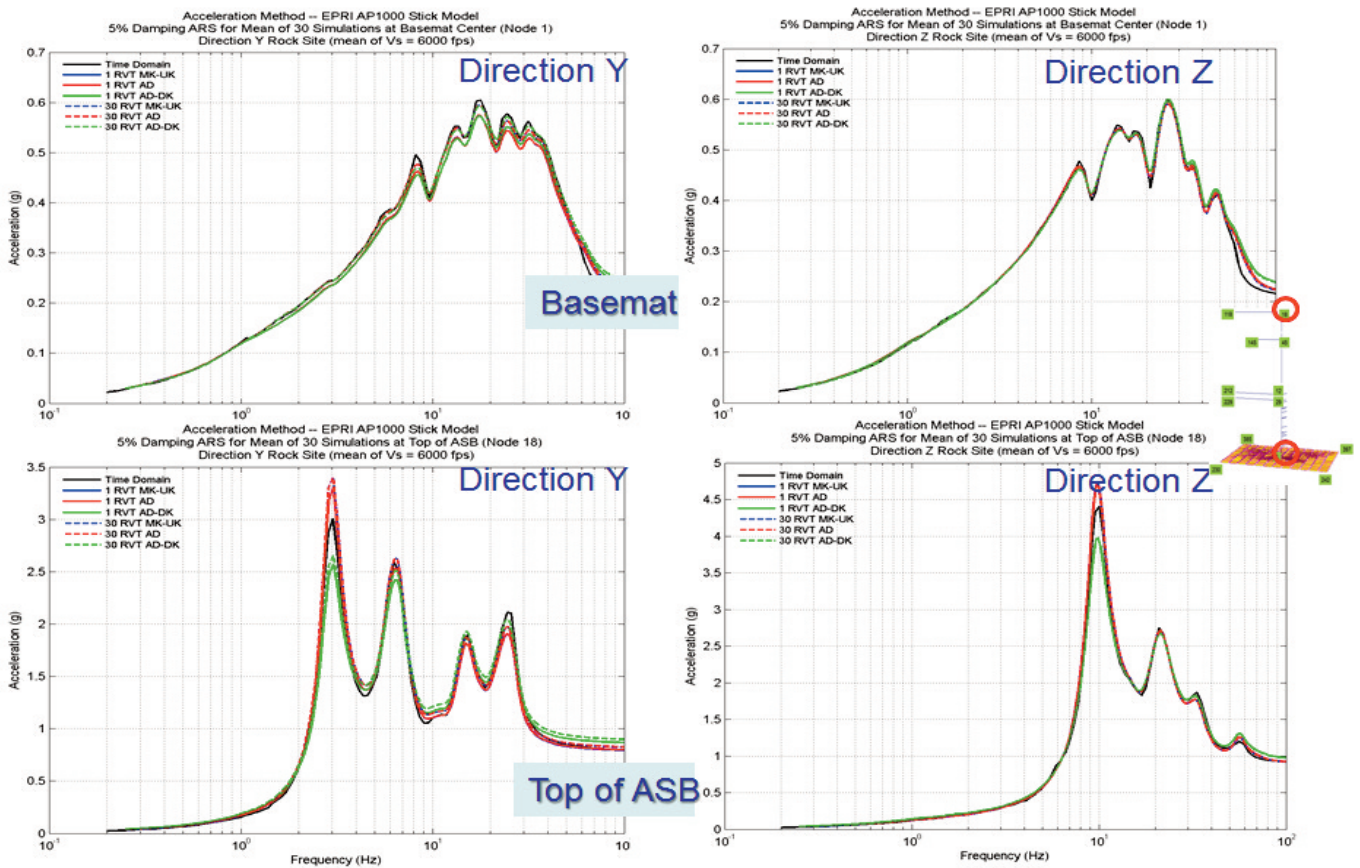


Figure 2 Probabilistic Mean ISRS and RVT ISRS at for Rock Site Using Acceleration Method

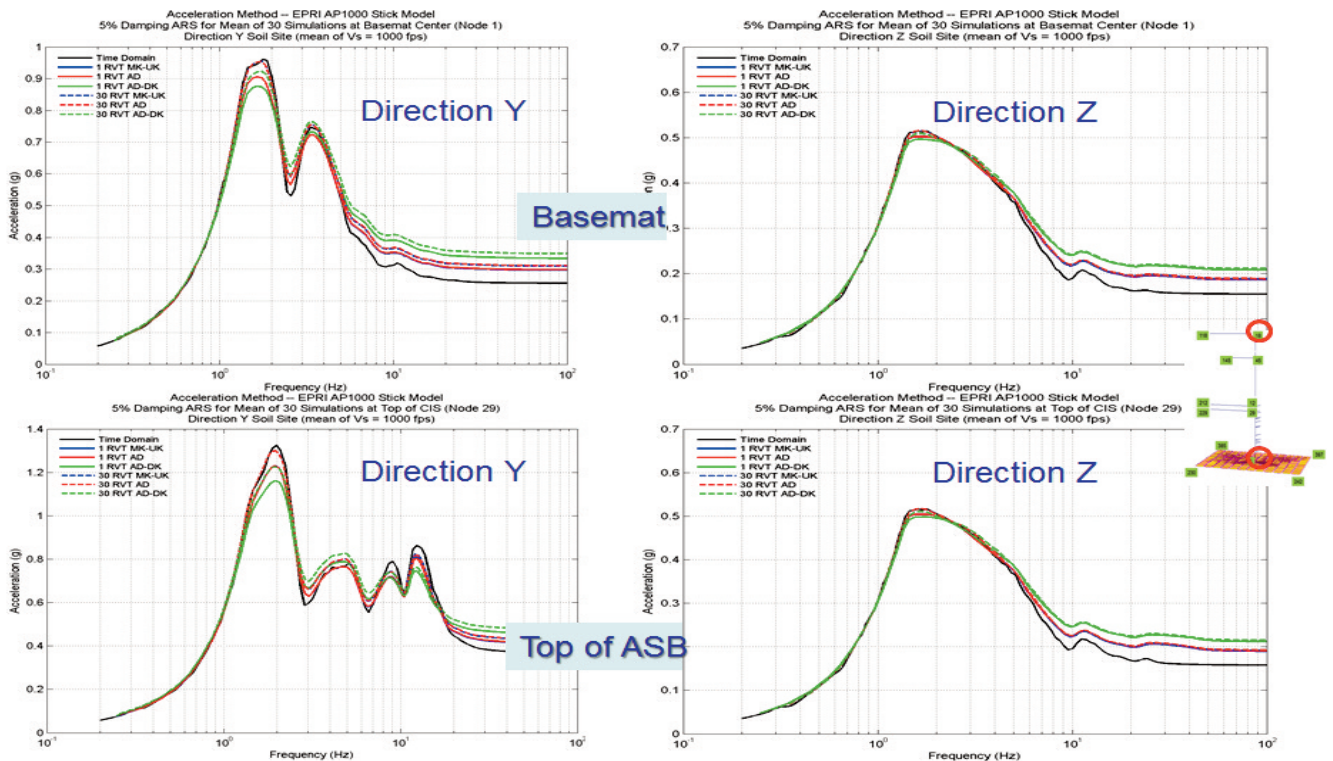


Figure 3 Probabilistic Mean ISRS and RVT ISRS at for Rock Site Using Acceleration Method

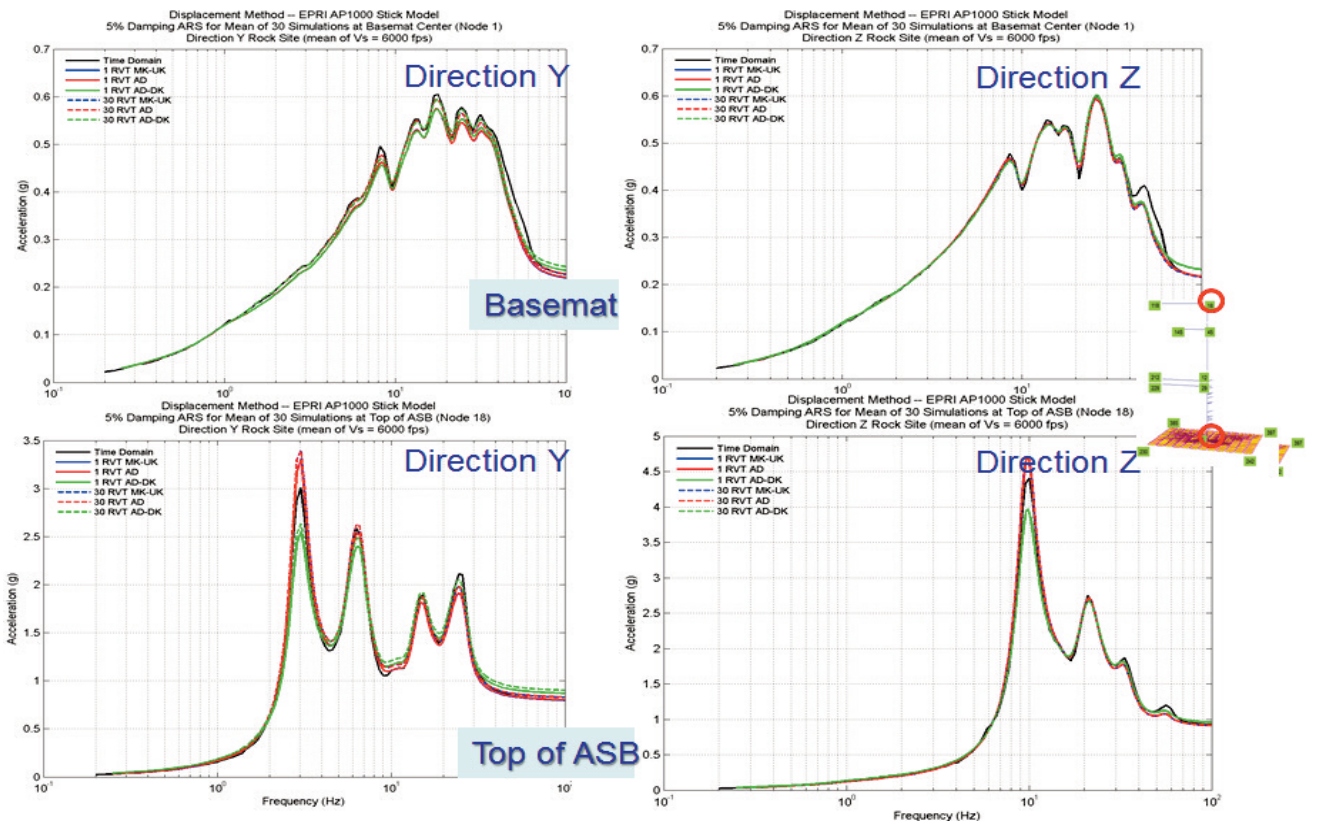


Figure 4 Probabilistic Mean ISRS and RVT ISRS at for Rock Site Using Displacement Method

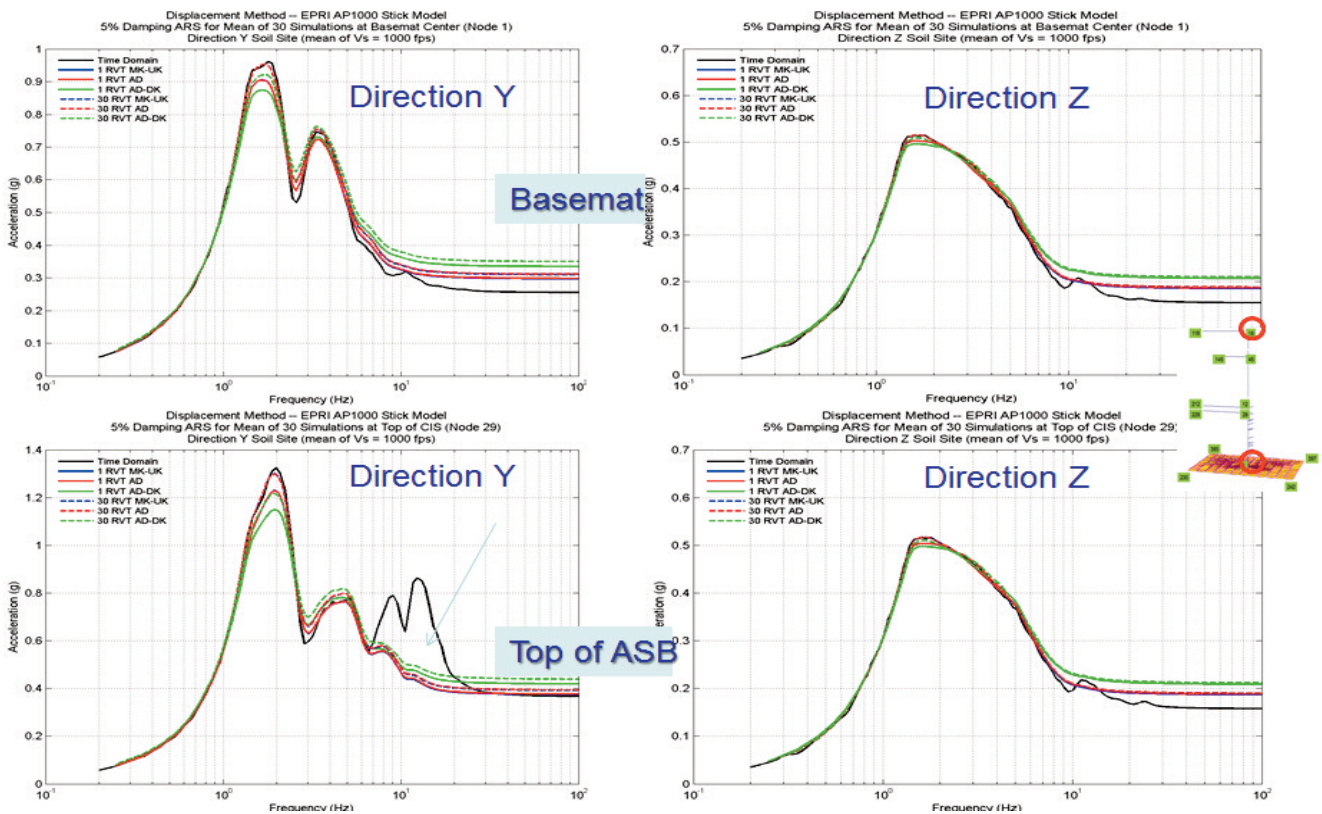


Figure 5 Probabilistic Mean ISRS and RVT ISRS at for Soil Site Using Displacement Method

**Deeply Embedded SMR Model:**

Figure 6 (left) shows the SMR SSI model considered for the study. The SMR structure has a size of 200ft x 100ft x

100ft (H x L x W) and an embedment of 140ft depth. The soil profile shown in Figure 6 (right) is highly non-uniform with a soil stiffness inversion within the

SMR embedment depth. The seismic control motion was input at the foundation level (FIRS) at 140ft depth (elevation 0ft).

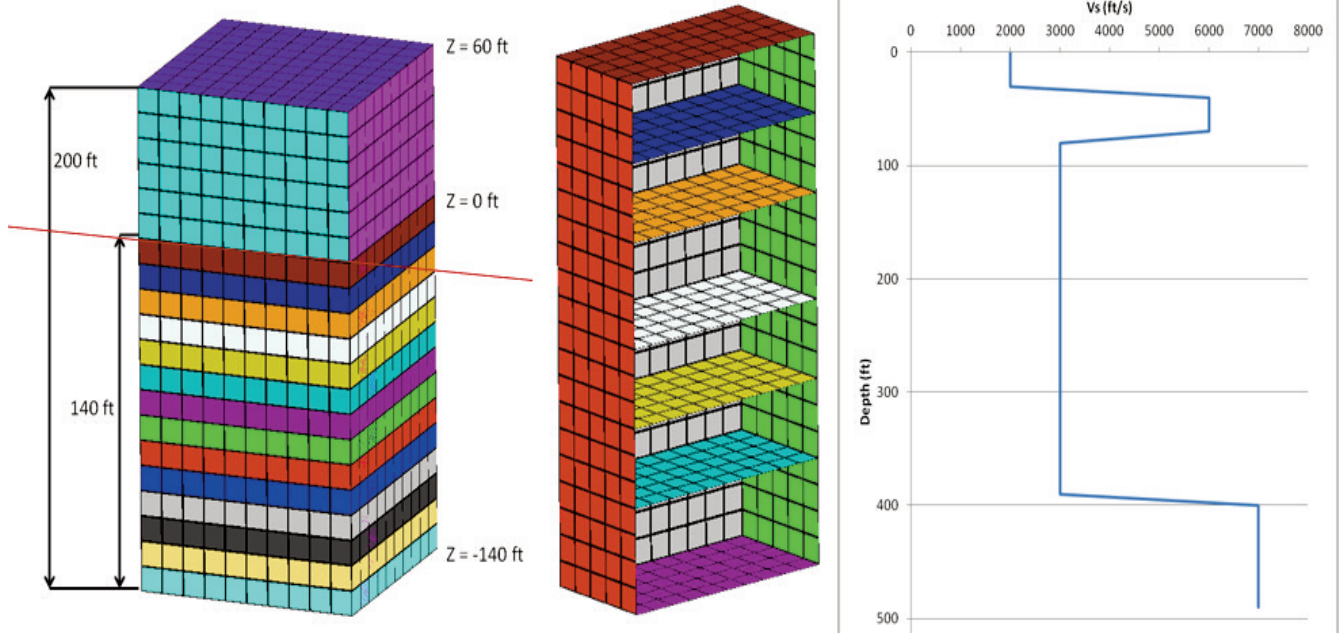


**Figure 6** 140ft Embedded SMR SSI FE Model (left) and Nonuniform Soil Profile (right)

Figure 7 and 8 show a comparison of the 5% damping mean ISRS computed using the RVT SSI approach and "standard" deterministic SSI approach as the reference approach. The RVT SSI approach results includes the MK-UK, AD and AD-DK PSD-RS transformation options implemented for the Acceleration (solid lines) and Displacement (dotted lines) methods. The "standard" deterministic SSI approach (black line) uses the mean ISRS computed for 5 (five) sets of input acceleration histories compatible with the FIRS input. The input acceleration histories were computed as in-column FIRS motions from the outcrop FIRS motion via the site response analysis. It

should be note that the input acceleration histories have a total duration of 20 seconds. For the RVT approach, it was assumed that the intense, stationary segment of the SSI motion duration is 10 seconds that appears to be a quite likely value for a 20 seconds simulated earthquake motion. Figures 7 and 8 ISRS comparisons indicate similar trends as previously noted for the surface EPRI AP1000 stick model. The mean RVT ISRS computed using MK-UK (green line) and AD (blue) algorithms with the Acceleration Method (solid lines) are by 15-20% different than the reference mean ISRS computed with the deterministic SSI approach (black solid line). The MK-UK

and AD algorithms provide basically identical results with slightly higher ISRS peaks than deterministic ISRS peaks in mid and high frequency range. However, the AD-DK algorithm (red line) fails to provide reasonable results for all locations. The Displacement Method (dotted lines) provides very poor results with missing ISRS peaks. For very low frequency below 3 Hz, all RVT approaches provide good accuracy. *Thus, reasonably accurate RVT ISRS for the deeply embedded SMR FE model can be obtained only by using the MK-UK and AD algorithms (not AD-DK) with the Acceleration Method (not with the Displacement Method)*

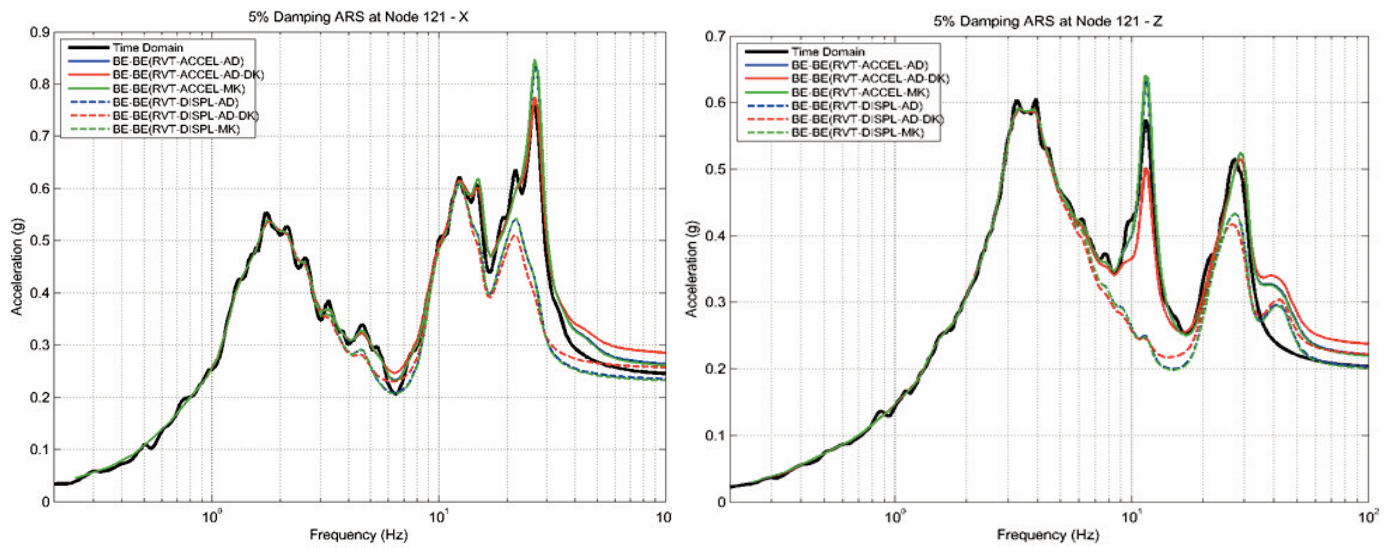


**Figure 7** Horizontal and Vertical Mean ISRS at Basemat Elevation (0 ft) Using RVT SSI MK-UK, AD and AD-DK with Acceleration (solid line) and Displacement (dotted) Methods and Deterministic SSI Approach Using Average ISRS for 5 FIRS Compatible Acceleration Input Sets (black line)

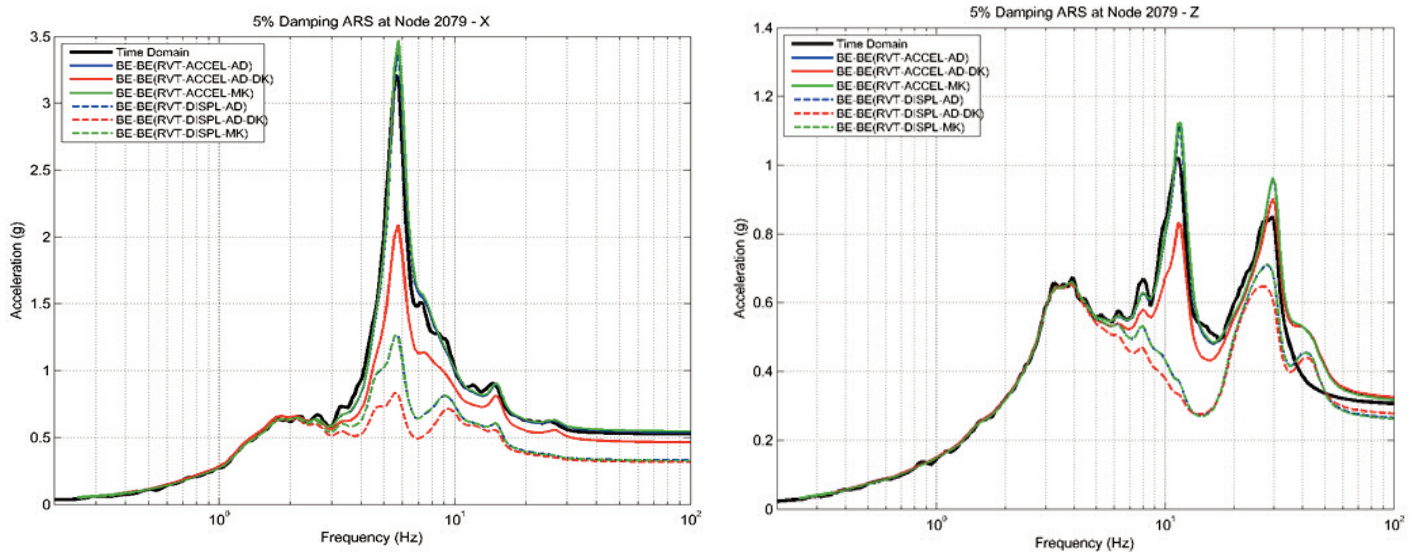


**Figure 8** Horizontal and Vertical Mean ISRS at Roof Elevation (200 ft) Using RVT SSI MK-UK, AD and AD-DK with Acceleration (solid line) and Displacement (dotted line) Methods and Deterministic SSI Approach Using Average ISRS for 5 FIRS Compatible Acceleration Input Sets (black line)

Further, the RVT SSI approach is compared with the probabilistic SSI approach. For probabilistic SSI, the outcrop FIRS spectral shapes were randomized based on the probabilistic site response analysis, as described in a separate paper (Ghiocel, 2015). No random variability was assumed for the soil profile or structural properties (assumed with uncracked

concrete and 4% damping). Figures 9 and 10 show comparisons between the mean 5% damping ISRS computed using the RVT SSI approach (colored lines) and probabilistic SSI approach (black line). The SMR ISRS results have some similarities with the AP1000 stick ISRS results, but also include new aspects with important implications on the RVT SSI approach

application in practice. Figure 10 shows the mean ISRS at the SMR roof elevation (200 ft). It should be noted that the RVT SSI approach using the Acceleration Method and the MK-UK and AD algorithms provide mean ISRS that are by 20% lower than the reference mean ISRS computed using the probabilistic SSI simulations.

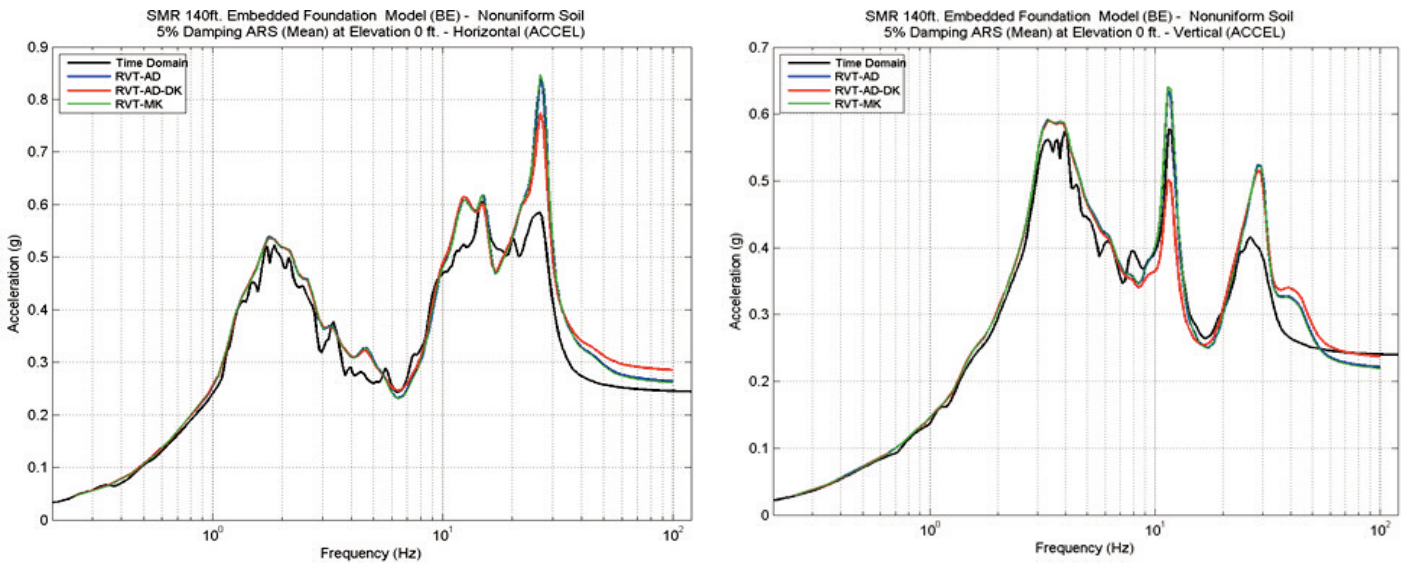


**Figure 9** Horizontal and Vertical Mean ISRS at Basemat Elevation (0ft) Using RVT SSI MK-UK, AD and AD-DK with Acceleration Method (colored) Vs. 60 Randomized FIRS Input Samples (black)

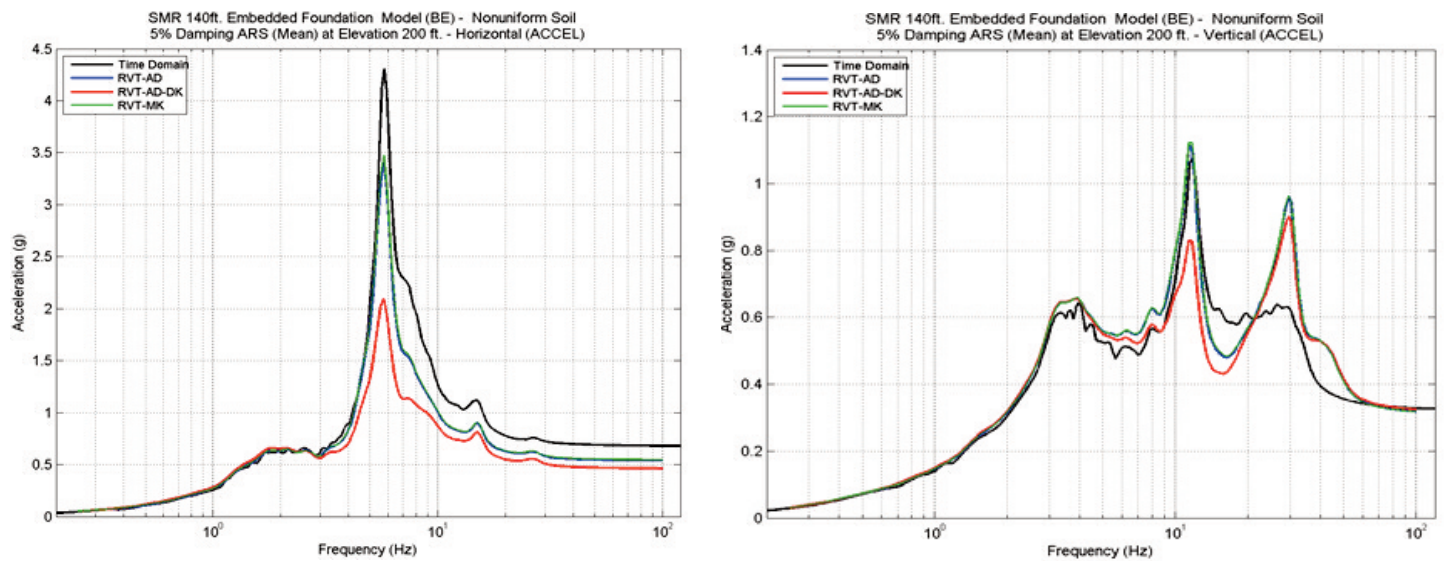


**Figure 10** Horizontal and Vertical Mean ISRS at Roof Elevation (200ft) Using RVT SSI MK-UK, AD and AD-DK with Acceleration Method (color) Vs. 60 Randomized FIRS Input Samples (black)

Figures 11 and 12 show comparisons between the 84% NEP ISRS computed using the RVT SSI approach (colored lines) and the probabilistic SSI approach (black line). It should be noted that all the RVT SSI approach algorithms produce highly

unconservative, unacceptable results for the 84% NEP ISRS computed at the SMR roof elevation (200 ft). The RVT SSI approach results are better at the basemat level, but by at least 20% unconservative for some ISRS peaks at the higher elevation. These

results suggest serious limitations of the application of the RVT SSI approaches to compute 84% NEP ISRS. *These results confirm the previous results published in the SMiRT22 proceedings (Ghiocel and Grigoriu, 2013).*

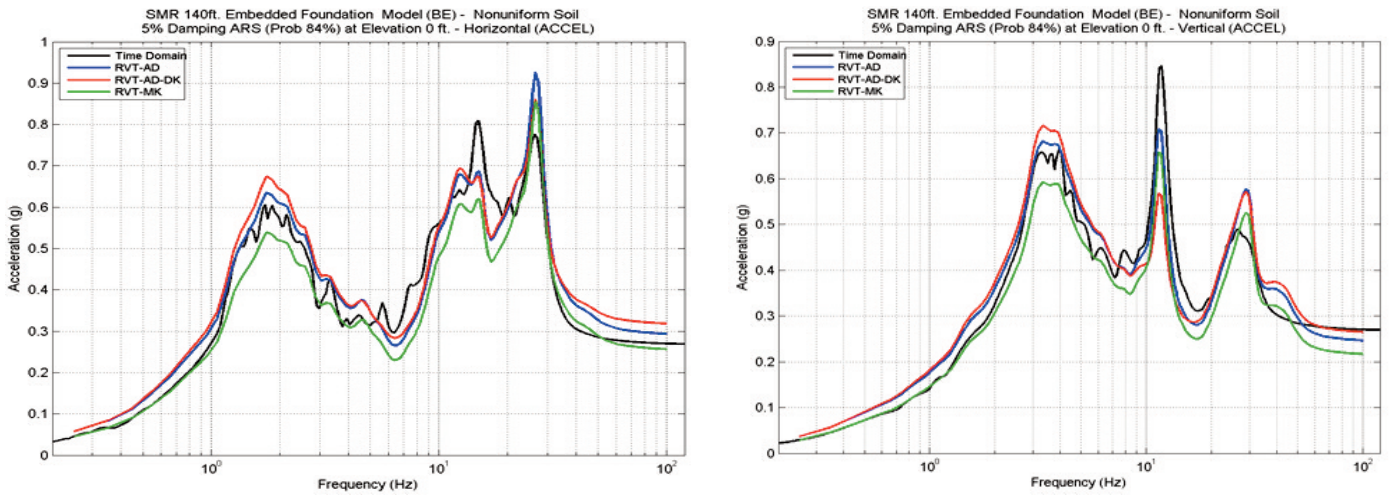


**Figure 11** Horizontal and Vertical 84% NEP ISRS at Basemat Elevation (0ft) Using RVT MK-UK, AD and AD-DK with Acceleration Method (color) Vs. 60 Randomized FIRS Input Samples (black)

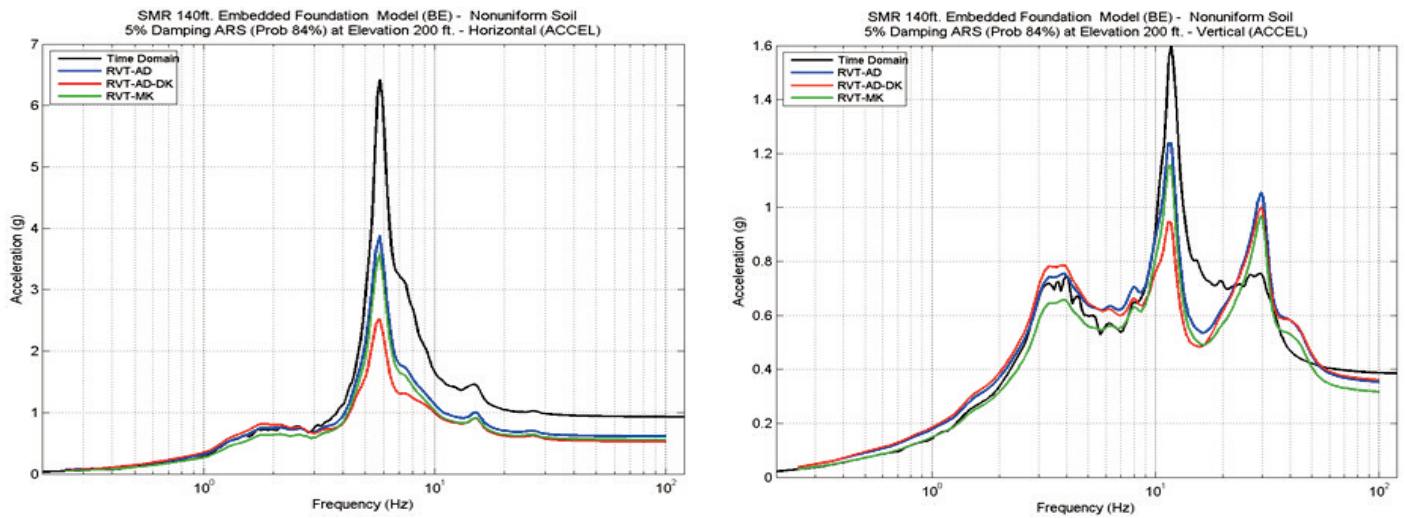


**Figure 12** Horizontal and Vertical 84% NEP ISRS at Roof Elevation (200ft) Using RVT MK-UK, AD and AD-DK with Acceleration Method (color) Vs. 60 Randomized FIRS Input Samples (black)

**CONCLUSIONS**

Based on the research investigations included in this paper, the application of the RVT SSI approach appears to be limited to the approximation of the mean ISRS based on the Acceleration Method with the MK-UK and AD algorithms, especially for the soft soil sites. The Displacement Method fails sometimes to provide reasonable results for soft soil sites. All RVT algorithms fail to provide reasonable

estimates for the 84% NEP ISRS. The RVT SSI approach accuracy varies widely on a case-by-case basis. In this paper we selected bad case study examples. There are also better situations, especially for surface models. We believe that additional, in-depth validation studies of the RVT SSI approaches should be performed by the SSI analysts before accepting them for application to nuclear projects. This paper is a warning on the

application of the RVT SSI approaches without a sufficient validation on a case-by-case basis.

**REFERENCES**

Ghiocel, D. M. (2015). "Probabilistic-Deterministic SSI Studies for Surface and Embedded Nuclear Structures on Soil and Rock Sites", the SMiRT23 International Conference, Division V, Paper #107, Manchester, UK, August 10-14